NTNU – Trondheim
Norwegian University of
Science and Technology

Design and Testing of Non-Axisymmetric Propeller Ducts

Andreas Stangeland Haavik

Marine Technology
Submission date: June 2015
Supervisor: Sverre Steen, IMT
Co-supervisor: Vladimir Krasilnikov, MARINTEK

Norwegian University of Science and Technology
Department of Marine Technology

NTNU Trondheim
Norwegian University of Science and Technology
Department of Marine Technology

MASTER THESIS IN MARINE TECHNOLOGY

SPRING 2015

FOR

Andreas Stangeland Haavik

Design and testing of non-axisymmetric propeller ducts

Ducted propellers are applied on a large range of specialized vessels, such as tugs, anchor handlers, fishing vessels etc. In the later years, we have seen the development of improved propeller duct designs. There have also been developments in manufacturing techniques, which means that it might be easier and less costly to manufacture ducts with customized geometry. Propellers have since long been designed to fit the particular wake field of the particular ship it will be used on. With the mentioned developments in manufacturing technology, the potential of making duct geometries that are customized to fit the wake field should therefore be explored – and then it is mainly the potential for making non-axisymmetric ducts that is most tempting.

Therefore, the aim of the master thesis is to explore the potential benefits of non-axisymmetric ducts. The following topics should be covered:

- Give a brief review of propeller theory for ducted propellers, and design methodology for propeller ducts.
- Describe the design criteria for a ducted propeller.
- Develop a design procedure for designing a non-axisymmetric propeller duct, which should be optimum for a given non-axisymmetric wake field.
- Use the design procedure to design at least two alternative non-axisymmetric propeller ducts.
- Perform tests in the large cavitation tunnel with the designed ducts, as well as a 19A reference duct.
- Analyze the test results and give recommendations for design of non-axisymmetric ducts.

In the thesis the candidate shall present his personal contribution to the resolution of problem within the scope of the thesis work.

Theories and conclusions shall be based on mathematical derivations and/or logic reasoning identifying the various steps in the deduction.

The thesis work shall be based on the current state of knowledge in the field of study. The current state of knowledge shall be established through a thorough literature study, the results of this study shall be written into the thesis. The candidate should utilize the existing possibilities for obtaining relevant literature.

NTNU Trondheim
Norwegian University of Science and Technology
Department of Marine Technology

The thesis should be organized in a rational manner to give a clear exposition of results, assessments, and conclusions. The text should be brief and to the point, with a clear language. Telegraphic language should be avoided.

The thesis shall contain the following elements: A text defining the scope, preface, list of contents, summary, main body of thesis, conclusions with recommendations for further work, list of symbols and acronyms, reference and (optional) appendices. All figures, tables and equations shall be numerated.

The supervisor may require that the candidate, in an early stage of the work, present a written plan for the completion of the work. The plan should include a budget for the use of computer and laboratory resources that will be charged to the department. Overruns shall be reported to the supervisor.

The original contribution of the candidate and material taken from other sources shall be clearly defined. Work from other sources shall be properly referenced using an acknowledged referencing system.

The thesis shall be submitted electronically (pdf) in DAIM:

- Signed by the candidate
- The text defining the scope (signed by the supervisor) included
- Computer code, input files, videos and other electronic appendages can be uploaded in a zip-file in DAIM. Any electronic appendages shall be listed in the main thesis.

The candidate will receive a printed copy of the thesis.

Supervisor : Professor Sverre Steen
Advisor : Vladimir Krasilnikov
Start : 15.01.2015
Deadline : 09.06.2015

Trondheim, 15.01.2015

Sverre Steen
Supervisor

Preface

This thesis is written at the Department of Marine Technology at the Norwegian University of Science and Technology (NTNU) during the spring 2015. It is submitted as a requirement for the degree of Master of Science.

Working on the subject has been of great academic value. During the semester have I developed an improved understanding of hydrodynamics, especially propeller theory. Doing experiments has been very exciting and challenging, including both preparation and performance of the tests.

I would like to thank my supervisor Professor Sverre Steen. His guidance during the semester has been invaluable. Professor Sverre Steen has provided me with constructive and concise feedback throughout the semester, and has always given rapid and helpful answers to my questions.

During the design process have both Vladimir Krasilikov and Lars Øien helped me. They provided me with theory, experience and computer skills. At the cavitation tunnel have Luca Savio and Terje Rosten guided me through the experiments. Both have lots of knowledge and experience, which they gladly shared. Thanks to Steinar Aasebø at Rolls Royce Marine for sharing information and material I needed for my thesis.

I would also like to extend my gratitude to Rolls Royce Marine for financial assistance of the model test. Their contribution has made it possible to do research on this special propulsion unit.

A special thank will I send to my office A1.019 at Marine Technology Center, for both constructive and non-constructive discussions during the last year at NTNU.

Last, but not least, will I thank my family for supporting me through all years at NTNU. They have served me with everything from thoughtful conversations and beautiful vacations to pure cash.

Trondheim, June 10, 2015

Andreas Stangeland Haavik

Summary

Ducted propellers are widely used on large range of vessels, especially for increased thrust, which is important on vessels like anchor handlers and trawlers.

In the later years new manufacturing techniques have been developed for production of propeller ducts. For that reason it might be easier and less costly to manufacture ducts with customized geometry. Propellers have since long time been customized to a given wake field. This type of customizing is suited for ducts as well. The main goal is to design a duct that generates homogenous flow into the propeller, as well as increasing the efficiency. This shall reduce the risk of cavitation. Cavitation is considered to only have negative contributions, like reduction of thrust and generation of noise and vibration.

A design procedure for the design of non-axisymmetric propeller ducts is developed. The script Haavik's model reads a given wake field from an arbitrary vessel, and divide the duct into sections. Then the script proposes a duct that consisting of different duct cross sections. The duct will accelerate or decelerate the flow, depending on the wake field, so the flow into the propeller becomes homogeneous. The duct cross sections are presented in a duct library.

During this master thesis two non-axisymmetric ducts are designed and tested. The ducts are tested against a reference duct, the well-known and axisymmetric 19A. The following tests for comparing the ducts are performed: open water test, cavitation bucket, pictures and noise measurements. All tests are done in the cavitation tunnel at MARINTEK, Trond-

heim.

The open water tests shows that the efficiency is higher for the non-axisymmetric ducts, compared to the 19A. The open water tests show also that the thrust is increased and that the torque is unaffected. The results from the cavitation tests shows that bubble cavitation reduce the total thrust. Thus, the non-axisymmetric ducts are less affected by this type of cavitation, compared to the 19A.

Duct cavitation occurred only at the 19A duct. That phenomenon happened at low cavitation numbers.

As a conclusion I mean that the tests of the non-axisymmetric ducts shows good results. The efficiency is high, and the effect of bubble cavitation is reduced. The design procedure should be improved so more accurate results could be obtained. The duct library should expand so the transitions between the cross sections will be smoother, thus more accurate calculations. CFD calculations might be efficient to tell how the duct influences the flow into the propeller.

Sammendrag

Dysepropeller blir brukt på en stor mengde spesialskip, hovedakelig for å øke thrusten. Dette er svært viktig for blant annet ankerhåndtererfartøy og fisketrålere.

I løpet av de senere årene har nye produksjonsmetoder blitt utviklet for design av dyser. Av den grunn er det blitt aktuelt å designe dyser etter medstrømmen fra skipet. Denne type tilpassing har i lang tid blitt gjort for propeller. Målet er at innstrømningen på propeller skal bli homogen, samtidig som virkningsgraden forblir så høy som mulig. Dette designet skal redusere risikoen for kavitasjon. Kavitasjon er antatt å kun påvirke negativt, som redusert thrust samt kilde til støy og vibrasjoner.

Jeg har utviklet en framgangsmåte for å designe ikke-rotasjonssymmetriske dyser. Skriptet "Haavik's model" leser en gitt medstrøm, og deler dysen inn i seksjoner. Deretter foreslår skriptet en dyse bestående av ulike tverrsnitt. Dysen vil akselerere eller redusere hastigheten på strømmen, slik at strømmen inn på propellen blir homogen. Tverrsnittene blir hentet fra et selvlaget dysebibliotek og kan settes sammen til en dyse.

I denne masteroppgaven har jeg designet og testet to ikke-rotasjonssymmetriske dyser. Dysene har jeg testet mot en referansedyse, den kjente og rotasjonssymmetriske 19A dysen. Følgende tester er utført: friprøve, "cavitation bucket", bilder og lydmålinger. Alle tester er gjennomført ved kavitasjonstunnelen ved MARINTEK, Trondheim.

Resultatene fra friprøvene viser at virkningsgraden blir høyere på de ikke-rotasjonssymmetriske dysene, sammenlignet med referansedysen. Resul-

tatene fra kavitasjonstestene viser at boblekavitasjon reduserer thrusten. De ikke-rotasjonssymmetriske dysene blir mindre påvirket av disse typene kavitasjon, sammenlignet med referansedysen.

"Tip vortex"-kavitasjon er en type kavitasjon som forbindes med støy. Resultatene fra testene viser at denne type kavitasjon oppstår ved omtrent likt kavitasjonstall for alle tre dysene. Lydmålingene forteller også at det ikke er store variasjoner mellom dysene.

Dysekavitasjon oppstår kun på referansedysen. Dette skjedde ved lave kavitasjonstall.

Jeg mener at testene som er gjort på de ikke-rotasjonssymmetriske dysene viser solide resultater. Virkningsgraden er høy og effekten av boblekavitasjon er redusert. Framgangsmåten kan forbedres ved å inkludere tangentielle hastigheter, slik at mer nøyaktige målinger kan foretas. Dysebiblioteket bør utvides slik at blant annet overgangene mellom tverrsnittene blir mykere og mer nøyaktig.

Contents

List of Figures

List of Tables

Nomenclature

Momentum theory

Symbol	Units	Description
δ	m/s	Duct induced velocity
η	$-$	Propeller efficiency
τ	$-$	Duct loading coefficient
ρ	kg/m^3	Density of water
A_P	m^2	Propeller disk area
C_T	$-$	Dimensionless propeller thrust
P	kW	Power
Δp	Pa	Pressure difference
T_P	N	Propeller thrust
T_d	N	Duct thrust
U_A	m/s	Propeller induced axial velocity
V	m/s	Velocity
V_p	m/s	Velocity at propeller plane

Lifting line theory

Symbol	Units	Description
Γ	m^2/s	Circulation
γ_ϕ	$-$	Strength per unit length of duct vortex distribution
Γ	m^2/s	Propeller vortex strength per unit area
G	$-$	Blade circulation coefficient at the duct/propeller

K_{TT}	$-$	Total thrust coefficient
K_{TP}	$-$	Propeller thrust coefficient
K_{TD}	$-$	Duct thrust coefficient
P_i	$-$	Propeller pitch ratio
p_0	Pa	Pressure, free stream
p_v	Pa	Pressure, vapor
p_∞	Pa	Pressure, static
T_D	N	Duct thrust
T_P	N	Propeller thrust
T_T	N	Total thrust
u_T	m/s	Induced tangenital velocity
u_A	m/s	Induced axial velocity
$u^*_{A\gamma}$	$-$	Non-dimensional axial velocity induced by a vortex ring
$u^{**}_{A\gamma}$	$-$	Non-dimensional axial velocity induced by a semi-infinite tube of ringvortices
u^*_{Aq}	$-$	Non-dimensional axial velocity induced by a source ring
V_A	m/s	Advance velocity
z	$-$	Number of blades

Propeller properties

Symbol	**Units**	**Description**
η_0	$-$	Propeller efficiency
σ	$-$	Cavitation number
D	m	Propeller diameter
J_A	$-$	Advance ratio
K_Q	$-$	Torque coefficient
K_T	$-$	Thrust coefficient
n	Hz	Number of revolutions
Q	Nm	Torque
T	N	Thrust

Statistics

Symbol	Units	Description
P_X	$-$	Precision limit
S_X	$-$	Standard deviation

Chapter 1

Introduction

Ducted propellers are widely used in marine propulsion system for several reasons. The main reason is to achieve high thrust at low speed, which is preferable in towing and trawling condition.

There are nominally two types of duct shape, accelerating and decelerating. As the name implies, the accelerating duct increases the velocity through the duct. The opposite happens with the decelerating shape. The main advantage with accelerating duct shape is increased thrust. The main advantage with decelerating duct is reduced risk of cavitation.

A non-axisymmetric duct can contain both an accelerating part and a decelerating part, depending on the wake field from the ship it will be used on.

New manufacturing techniques have been developed the later years for producing propeller ducts, which means it might be easier and less costly to produce ducts with customized geometry. Now, the leading design procedure for duct design is to make the ducts symmetrical. Propellers have since long time been designed to fit the particular wake field from the ship. This type of fitting is suited for duct design as well.

This master thesis should cover the following scope:

- Give a brief review of propeller theory for ducted propellers, and

design methodology for propeller ducts.

- Describe design criteria for a ducted propeller.
- Develop a design procedure for designing a non-axisymmetric propeller duct, which should be optimum for a given non-axisymmetric wake field.
- Use the design procedure to design two alternative non-axisymmetric propeller ducts.
- Perform test in the large cavitation tunnel with the designed ducts, as well as a 19A reference duct.
- Analyze the test results and give recommendations for design of non-axisymmetric ducts.

During the design phase and the testing will it be looked for both positive and negative effects regarding the non-axisymmetric duct design.

Part I

Ducted propeller theory

Chapter 2

Propeller theory for ducted propellers

2.1 Introduction

This chapter gives a review of ducted propeller theories. Afterwards are momentum theory and lifting line theory presented to get a deeper insight in the problem. Momentum theory is introduced because of its simple procedure when aiming for thrust and efficiency.

The software AKPA is used for calculating the duct induced velocities. The lifting line theory is presented by introducing a method for calculation of the duct induced velocities, and to explain different properties, like why duct induced velocities changes with different propellers and how duct design can be determined.

2.1.1 Literature study

The ducted propellers didn't come into practical use until the early 1930's when Luigi Stipa and later on L. Kort experimentally proved the advantages connected with this propulsion device. Due to the pioneer work

done by Kort the application of ducted propeller has become common practice. For that reason ducted propellers are sometimes named Kort nozzle.

The first attempt to calculate a ducted propeller were based on the momentum theory. Using this method the total thrust, ideal power and the ideal efficiency could be expressed in terms of the area and the velocity of the wake. The main drawback of the momentum theory was its inability to give a detailed knowledge of the induced velocity field and to determine the geometry of the duct and propeller.

In the early 40's Dickmann (1940) and Horn (1940) introduced the method of singularity in this field. Later on Horn and Amtsberg (1950) developed a method of design based on these theories, where the duct was represented by a distribution of ring vortices along the duct and the propeller by a sink-distribution at the propeller disk. By use of the Biot-Savart law the induced radial and axial velocities were determined at different points.

Dickmann and Weissinger (1955) pointed out that the duct and propeller has to be considered as a propulsion unit. They represented the propeller with a semi-finite tube of ring vortices emerging from the trailing edge of the duct. A comparison made between this theory and experiment shows a good agreement in the relation between the thrust of the duct, the potential wake induced by the duct and the propeller thrust coefficient. Dickmann and Weissinger assumed that the duct vorticity is known and calculated the shape of the duct.

Extensive systematic experiments have been performed at the Netherlands Ship Model Basin (NSMB) by Van Manen and Superina. This work gives proposals for the design of the optimum ducted propeller systems from the viewpoint of efficiency of ships. A review of this work was given by Oosterveld (1965).

Dyne (1967) introduced in the late 60's an accurate design method for practical use. The method use a combination of the method of singularities and momentum theory to simply the calculations. The blade circulation is arbitrary and the number of blades is finite.

Common for the mentioned research is the focus on axisymmetric ducts in a uniform flow. Not much has been written regarding non-axisymmetric ducts. In 1970 published Oosterveld (1970) his work on wake adapted ducted propellers. The design aim to make the flow at the propeller plane uniform. For accelerating and decelerating the flow he changed the exit area of the nozzle, thus only the aft part is non-axisymmetric. This kind of nozzle should minimize the propeller induced vibrations and cavitation problems, but also he found a reduction in DHP.

In June 1973 The Royal Institution of Naval Architects published a Symposium on Ducted Propellers (Turbal (1973)). He presented a theoretical solution of a non-axisymmetrical ducted propeller system in a non-uniform flow. Up to then the design of such ducts has been carried out semi-empirically. Those methods are both time consuming and includes drawbacks that are of importance in optimizing the ducts. This new theoretical method will make it possible to to evaluate the efficiency of the duct as a means of correcting the velocity field, and finding the range of application of this technique.

2.2 Momentum theory

This description of the theory is based on the presentation from Steen (2013).

The momentum theory assumes that the propeller only induces axial velocity, and that the induced velocity is uniform over the propeller disk area. See Figure 2.1.

The disk, which is located at the propeller plane, is considered to absorb all of the power of the engine and dissipate this power by causing a pressure jump. The pressure jump over the propeller disk gives the propeller thrust. By applying Bernoulli's equation we get the following, respectively in front of and behind the propeller:

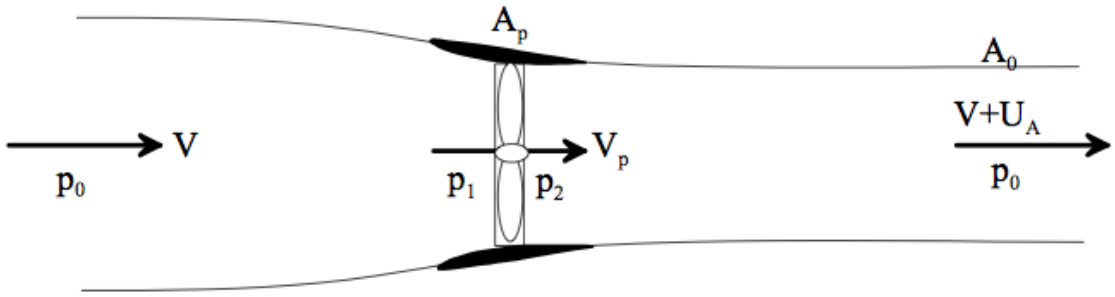

Figure 2.1: A sketch of a ducted propeller, explaining simple momentum theory (Steen (2013)).

$$\Delta p_1 = \frac{1}{2}\rho[V_p^2 - V^2] \tag{2.1}$$

$$\Delta p_2 = \frac{1}{2}\rho[(V + U_A)^2 - V_p^2] \tag{2.2}$$

where Δp is the change of pressure, V is the incoming water velocity and U_A is the axial velocity induced by the propeller.

Which gives the propeller thrust:

$$T_p = A_p(\Delta p_1 + \Delta p_2) = \rho A_p(V + \frac{1}{2}U_A) \cdot U_A \tag{2.3}$$

Here T_p is the propeller thrust.

The duct has the possibility to induce the velocity of the flow through the propeller disk, both positive and negative. The duct induced velocity is denoted δ.

The velocity will then be:

$$V_p = V + \frac{1}{2}U_A + \delta \tag{2.4}$$

The requirement of continuity gives the velocity through the disk:

$$V_p = \frac{A_0}{A_p}(V + U_A) \tag{2.5}$$

For the duct:

$$\frac{\delta}{V} = \frac{A_0}{A_p} + \frac{U_A}{V} \cdot (\frac{A_0}{A_p} - \frac{1}{2}) - 1 \tag{2.6}$$

The total thrust is given from the change in momentum:

$$T_0 = T_p + T_d = \rho A_p (V + \frac{U_A}{2} + \delta) \cdot U_A \tag{2.7}$$

where T_d is the duct thrust.

The power is given as:

$$P = \frac{1}{2}\rho A_p [V + \frac{U_A}{2} + \delta] \cdot [(V + U_A)^2 - V^2] \tag{2.8}$$

The efficiency is:

$$\eta = \frac{T_0 \cdot V}{P} = \frac{2}{2 + \frac{U_A}{V}} \tag{2.9}$$

Introducing dimensionless propeller thrust:

$$C_{Tp} = \frac{T_p}{\frac{1}{2}\rho V^2 A_p} \tag{2.10}$$

The induced velocity is given as:

$$\frac{U_A}{v} = \sqrt{1 + C_{Tp}} - 1 \tag{2.11}$$

If we combine the to last equations:

$$\eta = \frac{2}{1 + \sqrt{1 + \tau C_{t0}}} \tag{2.12}$$

where τ is the duct loading coefficient. The optimum duct loading coefficient approaches 0.5, which is a common approximation for ducted propellers (Steen (2013)).

If we use the approximation that $\delta = \frac{U_A}{2}$ we get that:

$$\tau = \frac{1 + \sqrt{1 + C_{Tp}}}{2\sqrt{1 + C_{Tp}}} \tag{2.13}$$

2.3 Lifting line theory for ducted propeller

Lifting line is one step closer the real world. The method I present is made by Dyne (1967). The method was for the design of ducted propellers in a uniform flow, and is based on the lifting line theory.

The method is developed to get an accurate method for practical use. To simplify some calculations a method of singularities and the momentum theory is used.

Due to the above mentioned reasons, the method presented by Dyne is suited to my case. The duct induced velocities are calculated as one propulsion unit.

2.3.1 Vortex system of the propeller and its induced velocities

According to the ordinary lifting line theory the propeller and its slipstream can be represented by vortex systems consisting of a free vortex line along the propeller axis, a bound vortex representing the propeller blade and and a free helical vortex line starting at the blade at radius r′. See Figure 2.2.

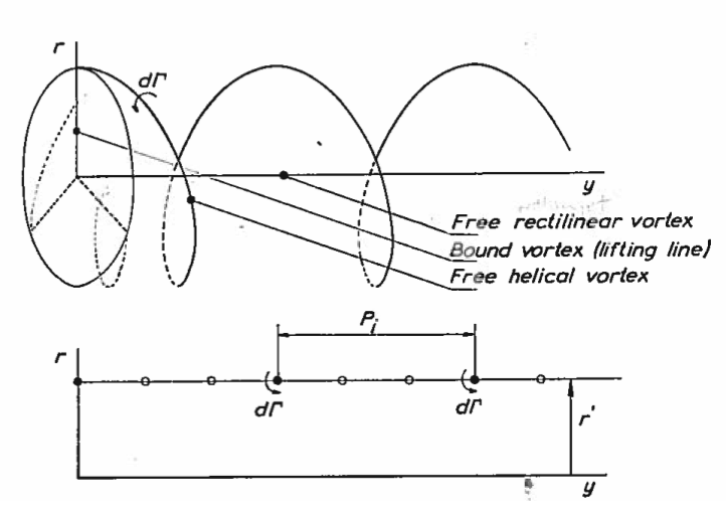

Figure 2.2: Vortex system according to lifting line theory (Dyne (1967)).

If the total circulation is $\Gamma(r')$, the strength of the vortex is $\frac{d\Gamma}{dr'}dr'$. The pitch of the helical vortex line depends on the local velocities. Since they are changing rapidly in the area of the propeller both the pitch and the radius of the helical vortex line are varying in the axial direction. As a simplification we replace the real helical vortex with an equivalent vortex with constant pitch and radius.

The velocities induced by the vortex system are determined by the Biot-Savart law, which states that the velocity at a point induced by a vortex element become:

$$\vec{dv} = \frac{\Gamma}{4\pi}\frac{\vec{ds} \times a}{a^3} \tag{2.14}$$

where $\vec{a}$ is the vector distance between the vortex element and the point considered.

Lerbes (1952) introduced induction factors, and solved the resulting equations analytically for the induced axial and tangential velocities at the propeller blade. The expression for the total propeller induced velocities can be simplified when assuming infinite number of blades, and are given as:

$$\frac{u_A}{V_A} = \frac{1}{2}\int_{xH}^{1} i_A \frac{dG_L}{dx'} \cdot \frac{dx'}{x - x'} \tag{2.15}$$

$$\frac{u_T}{V_A} = \frac{1}{2}\int_{xH}^{1} i_T \frac{dG_L}{dx'} \cdot \frac{dx'}{x - x'} \tag{2.16}$$

where

$$G_L = \frac{\Gamma}{\pi D V_A} \tag{2.17}$$

and

$$x = \frac{r}{D/2} \tag{2.18}$$

When designing a ducted propeller, the propeller induced velocities must be calculated also at several number of points ahead of and behind the propeller. It requires very complicated numerical calculations to obtain the values, and will not be shown here (Hough and Ordway (1965)).

As shown by Hough and Ordway (1965) the velocity at any field point consists of fluctuating components. When determining the shape of the duct only the steady velocities are of interests. Since the steady component is independent of number of blades, the propeller in this calculations assumes to have infinite number of blades.

For a propeller with infinite number of blades the vortex system will look like Figure 2.3 on the following page. The horse-shoe vortices induce tangential velocities and the ring vortices induces axial and radial velocities.

The strength per unit area of γ of the different vortices is determined by the following expressions:

For the horseshoes vortices:

$$\gamma_\phi = \frac{z\frac{d\Gamma}{dr'}}{2\pi r'} \tag{2.19}$$

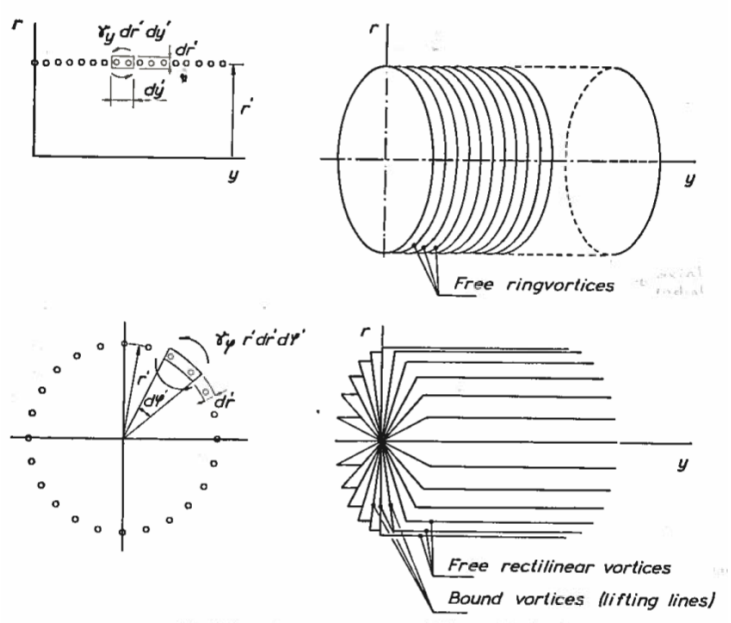

Figure 2.3: Vortex system for a propeller with infinite number of blades (Dyne (1967)).

For the ring vortices:

$$\gamma_y = -\frac{z\frac{d\Gamma}{dr'}}{P_i} \tag{2.20}$$

The total tangential velocity induced by the propeller at the radius x is given as:

in the slipstream:

$$\frac{u_T}{V_A} = \frac{z \cdot G_L}{x} \tag{2.21}$$

outside the slipstream:

$$\frac{u_T}{V_A} = 0 \tag{2.22}$$

The total axial velocity induced by the total vortex system can be determined by solving the following equation;

$$\frac{u_A}{V_A} = -\frac{1}{2}\int_{xH} 1 \frac{z\pi u_{Ay}^{**}}{P_i/D}\frac{dG_L}{dx'}dx' + \frac{1}{2}\frac{z\pi u_{Ay}^{**}}{P_i/D}G_{LD} \tag{2.23}$$

For a conventionally propeller, the circulation falls gradually to zero at the blade tips, where a pressure equalizer between the pressure and suction side of the blade tips takes place. If the propeller is surrounded by a duct there is no need for this equalization and the circulation can have a finite value at the blade tips.

2.3.2 Relation between thrust, circulation and induced velocities

I will now introduce a relation between the propeller induced velocities and the blade circulation.

Due to the tangential velocity component behind the propeller the pressure p_∞ differs from the free stream pressure p_0 outside the slipstream. Since the pressure forces must balance the centrifugal forces, then

$$p_\infty - p_0 = -\rho\int_{r\infty}^{R\infty}\frac{u_{T\infty}^2}{r_\infty^2}dr_\infty \tag{2.24}$$

where R_∞ is the radius of the slipstream.

The total thrust is obtained from the momentum theory and can be written as:

$$T_{Ti} = \frac{1}{2}\rho V_A^2\cdot 2\pi\cdot(\int_{r_H}^{R}[2(1+\frac{u_{A\infty}}{V_A})\cdot(\frac{u_{A\infty}}{V_A})\dot{r}dr - 2\int_{rH}^{R\infty} r_\infty dr_\infty \int_{r\infty}^{R\infty}(\frac{u_{T\infty}}{V_A})^2\cdot\frac{dr_\infty}{r_\infty}] \tag{2.25}$$

The thrust of the propeller can now be written as

$$T_{Pi} = 2\pi \int_{r_H}^{R} \Delta p r dr = \frac{1}{2}\rho V_A^2 \cdot 2\pi \cdot \int_{r_H}^{R} [2\frac{u_{A\infty}}{V_A} + (\frac{u_{A\infty}}{V_A})^2 + (\frac{u_{T\infty}}{V_A})^2 - (\frac{u_{T\infty}}{V_A})^2 - 2\int_{r\infty}^{R\infty} (\frac{u_{T\infty}}{V_A})^2 \cdot \frac{dr_\infty}{r_\infty}] dr dr \quad (2.26)$$

For lightly and moderately loaded propellers the contraction of the slipstream can be ignored which means that:

$$u_{T\infty} = u_{T0+}$$
$$r_\infty = r$$
$$R_\infty = R \quad (2.27)$$

If Equation 2.27 is inserted in Equation 2.25 and2.26 we can introduce non-dimensional expressions for the propeller thrust

$$K_{TPi} = \frac{T_{Pi}}{\rho D^4 n^2} = \frac{\pi}{2} J^2 \int_{xH}^{1} [\frac{u_{A\infty}}{V_A} + \frac{1}{2}(\frac{u_{A\infty}}{V_A})^2 - \int_x^1 (\frac{u_{T\infty}}{V_A})^2 \cdot \frac{dx}{x}] x dx \quad (2.28)$$

and for the total thrust

$$K_{TTi} = \frac{T_{Ti}}{\rho D^4 n^2} = \frac{\pi}{2} J^2 \int_{xH}^{1} [\frac{u_{A\infty}}{V_A} + \frac{u_{A0}}{V_A} \cdot \frac{u_{A\infty}}{V_A} - \int_x^1 (\frac{u_{T\infty}}{V_A})^2 \cdot \frac{dx}{x}] x dx \quad (2.29)$$

We find the duct thrust by subtract the propeller thrust from the total thrust (equation 2.28 and 2.29):

$$K_{TDi} = \frac{T_{Di}}{\rho D^4 n^2} = \frac{\pi}{2} J^2 \int_{xH}^{1} \frac{u_{A\infty}}{V_A} (\frac{u_{A0}}{V_A} - \frac{1}{2}\frac{u_{A\infty}}{V_A}) x dx \quad (2.30)$$

or, since $u_{A0} = u_{AP0} + u_{AD0}$ and $u_{AP0} = \frac{1}{2} u_{A\infty}$

$$K_{TDi} = \frac{T_{Di}}{\rho D^4 n^2} = \frac{\pi}{2} J^2 \int_{xH}^{1} \frac{u_{A\infty}}{V_A} \cdot \frac{u_{AD0}}{V_A} \cdot x dx \tag{2.31}$$

Thus the velocities u_{AD0} induced by the duct at the propeller disk is directly determine the thrust of the duct.

The pressure jump Δp is determined as

$$\Delta p = \frac{dT_{Pi}}{2\pi r dr} \tag{2.32}$$

where dT_{Pi} is the thrust of the bound vortices, and is obtained by applying the law of Kutta-Joukowski and assuming the induced tangential velocity at the propeller to be the mean value of the velocities immediately ahead of and behind the propeller.

$$dT_P = z\rho\Gamma(2\pi r n - \frac{1}{2} u_{T0}) dr \tag{2.33}$$

After simplifying and making it non-dimensional we get:

$$\Delta p = \frac{1}{2}\rho V_A^2 \frac{2z G_L}{x} (\frac{\pi x}{J} - \frac{1}{2}\frac{u_{T\infty}}{V_A}) \tag{2.34}$$

Using the expressions for δp and inserting Equation 2.24 and 2.27 it can now be shown that the following relation between the blade circulation and the propeller induced velocity is:

$$\frac{z\pi}{J} G_L = \frac{u_{A\infty}}{V_A} + \frac{1}{2}(\frac{u_{A\infty}}{V_A})^2 + \frac{1}{2}(\frac{u_{T\infty}}{V_A})^2 - \int_x^1 \frac{dx}{x} \tag{2.35}$$

2.3.3 Strength of the ring vortices of the propeller

The strength γ_y of the ring vortices is

$$\gamma_y = -\frac{z\frac{d\Gamma}{dr'}}{P_i} \tag{2.36}$$

where P_i is the pitch of the helical free vortex of the finite bladed propeller. As this vortex lie along a streamline the pitch is determined by the local velocities, which varying in the axial direction. The variation in Γ_y is shown Figure 2.4

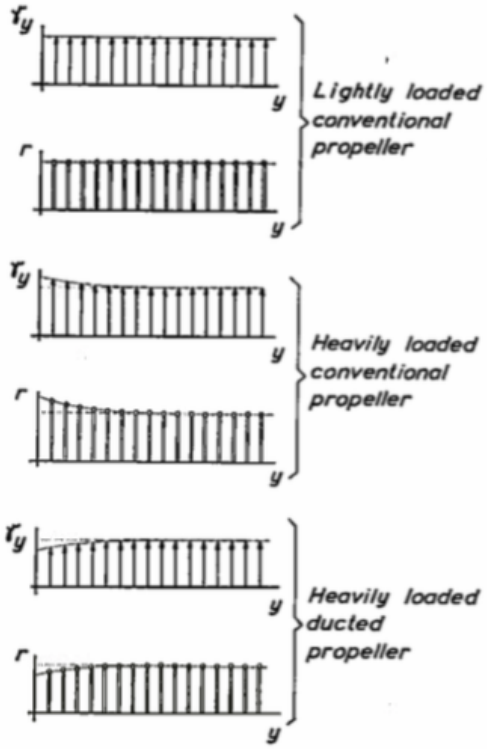

Figure 2.4: Axial variation in radius and strength of a ringvortex (Dyne (1967)).

If the propeller is surrounded by a duct the additional velocities induced by the duct change the vortex distribution γ_y of the propeller. An accelerating duct decreases both the ratio $\frac{\gamma_{y0}}{\gamma_{y\infty}}$ and the contraction of the slipstream. See Figure 2.4. A decelerating duct has the opposite effect.

When calculating the propeller induced velocities the actual vortex system is replaced by an equivalent system with constant strength γ_{ye} and radius. The strength γ_{ye} is determined so that the velocities induced by the equivalent system of ring vortices are equal to those obtained form the momentum considerations.

So, the vortex strength γ_{ye} depends upon the conditions far behind a conventional propeller. If the propeller is surrounded by a duct the local value of γ_y is changed. Because this change is concentrated to the field near the propeller it seems that we can assume that also for ducted propeller the vortex strength γ_{ye} of the vortex system is determined by the vortex pitch far behind the propeller.

2.3.4 Duct induced velocities

The thickness of the duct is represented by a distribution of ring sources and sinks along the duct. The strength q_D per unit area of the distribution is determined from the equation of continuity as

$$q_D = \frac{\delta[t_d(V_A + u_A)]_D}{\delta y'} \tag{2.37}$$

If the radius of the duct is made constant ($r_D = R$) the following expression for the axial velocity induced by the duct is:

$$u_A = \frac{1}{2\pi R} \int_{-L/2}^{L/2} q_D u^*_{Aq} dy' \tag{2.38}$$

where u^*_{Aq} is obtained from 2.5 on the next page, results made by Küchemann and Weber (1953).

If the ring vortices are placed on a cylinder with constant radius R and the strength per unit length if the vortex distribution is γ_D then the induced axial velocity be calculated from

$$u_A = \frac{1}{2\pi R} \int_{-L/2}^{L/2} \gamma_D u^*_{A\gamma} dy' \tag{2.39}$$

L is the duct length and γ_D is the vortex distribution. $u^*_{A\gamma}$ is obtained from Figure 2.6 on page 19, made by Küchemann and Weber.

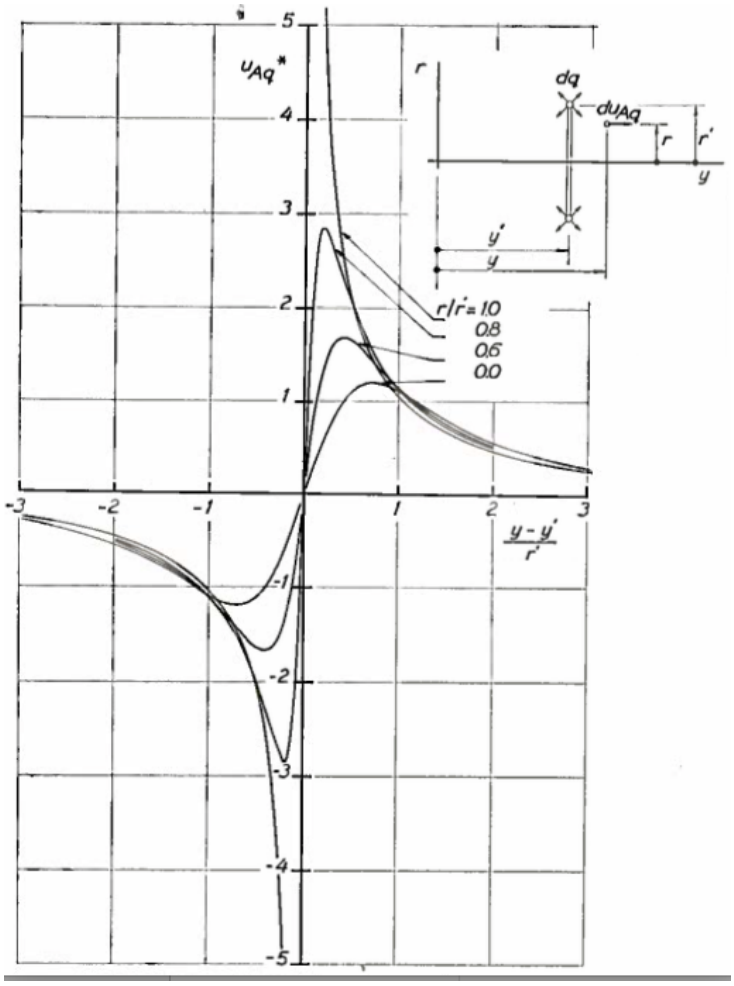

Figure 2.5: Axial velocities induced by a source ring (Dyne (1967))

2.3.5 Thrust of duct and propeller

The thrust of the duct and propeller are determined in an iteration process as follows:

- Approximate values for blade area, total axial velocity at the propeller disc and along the duct, tangential velocity at the propeller disk and blade circulation
- The strength of the source distribution for the duct are calculated from equation 2.37, and the corresponding axial velocities from equa-

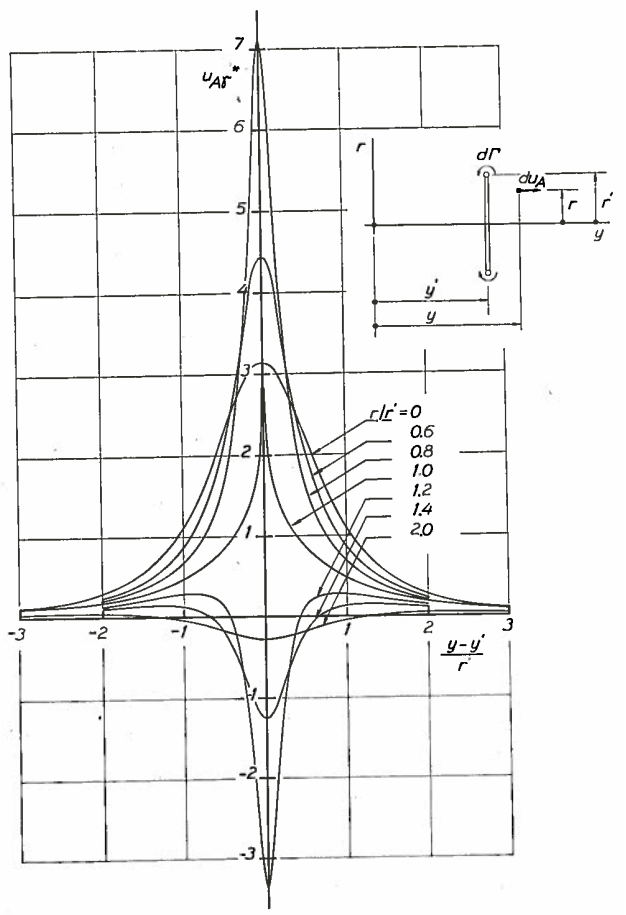

Figure 2.6: Axial velocities induced by a vortex ring (Dyne (1967)).

tion 2.38.

- Due to the axial components of the drag caused by the duct, the ducted propeller must be designed to give a total thrust K_{TTi} higher than the thrust desired, K_{TT}.

$$K_{TTi} = K_{TT} + \frac{z}{8} \cdot J^2 \int_{xH}^{1} C_D \cdot \frac{l}{R} \cdot \frac{V}{V_A}(1 + \frac{u_{A0}}{V_A})dx + \frac{\pi}{4} \cdot J^2 C_D \cdot \frac{L}{R} \tag{2.40}$$

- The total thrust K_{TTi} is obtained from momentum considerations and compared with the thrust obtained from equation 2.40

- If the two values of the total thrust differ the blade circulation G_L is corrected. After that the total axial velocity at the propeller disk and along the hub and the duct is determined. The contributions are the advance velocity V_A, the propeller (equation 2.23), the source distribution of the duct (equation 2.38) and the vortex distribution of the duct (equation 2.39).

  Calculations are repeated until convergence is obtained.

- When this is ok, the thrust of the propeller is determined by:

$$K_{TP} = K_{TPi} - \frac{z}{8} \cdot J^2 \int_{xH}^{1} C_D \cdot \frac{l}{R} \cdot \frac{V}{V_A}(1 + \frac{u_{A0}}{V_A})dx \tag{2.41}$$

  The thrust of the duct is:

$$K_{TD} = K_{TT} - K_{TP} \tag{2.42}$$

- For a given blade profile the effective camber is determined form the blade circulation using two-dimensional profile data (Abbot and von Doenhoff (1949)). From these data also the critical cavitation number and the thickness and camber of the blade profile is given.

2.4 Design methodology for propeller ducts

According to Gilbert Dyne, a well designed duct meet the following requirements:

- The duct induces axial velocities at the propeller disk, and thrust is generated.
- The internal surface of the duct is cylindrical at the propeller disk.
- The pressure distribution along the duct is suitable to avoid flow separation.

With those requirements in mind, I will introduce and explain two methods for the design of ducts.

2.4.1 The boundary condition method

The most common method is the boundary condition method. It is based on that the normal velocity must vanish at the duct surface.

The radial and axial mean velocities u_R and u_A induced by the singularities represents the propeller and the duct. Those are calculated at the duct surface. Then the boundary condition

$$\frac{dr_D}{dy} = \frac{u_R}{V_A + u_A} \tag{2.43}$$

gives a first approximation of the duct camber line $r_D(y)$. The exact duct shape can be determined by an iteration process where the ring vortices and ring sources of the duct and the ring vortices representing the propeller are placed to the calculated stream tubes if the duct and propeller slipstream after which the calculations are repeated.

2.4.2 Continuity law method

In this method the radial distribution of the axial velocity induced by the singularities of the propeller and duct are calculated at a number of sections along the duct. The internal surface of the duct is then determined to a first approximation using the law of continuity:

$$2\pi \int_{rH}^{Di} (V_A + u_A) r_y dr_y = constant \tag{2.44}$$

The axial velocity u_A at the stream tube which passes the propeller disk at the radius $r_y = r$ is assumed to be equal to the velocity calculated at an equivalent cylinder with constant radius r.

Also for the continuity law method must an iteration process be used to obtain the exact shape of the duct. The iterations necessary to determine the exact shape of the duct are extremely complicated especially if the propeller blade circulation is varying in the radial direction. Therefore only the first approximation of the shapes are discussed in the following. This approximation is valid for both methods.

For both methods the radial velocities strongly influence the shape of the duct. They are mainly induced by the outer part of the propeller vortex system. When the radial velocities are calculated the actuator disk assumption is used (the propeller is assumed to be infinitely thin).

The axial velocities induced by the duct are obtained from Equation 2.5 in Chapter 2.3.4.

From Figure 2.7 we can see that the boundary condition method magnifies the contraction of the stream tubes just outside the vortex tube in relation to the stream tubes just inside the tube in such a way that the law of continuity is not fulfilled. As seen the stream tubes passing $r/R = 0.9$ and 1.1 at $y/R = 0$ in the actual example cross each other at $y/R = 0.5$.

To satisfy the law of continuity the velocity vector close outside the vortex tube must be parallel to the corresponding vector close inside the tube. The total velocity can be divided in three parts:

- The velocity $\gamma/2$ induced by the local vortices
- The mean velocities u_A and u_R induced by the rest of the vortex tube
- The undisturbed velocity V_A

The radial velocities strongly influence the shape of the duct and are induced by the outer part of the propeller vortex system. Because these vortices are located inside the duct, the boundary condition method magnifies the duct shape in either direction as soon as the slipstream deviates from the cylindrical form.

When the radial velocities are calculated the actuator disk assumption is generally used, i.e. the propeller is assumed to be infinitely thin. In reality

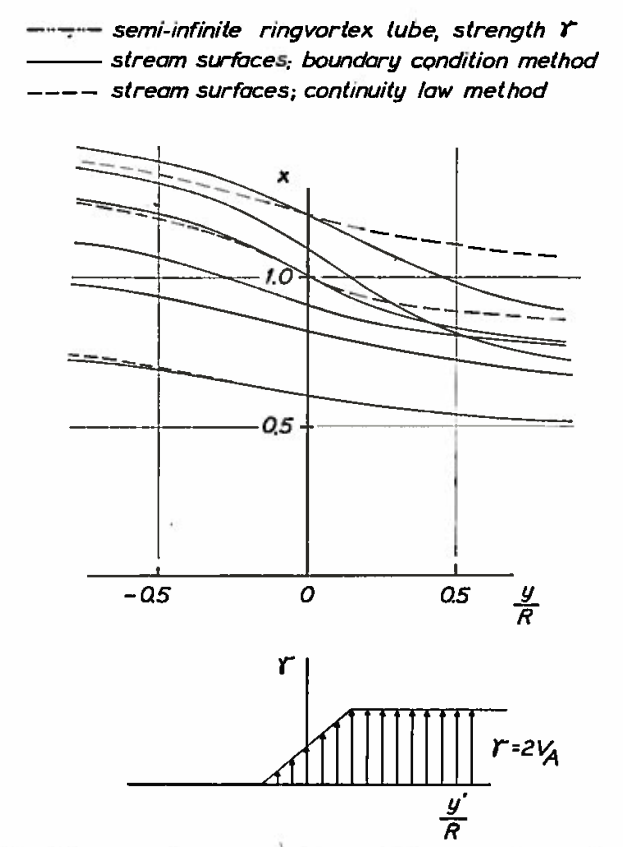

Figure 2.7: Induced stream tubes, calculated by the two different methods (Dyne (1967).

the axial extension of the propeller is finite. In the first case the vortex strength γ_y of the propeller is increased suddenly from zero to its full value at $y = 0$. In the second case however the increase in γ_y occurs gradually from zero at the propeller blade leading edge to its full value at the blade trailing edge. Quite different radial velocities are obtained near the vortex tubes at $y = 0$ in the two cases. So, if the actuator disk assumption is used, the contraction of the slipstream and the duct is overestimated.

As a result of the discussion, the continuity law is preferred. Hereby the axial velocities induced by the duct are obtained from the following equations:

Axial velocity induced by the duct source distribution:

$$u_A = \frac{1}{2\pi R} \int_{-L/2}^{L/2} \gamma_D u^*_{A\gamma} dy' \tag{2.45}$$

Tests done by (Dyne (1967)) shows the importance of the accuracy required in the design method. Small alterations in the duct shape can cause considerable changes in the thrust.

Part II

Design and testing of non-axisymmetric ducts

Chapter 3

Design criteria for a ducted propeller

Different vessels generate different wake fields. As a general rule they are non-axisymmetric. Therefore the possibility to neutralize the effect of the wake field into the propeller will be studied. By designing the ducts the aim is to achieve a homogeneous inflow to the propeller. The main goal is to decrease the risk of cavitation and still make the ducts efficient.

To achieve a homogeneous flow into the propeller the ducts will be designed with respect to the given wake field (presented in Chapter 5.2). The given wake field contains only axial velocities. Thus the tangential velocities are not given and therefore not taken into account in this thesis. One of the reasons for not including the tangential velocities is that mesh (shroud) is used to generate the given wake field. By use of this method is it more difficult to achieve the correct tangential velocities, compared to installing an aft ship in the tunnel.

Duct cross sections are presented as a function of duct induced axial velocity. As a simplification, the induced axial velocity is calculated at the propeller plane, not considered in front of or behind the propeller. It is used that the duct induced axial velocity at the propeller plane is the resulting velocity.

The duct cross sections has been designed by changing the parameters; camber, thickness, angle of attack and length. It has to be known that the duct has to be customized for each propeller and each wake, as they interfere with each other, see Chapter 4.5.

Chapter 4

Design procedure for asymmetric ducts

This chapter presents the developed design procedure for designing non-axisymmetric propeller ducts.

4.1 Procedure for the MATLAB script: Haavik's model

A MATLAB-script is developed to design non-axisymmetric ducts. The script is named Haavik's model and is found in the Appendix.

The procedure for Haavik's model is:

1. The script reads the given wake field.
2. It separates the wake field into sections of 30 degrees (can be edited), so the wake field is divided into 12 sections, of 30 degrees. The script then finds mean the velocity over each section.
3. The script will also average the velocity over the radius of the propeller blades. The script uses the velocity on the propeller at $0.7R$. One can also weight the velocity over the area.

4. A matrix is generated, which contains the mean velocity for each section at $0.7R$. This is the resulting velocity used to determine the best duct profile for each section.
5. From the sections made at point 1, the script finds the section that has the highest water velocity in the wake field. This section is now the reference section.
6. The script calculates required velocity for each section of the duct, to achieve a homogeneous flow into the propeller.
7. A final matrix will be generated, with numbered duct profiles. A row is included in the matrix that tells where the ducts should be placed in degrees (see Figure 4.2 on page 32). The duct cross sections are found in the duct library.

4.2 Library of ducts

A library of duct cross sections is developed, and attached electronically. The duct cross sections are presented as a function of duct induced axial velocities.

The Wageningen 19A duct is used as basis for designing duct cross sections. Four parameters are varied; angle of attack, camber distribution, thickness distribution and length of duct. See Figure 4.1. By changing those parameters one is able to both accelerate and decelerate the duct induced velocity. The software AKPA 6.0 was used to calculate the duct induced axial velocities. AKPA was verified as being a suitable program during the project thesis Haavik (2014). The duct induced velocities have been calculated together with the propeller P1374, which is further presented in Chapter 5.2.

Separation at leading edge is tried avoided when designing the ducts. Separation is considered to only have negative effect on the propulsion.

All duct cross sections are designed so propeller tip and duct has constant

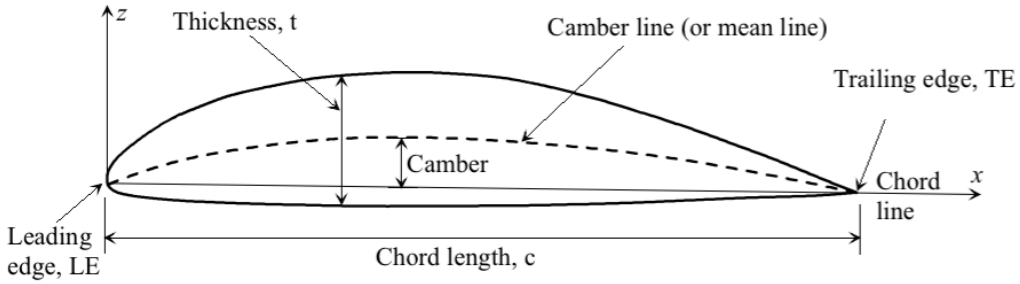

Figure 4.1: Definitions of geometry of a foil cross section (Minsaas and Steen (2012)).

and minimized gap; $1.5mm$. This is done to minimize the pressure difference at different blade positions. The consequence is that at $30\% - 70\%$ of the duct length, the inner part is horizontal. This can be seen on Figure 4.9 on page 37 .

When using AKPA 6.0 for calculating the duct induced velocities, the values are found in the file named IndVelField.duc in the project folder. Notice that all induced velocities in AKPA should be given with the main sign convention, and in the main coordinate system. It means that positive axial velocities are upstream, and negative velocities are downstream. In the case of ducts, positive induced velocities should mean that the duct decelerates the flow, while negative induced velocities would mean that it accelerates the flow.

4.3 Mount the duct cross sections

Next step after receiving the matrix from Haavik's model, is to mount the duct cross sections.

If the proposed duct contains cross sections with different lengths is it recommended that the cross sections are mounted so the propeller always works at the center of the duct length. Mounting the cross sections at leading or following edge are possibilities.

The problem with mounting at leading edge is that most of the "work" (regarding axial induced velocities) is done at leading edge. Mounting of the ducts at leading edge vanish the gain from the design.

Meeting at following edge is possible. One problem is that the propeller always should operate at the horizontal level (as explained in Chapter 4.2), due to the non-axisymmetric form. If the cross sections should meet at following edge the horizontal level will move due to different lengths of cross sections. It means it requires changes of geometry of the cross section. Thus, the induced velocities changes and the accuracy of the method decreases.

Because the duct cross sections are chosen as a function of induced velocities, I recommend that the ducts will be centered to achieve the calculated induced velocities.

4.4 Presentation of Duct A and B

The final matrices generated by Haavik's model are presented for Duct A and B in Figure 4.2 and 4.3.

The reason for the different proposals can be divided in two.

First of all, the reason is due to design procedure. In the script, Haavik's model is it used a different method for considering radial velocity. For Duct A is it used the velocity at $0.7R$. For Duct B is it weighted over the area.

Secondly, Duct B was made at a later date when the duct library was expanded.

As one understand form the matrix for Duct B in Figure 4.3, Duct B should contain four different duct profiles. From Figure 4.5 one can see it consists of only three duct cross sections. It was not possible to place the fourth cross section when the duct was modeled on the computer. The smoothing technique requires a part of the duct for transition. Duct A is presented in

```
placementOfDuctCrossSection =

     0     0     1     0     0     0     0    30
     0     0     0     0     1     0     0    60
     0     0     0     0     0     1     0    90
     0     0     0     0     0     0     1   120
     0     0     0     0     0     0     1   150
     0     0     0     0     0     0     1   180
     0     0     0     0     0     0     1   210
     0     0     0     0     0     0     1   240
     0     0     0     0     0     0     1   270
     0     0     0     0     0     1     0   300
     0     0     0     0     1     0     0   330
     0     0     1     0     0     0     0   360


ductCrossSectionNumber =

     1     2     3     4     5     6     7
```

Figure 4.2: The matrix generated for Duct A.

the means of cross sections in Figure 4.4.

The coordinates for the duct cross sections are found in Appendix E.

Figure 4.6 on page 34 presents a flowchart that summarize the design procedure.

The most accelerating duct cross section in the library induces axial velocity $1.34m/s$. The given wake field requires the duct to induce the velocity $1.56m/s$ at top position to achieve a uniform flow. Thus, the theoretical velocity at top position is 86% of the velocity at bottom position, so the flow is close to uniform at the propeller plane. The flow into the propeller is presented in Figure 4.7. An ideal case for uniform flow, should the plots be a line on the x-axis.

```
postionForDuctCrossSection =

     0     0     1     0     0     0     0     0     0     0    30
     0     0     0     0     0     1     0     0     0     0    60
     0     0     0     0     0     0     0     0     1     0    90
     0     0     0     0     0     0     0     0     0     1   120
     0     0     0     0     0     0     0     0     0     1   150
     0     0     0     0     0     0     0     0     0     1   180
     0     0     0     0     0     0     0     0     0     1   210
     0     0     0     0     0     0     0     0     0     1   240
     0     0     0     0     0     0     0     0     0     1   270
     0     0     0     0     0     1     0     0     0     0   300
     0     0     0     0     1     0     0     0     0     0   330
     0     0     1     0     0     0     0     0     0     0   360


ductCrossSection =

     1     2     3     4     5     6     7     8     9    10
```

Figure 4.3: The matrix generated for Duct B.

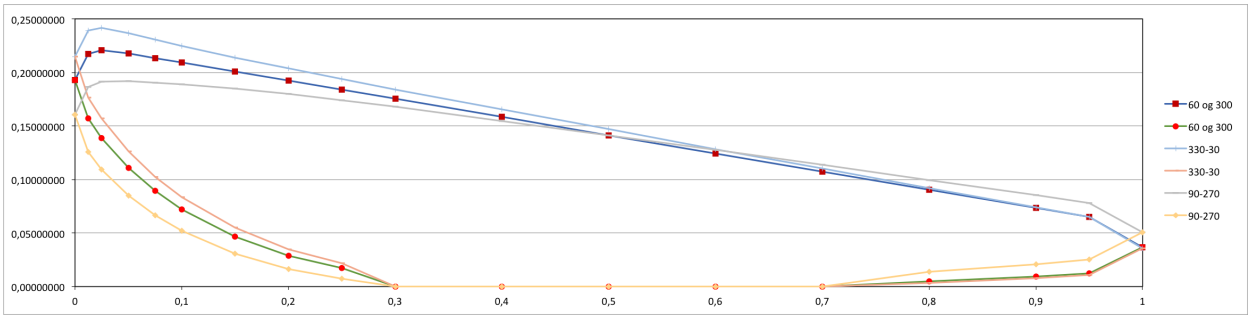

Figure 4.4: Duct cross sections for Duct A.

4.4.1 3D-modelling of the ducts

Electronically modeling of the ducts are required for production. The software Rhino was used for 3D drawing. The 3D drawings are attached electronically for both ducts in the Appendix.

The ducts are pictured in Figure 4.8, 4.9 and 4.10.

The gap between the propeller tip and the duct was set to 1.5mm. This value was decided after some discussion, 1mm gap was evaluated but rejected because the electronically smoothing may require some variations

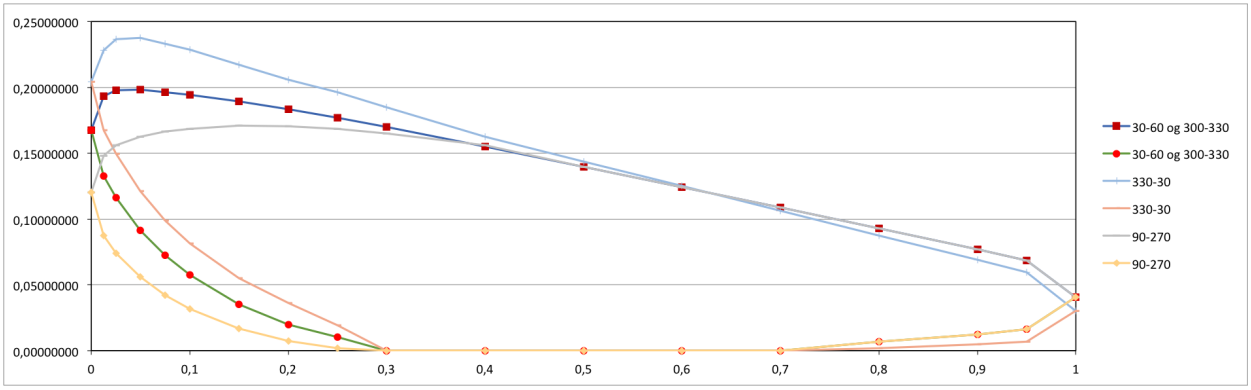

Figure 4.5: Duct cross sections for Duct B.

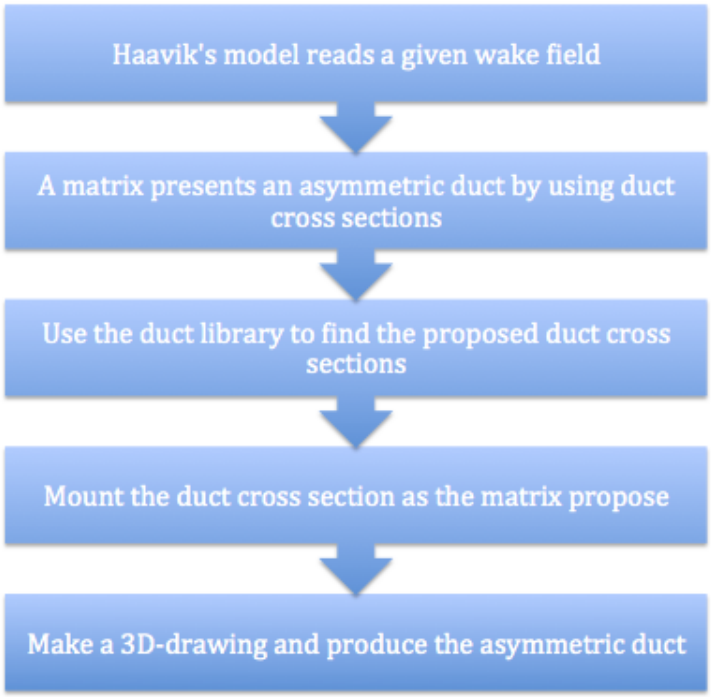

Figure 4.6: Flowchart of the design procedure for a non-axisymmetric duct.

in the inner circle.

The 3D-printer at MARINTEK was used for producing the ducts.

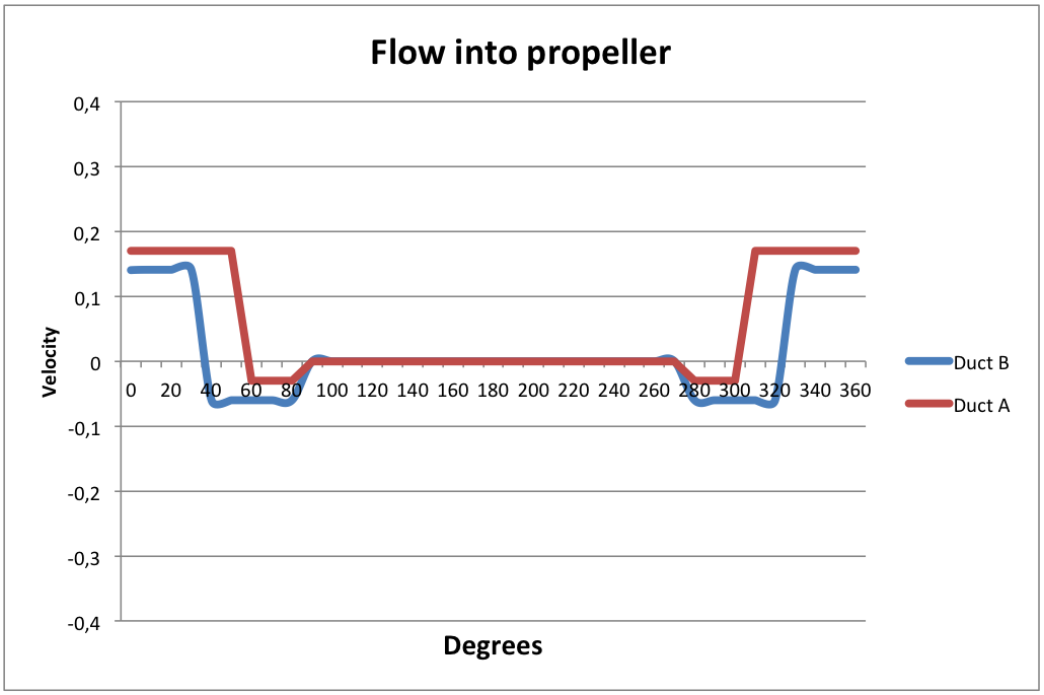

Figure 4.7: Flow into the ducted propellers.

4.5 Ducts with different propellers

It is important to know that the calculated induced axial velocities depend on which propeller is used.

The duct induced velocities will alter for different propellers. As described by Dickmann and Weissinger (1955), the ducted propeller should be considered as one propulsion unit. See Chapter 2.3 for details.

The velocities induced by the propeller change the vortex distribution γ_y of the duct. Which are used for calculating the propeller induced velocities and thrust.

A small test is done to verify the theory. The induced axial velocities are calculated for to different propellers, shrouded with the same duct, 19A. The first propeller is the one used in this thesis, P1374. The second propeller is the Wageningen Kcp 4-55. The Kcp 4-55 has similar diameter and the same number of blades as the P1374. $D = 0.25m$ and $Z = 4$.

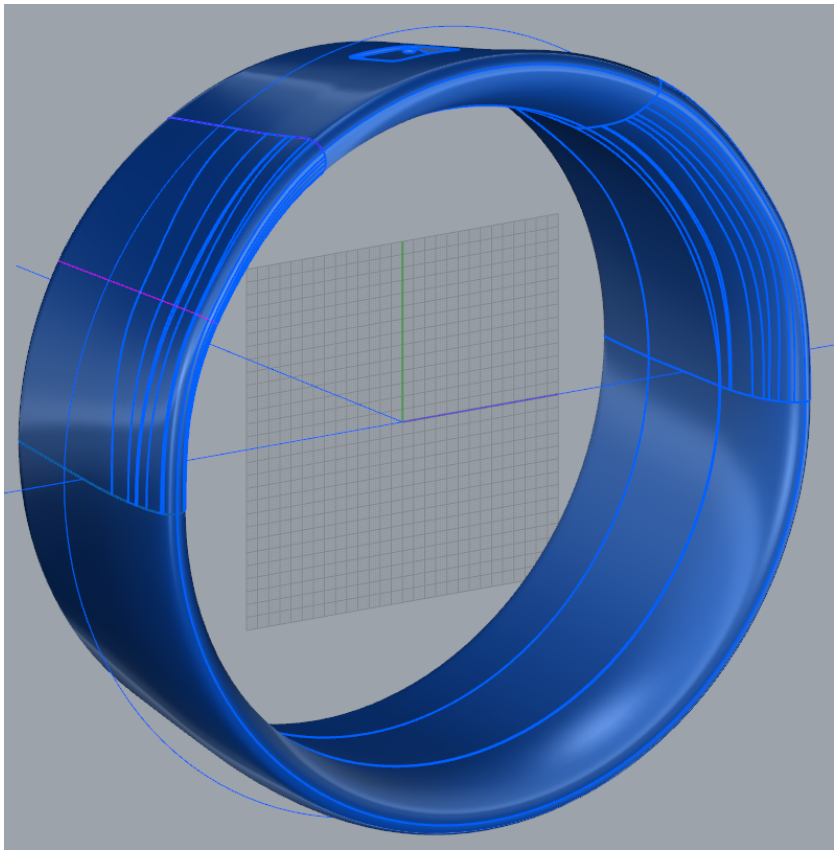

Figure 4.8: 3D picture of Duct A.

Table 4.1 presents the duct induced velocities at the propeller plane.

	P1374	Kcp 4-55
Duct induced axial velocity at the propeller plane:	0.6738 [m/s]	0.3365 [m/s]

Table 4.1: Table presenting the duct induced axial velocity for different propellers in the same duct.

As one understand from Table 4.1, the duct induced velocity strongly depends on which propeller is used.

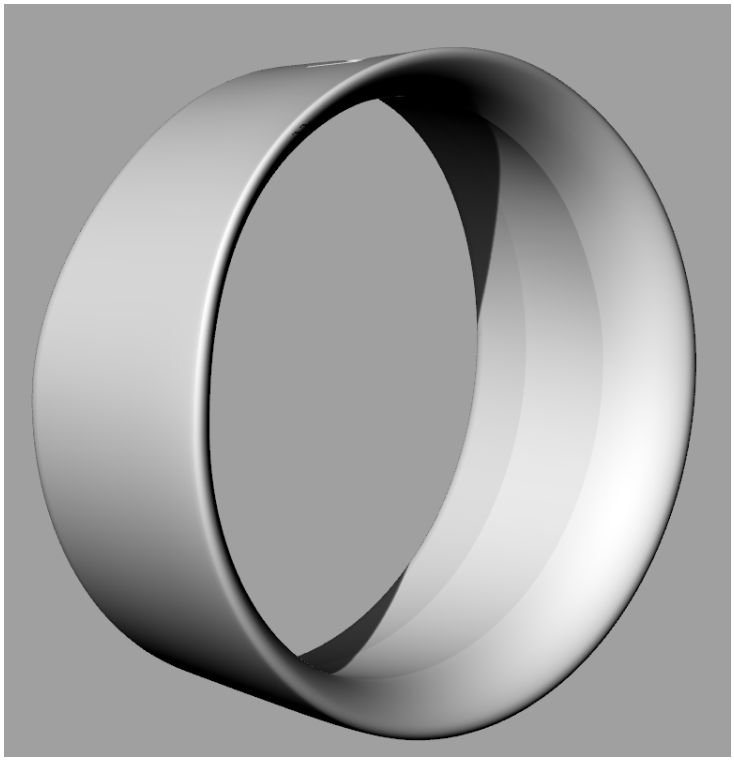

Figure 4.9: 3D picture of Duct B.

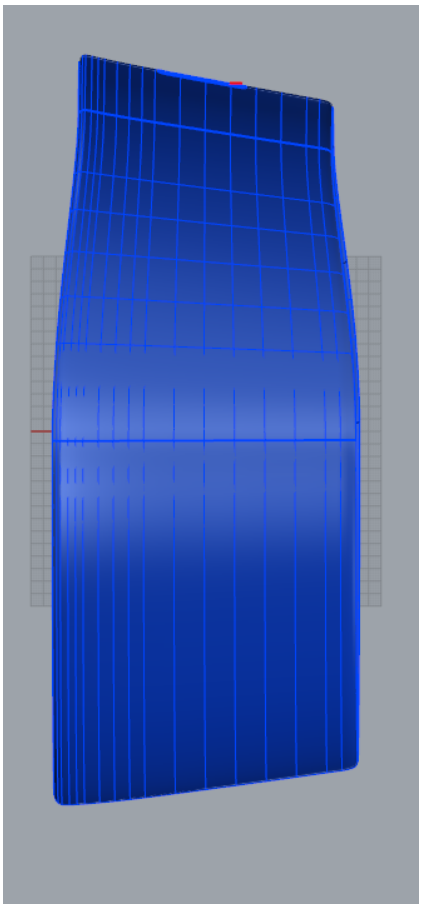

Figure 4.10: Picture taken from the side of Duct B.

Chapter 5

Cavitation tunnel test

5.1 Introduction

This chapter presents the cavitation tests done in week 9, 10, 17 and 18, 2015. The experiments were done at the cavitation tunnel at MARINTEK. A cavitation test is performed to find when, where and how the cavitation affects a (ducted) propeller.

5.2 Test setup

The cavitation tunnel at MARINTEK is pictured in Figure 5.1. Its dimensions are presented in 5.1.

Cavitation tunnel at MARINTEK		
Diameter of working section	1.20	m
Length of working section	2.08	m
Maximum water velocity	18	m/s
Maximum propeller RPM	3000	

Table 5.1: Properties of the cavitation tunnel

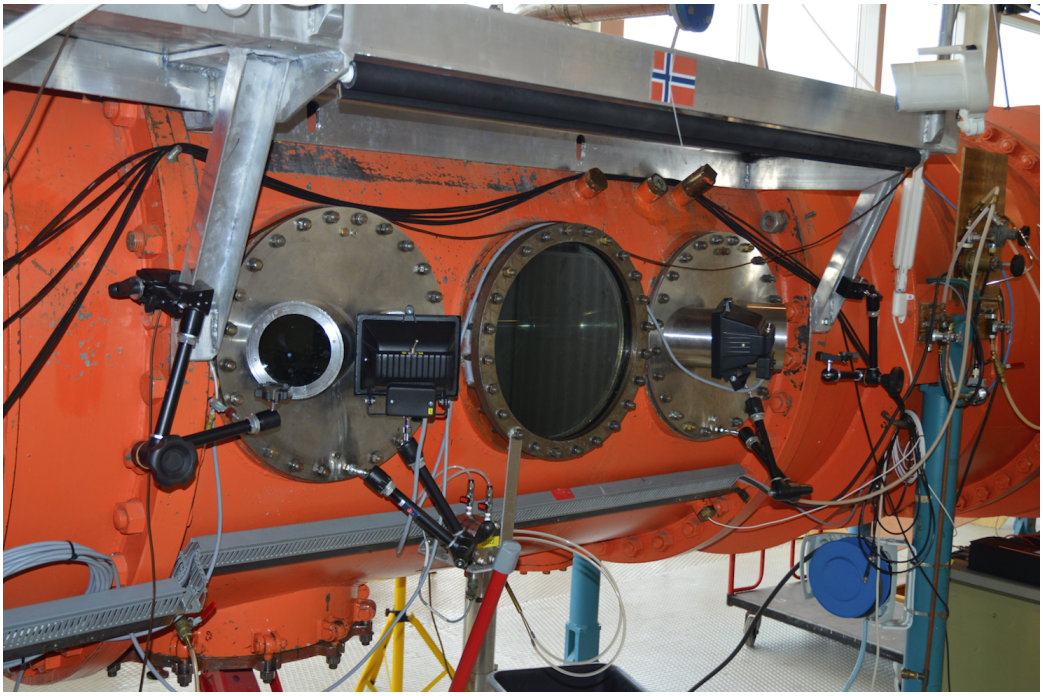

Figure 5.1: The working section at the cavitation tunnel at MARINTEK

A hydrophone for measuring the noise was installed at port side of the tunnel.

A digital amplifier is used, which is made by HBM (Hottinger Baldwin Messtechnik). The transducer is self-made at MARINTEK, and is based upon strain gauges.

The propeller P1374 is used for this experiment. Its dimensions are presented in 5.2. The duct is presented in Table 5.3.

Propeller	P1374	
Number of blades	4	-
Diameter	0.250	m
Pitch	1.1	-

Table 5.2: Properties of the propeller

Terje Rosten has made a mesh to let the ducted propellers operate in the decided wake field during the cavitation tests. See Figure 5.2.

Duct:	Wageningen 19A
Length:	0.121 m

Table 5.3: Properties of the duct

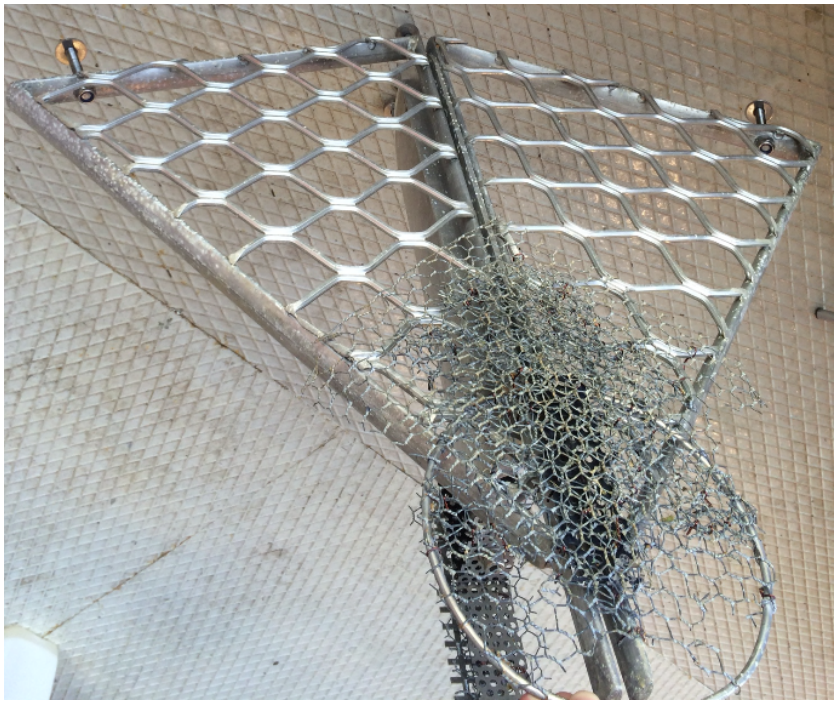

Figure 5.2: The mesh that generates the given wake field.

The mesh will act as an aft ship and is installed in front of the propeller, in the tunnel. The propeller together with the ducts was installed afterwards, through openings at the top of the tunnel.

The mesh represents an arbitrary one-shrouded ship. The wake field from the mesh is given in 5.3 and 5.4. More realistic wake simulations will produce more representative cavitation. The original wake field is presented together with the mesh made by Terje Rosten in figures in Appendix A.

For this study is it concluded that the most appropriate tests for the research on ducted propellers, in prioritized order, are:

- Open water test

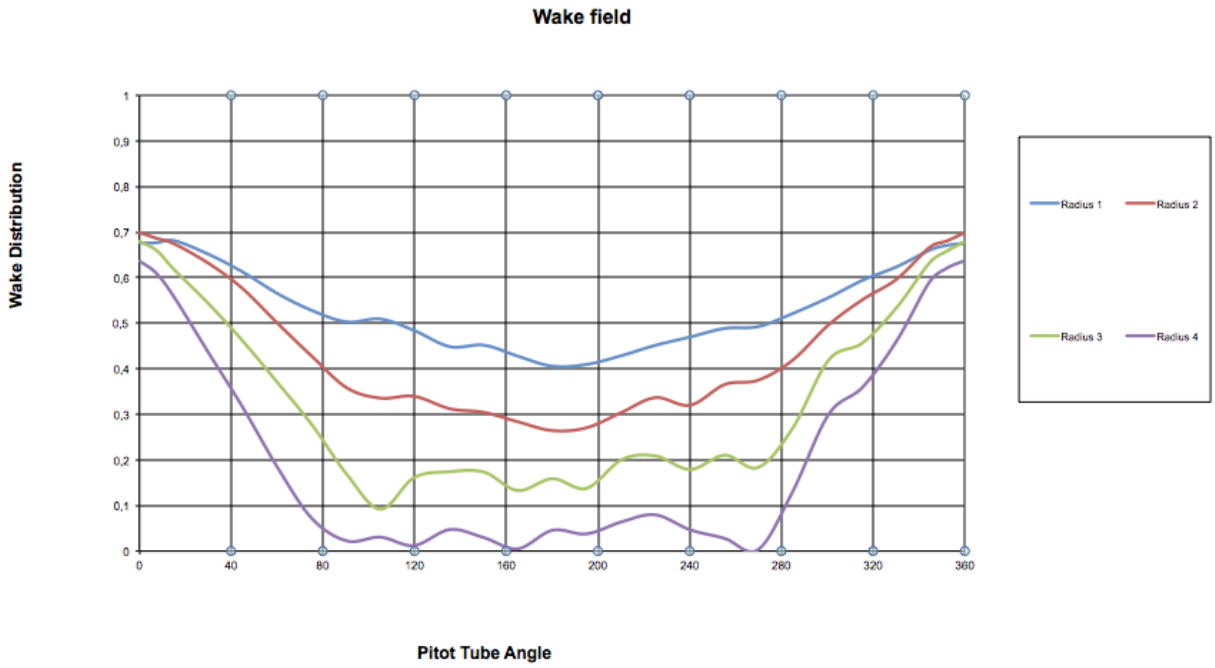

Figure 5.3: The measured wake field.

- Cavitation bucket
- Pictures
- Noise measurments

5.3 Background theory

5.3.1 Cavitation tunnel

A cavitation tunnel is a closed circuit water channel equipped with a vacuum pump, which allows reducing pressure in order to meet the desired cavitation number (Savio (2011)). The free stream velocity is controlled by by an impeller. The propeller is mounted on a shaft in the upper part of

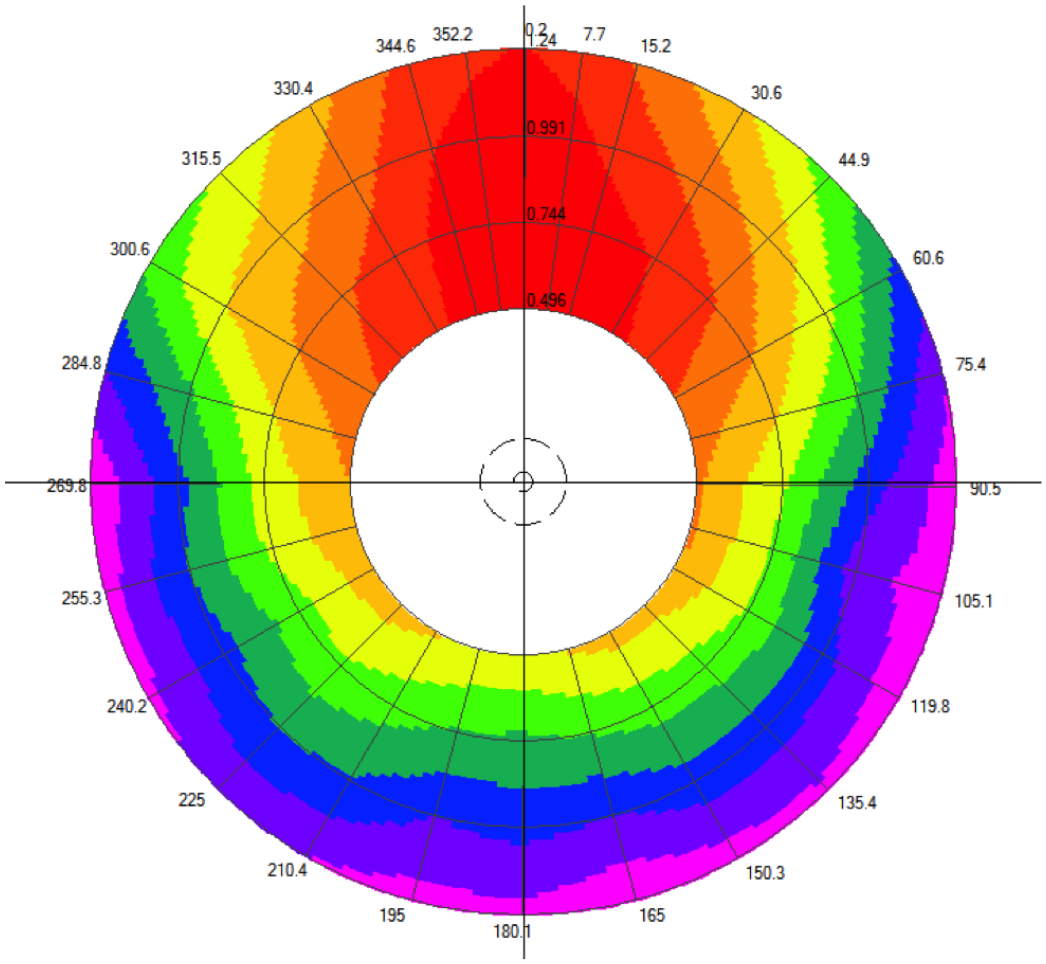

Figure 5.4: The measured wake field.

the tunnel, and provides rotational motion of the propeller. This is the test section of the tunnel. An important part of a cavitation test is visualization. This is done by using the windows at the test section. See Figure 5.5. The windows are positioned with different angles so it is possible so watch the propeller from different positions.

The most important parameters which impact the quality of experiments carried out in a cavitation tunnel are:

- Test section size: Both length and cross section is important. The cross section could be either circular or squared, and impacts the the

maximum propeller diameter. This is due to wall reflection. As a rule of thumb the propeller disk area should be less than $1/3$ of the cross section area of the test section.

- Maximum flow speed: Increasing the free stream velocity requires the propeller to rotate faster to meet the desired advance ratio and hence the operating Reynolds number is increased.
- Height of the tunnel: The lower horizontal arm is meant to eliminate all the traveling bubbles, which have been created in the upper part. To make the bubbles implode the velocity is also reduced by enlarging the tunnel section.
- Contraction area ratio: This is the ratio between the cross sections upstream the test section and the test section itself. Larger ratio gives smoother flow field at the test section inlet.
- Maximum and minimum cavitation number. Minimum cavitation number is particular important when tests are performed on high speed vessels.

5.3.2 Open water test

The main intention with an open water test is to show how the open water efficiency of a propeller is determined (Minsaas and Steen (2012)). The tests are done to check if the propeller requirements are fulfilled.

During an open water test in a cavitation tunnel is it possible to select the propeller speed, because as long as the advance ratio J corresponds to the required K_T is achieved. To get the correct condition adjust either the free stream velocity V_A or the revolutions n.

In practice, in order to obtain as high value of Reynolds number as possible for the flow over the blade sections, the requirement to run at the correct Froude number is ignored. It is unnecessary to follow Froude's law if sufficient submergence is maintained during the test. Instead, the open water test are carried out at a higher speed of advance, the advance ratio

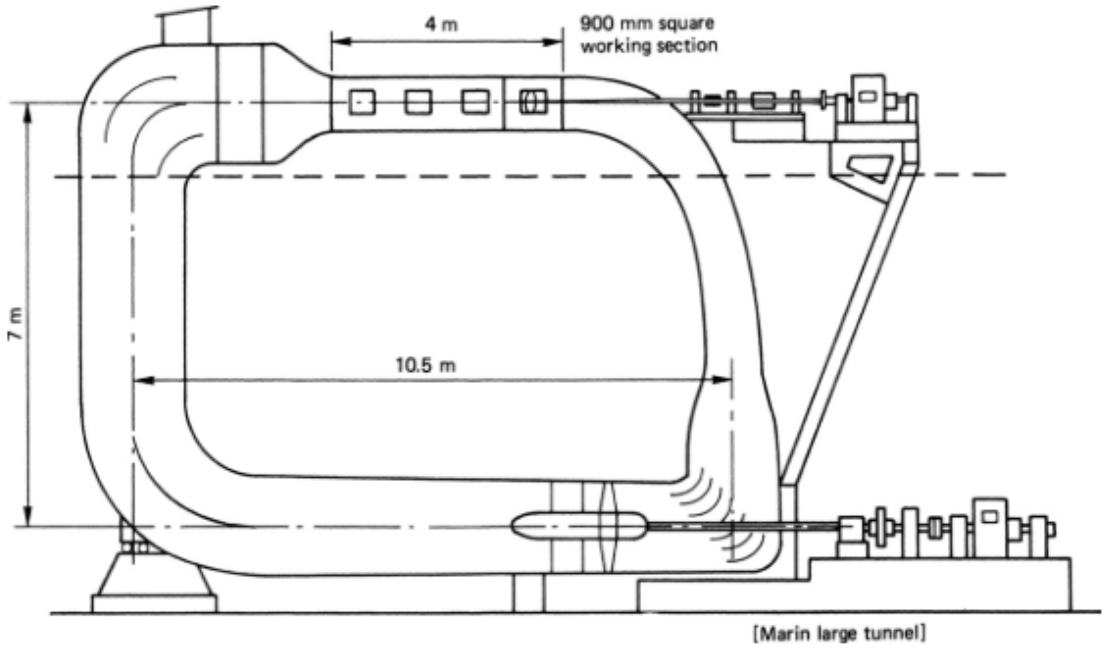

Figure 5.5: Typical cavitation tunnel. Test section in the upper horizontal arm (Kuiper (1981)).

being varied to cover the necessary range by a variation in revolutions. In other cases, the advance ratio range is covered by running at constant revolutions and varying the speeds of advance.

During open water propeller test, the values of thrust, torque, rate of revolutions and speed of advance are recorded during the measured trails.

5.3.3 Cavitation

Cavitation is a fluid mechanical phenomenon that can occur whenever a liquid is used in a machine which induces pressure and velocity fluctuations in the fluid.

Cavitation is called cold boiling because the temperature is hold constant during the process. In naval architecture it is considered to have only negative effects and hence avoided (Carlton (2007)). The effects may be (Min-

saas and Steen (2012)):

- Reduced efficiency
- Erosion
- Noise
- Vibration

The basic cavitation criterion is given as: $Ps \leq Pv$. Ps is the pressure in a given point. Pv is the vapor pressure at ambient temperature.

In the model cavitation test two scaling requirements have to be met. The first, geometrical similarity, means that that the structure in model and full scale has the same shape, only a scale ratio between. The second, dynamic similarity (flow similarity), requires that the cavitation number is similar. To satisfy this requirement a cavitation tunnel with the possibility to lower the pressure, from atmospheric, has to be used (Steen (2014)).

It exists several different types of cavitation, see Figure 5.6. Some of them are connected to more serious consequences than others. For example, bubble cavitation is always to be avoided due to its effect on erosion and thrust reduction.

Water quality and gas content in the water is important for when cavitation appears and for the extent of cavitation. For that reason, this is an important source of uncertainty.

Cavitation bucket

Cavitation buckets are made for presentation of the data. It is used to illustrate the development of cavitation.

The cavitation bucket for a propeller is presented in terms of inception for a given phenomenon versus K_T. It has to be read as follows: if propeller working point (K_T, σ_n) is located above a given inception curve the propeller will be free from that cavitation phenomenon; on the contrary the

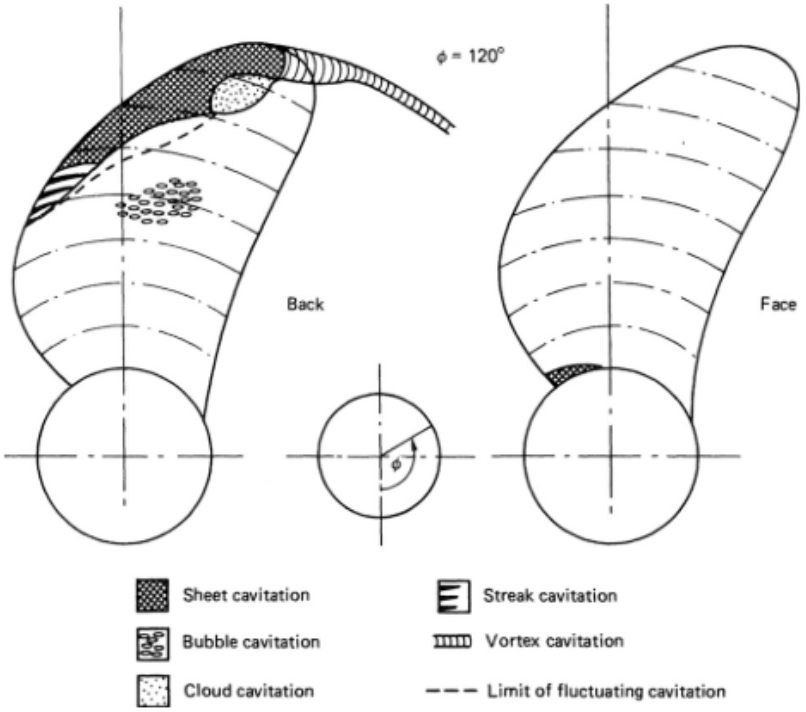

Figure 5.6: Sketch of cavitation types (Carlton (2007))

propeller will show all the cavitation phenomena whose inception index is higher that its cavitation number for a given K_T.

An example of a cavitation bucket is given in Figure 5.7.

In general, design point does not coincide with the full speed and it is carefully chosen to represents a good compromise considering different ship operation speeds. See Figure 5.8 for trends in propulsory design. As one can see, in order to avoid cavitation you may have to reduce the efficiency.

5.3.4 Propeller noise

Propeller noise is a part of the general topic ship noise. The propeller contribution to the ship overall noise varies significantly with the ship speed and is dominating in cavitating condition (Savio (2011)). Other sources of

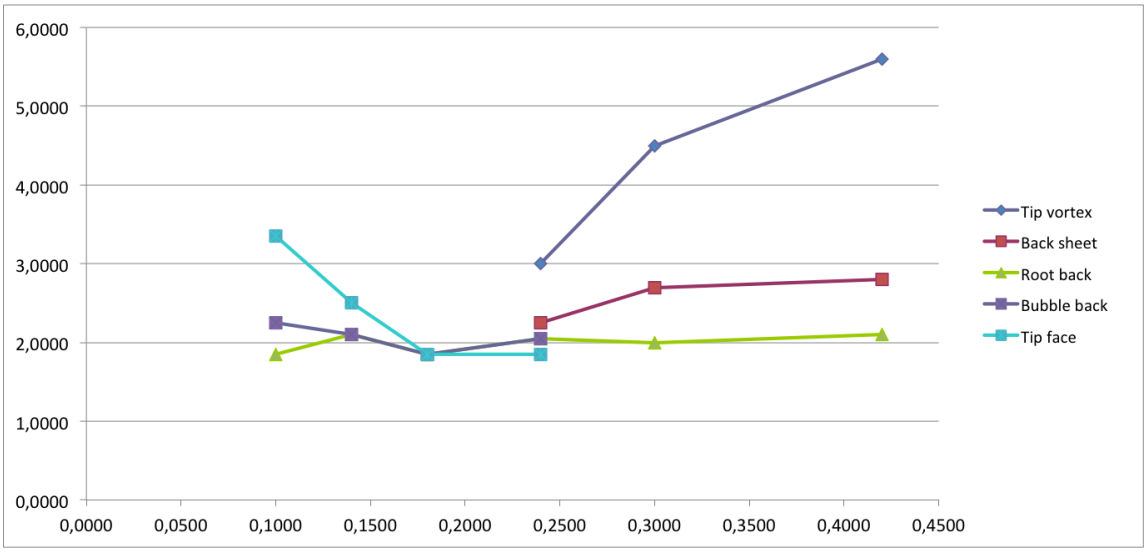

Figure 5.7: Example of a cavitation bucket.

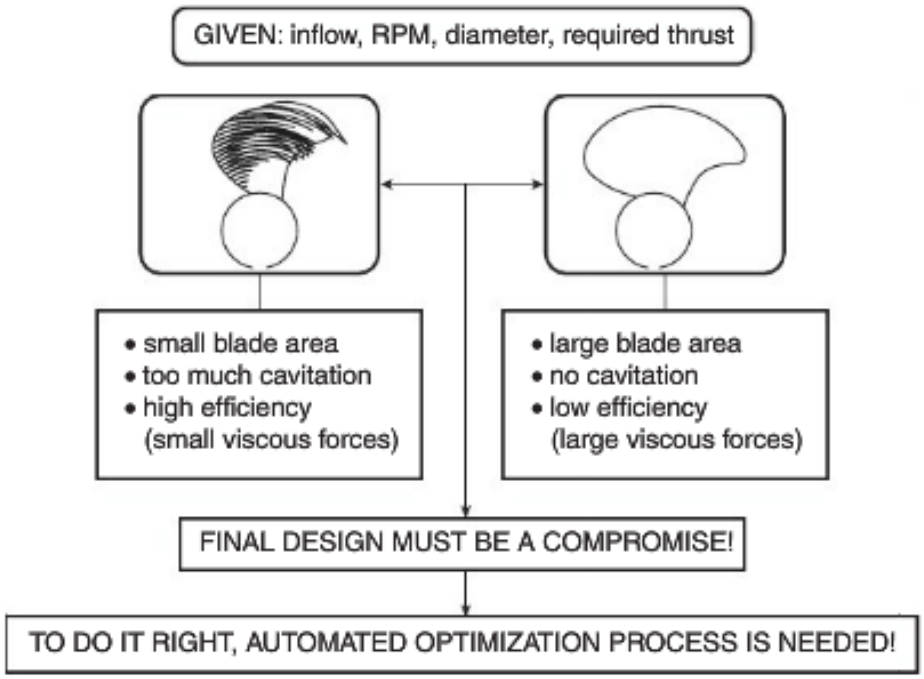

Figure 5.8: Trade-offs in propulsor design (Kerwin and Hadler (2010))

noise regarding ship could be boundary layer noise, machinery noise or electrical noise.

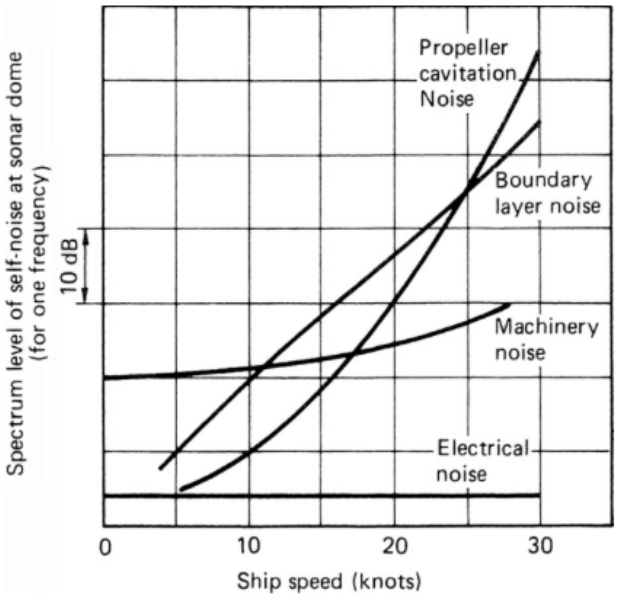

Figure 5.9: Ship noise and velocity (Carlton (2007)).

Propeller noise was until recently a concern only for naval ships and research vessels. Nowadays it is an increased attention towards environmental issues, which is leading to consider propeller noise also for merchant ship applications.

Reliable noise measurements are difficult to obtain from model scale tests. For example the wake field and the water quality effects the measurements. In addition to those effects, noise measurements are often spoilt by facility background noise. Noise generated by boundary layers can develop a wall on the hydrophone itself, which will reduce the signal for the hydrophone.

Propeller noise can be divided in hydrodynamic noise and cavitation related noise. Hydrodynamic noise occurs in both cavitating and non-cavitating condition.

It is common to present the noise in frequency spectra. The spectra of a cavitating propeller shows different features:

- Pure tones, discrete spectrum.

- Broadband signal, continous spectrum.

Figure 5.10 shows how different types of cavitation affect the spectra.

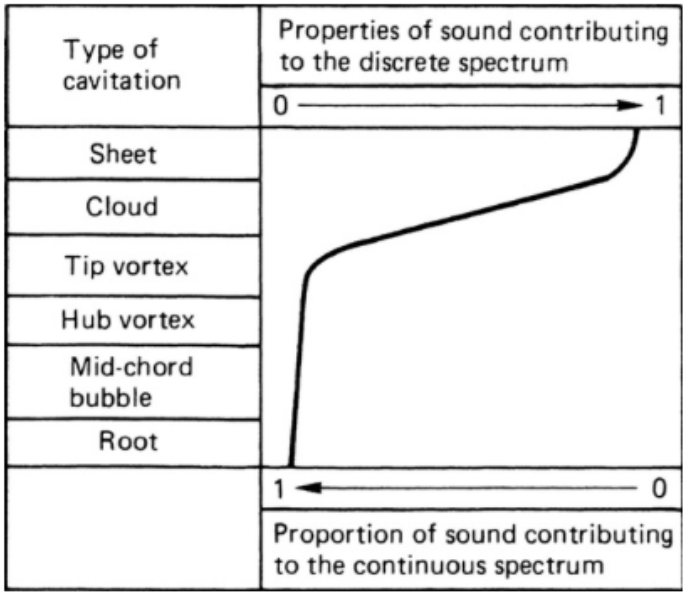

Figure 5.10: Impact of different cavitation phenomena on noise spectrum (Carlton (2007)).

It has to be known that the duct made by the 3D-printer is made of another material that the reference duct 19A. It is possible that the material used by the printer slightly works as a blockage of the noise to the hydrophone.

5.3.5 Calibration of equipment

As preparation for the cavitation test, the equipment needs to be calibrated to obtain reliable results. ITTC has made a document with recommended procedures and guidelines (ITTC (2011)) for a cavitation test.

Calibration of equipment is done to get a link between the measured signal and the correct physical value. This is done by applying different known loads, covering the expected range of measured values.

Vibrations of the model propeller shaft may have an influence on the steadiness of the cavitation on blades and the level of the pressure fluctuations. Attention should be paid to the level of vibration at each test condition.

5.3.6 Water quality

Water quality refers to the number and the size of cavitation nuclei (Savio (2011)). Nuclei change the water utensil strength which affect the inception cavitation number. If the nuclei number is too low, it will underestimate the real inception cavitation number and cavities behavior. A too high cavitation number will make it difficult to classify the different phenomena, due to reduced visibility inside the test section.

5.4 Test procedure

Calibration of equipment was done prior start of the test. This was done by Terje Rosten, who is engineer at the cavitation tunnel. The water temperature in the tunnel was measured, as well as the level of oxygen. Those measurements was done every morning before testing. See Table 5.4

Amount of gas in water	23-25	%
Water temperatur	18-19	C°

Table 5.4: Properties of the water.

To be able to discover cavitation on the propeller blades, is it used stroboscopic lights. The strobe lights works with the same frequency as the propeller, so it looks like the propeller doesn't rotate.

The test can be divided in four parts:

- Open water test
- Cavitation bucket
- Pictures

- Noise measurements

The same four measurements was done for each of the three ducted propellers.

The first test was an open water test. The open water test was done for J_A-values from 0.2 to 1.2, with an interval of 0.2. The same number of revolutions was used for all ducted propellers during the open water test; 15 rps. The open water test are made to check if the propeller requirements are fulfilled (Steen and Minsaas (2013)). The results of the test are presented dimensionless in an open water diagram as thrust coefficient K_T, torque coefficient K_Q, propeller efficiency η_0 and advance ratio J_A. The open water tests are done in non-cavitating conditions.

$$J_A = \frac{V_A}{nD} \tag{5.1}$$

$$K_T = \frac{T}{\rho \cdot n^2 \cdot D^4} \tag{5.2}$$

$$K_Q = \frac{Q}{\rho \cdot n^2 \cdot D^5} \tag{5.3}$$

$$\eta_0 = \frac{K_t \cdot J}{2\pi \cdot K_Q} \tag{5.4}$$

After finishing the open water test, the cavitation bucket was made. When making the cavitation bucket, observation of cavitation pattern is the most important task.

For making the cavitation bucket six K_T-values was picked. See Table 5.5. For each of the K_T-values I started measuring from atmospheric pressure and reduced the tunnel pressure until cavitation inception or a new type of cavitation occurred. Each type of cavitation was plotted, where it was focused on the types of cavitation that affects measurable properties, like thrust and noise.

The cavitation number is given as:

$$\sigma = \frac{P_0 - P_v + \gamma(h - 0.8R)}{\rho/2 \cdot (n \cdot D)^2} \tag{5.5}$$

n [rps]	Kt [-]
15	0.42
15	0.30
15	0.24
15	0.18
15	0.14
15	0.10

Table 5.5: Kt-values tested for cavitation bucket.

where:

P_0 = atmospheric pressure

P_v = vapor pressure of water

γ = specific gravity of water

h = immersion of propeller shaft

ρ = mass density of water

n = rate of revolutions

D = propeller diameter

Noise measurements and pictures were taken for each condition at three different blade positions. Also, the pictures are taken from both blade suction and pressure side of the ducted propellers.

Chapter 6

Error sources

In all kinds of physical experiments there is inherent uncertainty in all measured data. A test result is one example of the range of possible outcomes of the experiment. By repeating the experiment, it is unlikely that exactly the same result is obtained. To know how far the measured value could be from the true value, one has to perform uncertainty analysis.

In this analysis two types of errors are considered, precision and bias errors. Precision errors are "scatter" in the results, and are found by comparing the results of repeated tests. Bias errors are systematic errors, and are not revealed by repetition of tests.

The main results in this thesis are based on relative differences between the customized ducts and the reference duct. Therefore keeping the test conditions as equal as possible for the compared runs was of high priority. Variables such as oxygen level and water temperature was measured before every run.

6.1 Precision error

6.1.1 Precision error - cavitation test

The method used for calculation of precision limit is based on a method presented by Steen (2014) and Ersdal (2004).

Due to limited amount of time are four repeated tests done for one condition, and assumed that the precision limit found is representative for other conditions. The repeated tests are measured at $J = 0.95$, $K_{t,total} = 0.24$. The plots are presented in Figure 6.1. All other data are measured two times and presented as the mean value of those two measurements.

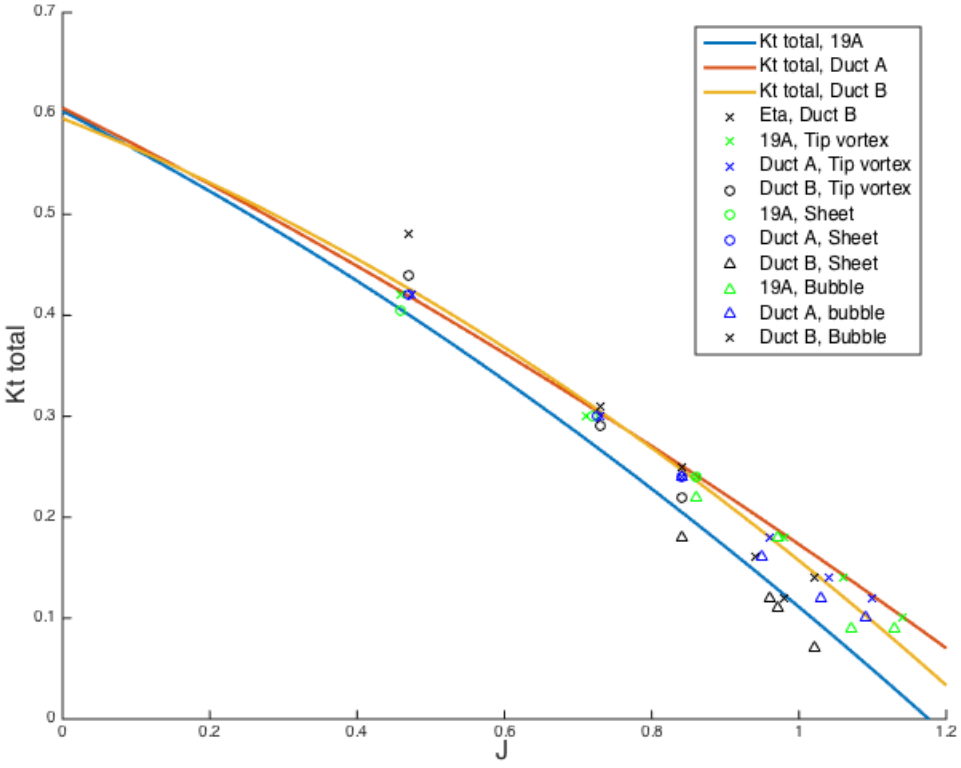

Figure 6.1: Plots of cavitation inception together with total thrust from open water test.

The standard deviation is given of the measured total thrust coefficient for the five tests is:

$$S_X = \sqrt{\frac{1}{N-1}\sum_{j=1}^{N}(X_j - \bar{X})^2} = 0.00077 \tag{6.1}$$

The precision limit is given as:

$$P_X = S_X \cdot t_4 = 0.00077 \cdot 3 = 0.00230 \tag{6.2}$$

where t is given in Figure 6.2, and is the weight for estimating confidence intervals. I have used the 95% confidence interval.

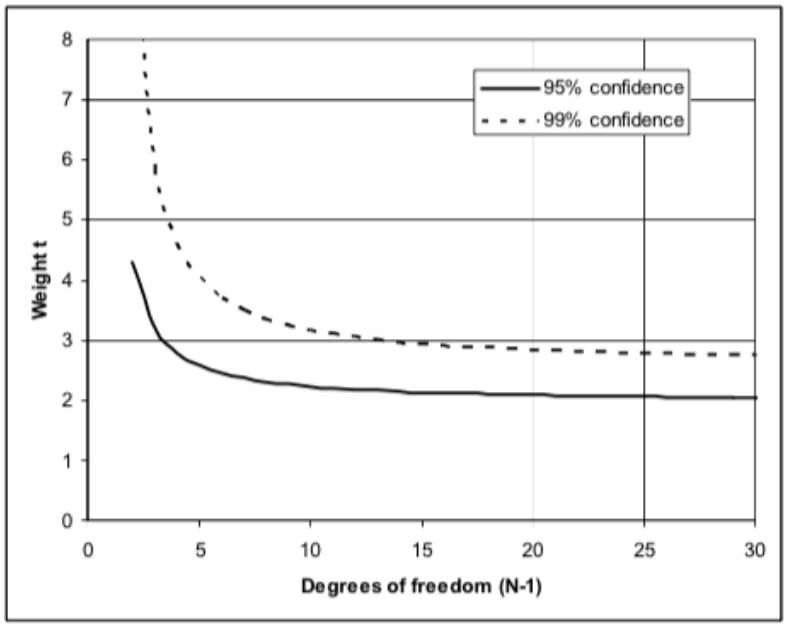

Figure 6.2: The weight t for estimating confidence intervals.

The average thrust coefficient for the four tests is 0.2399. The uncertainty of the measurements (of a single test) is then:

$$\frac{0.00230}{0.2399} = 0.0096 = 0.96\% \tag{6.3}$$

The standard deviation of the means of the four tests is $\frac{0.00077}{\sqrt{4}} = 0.00038$

This gives a precision limit for the mean:

$$P_{\bar{X}} = S_{\bar{X}} \cdot t_4 = 0.00038 \cdot 3 = 0.00115 \tag{6.4}$$

Which gives an uncertainty of:

$$\frac{0.00096}{0.2399} = 0.00399 = 0.399\% \tag{6.5}$$

From the results, the uncertainty is 0.40%.

The calculations are summarized in Table 6.1.

	n
	0.2395
	0.2403
	0.2408
	0.2391
Avg	0.2399
s^2	0.000768
Sx	0.000384
P(M)	0.00230
%	0.9590
P(S)	0.00115
%	0.480

Table 6.1: Calculation of precision error.

Table 6.1 shows that the measured quantities have reasonable accuracy for single runs. The accuracy is higher for multiple runs. This can be explained by the fact that higher values with difference of around the same order give a lower relative uncertainty.

6.1.2 Criterion for rejecting outliers

Data samples that deviates significantly from the majority are called wild points or outliers. If no physical explanation is found, the point might be disregarded.

Samples with higher deviation from the mean than the following criterion may be disregarded, following Chauvenet's criterion:

$$|X_j - \bar{X}| > t_{chauvenet} \cdot S_x \tag{6.6}$$

$t_{chauvenet}$ is found by using Figure 6.3.

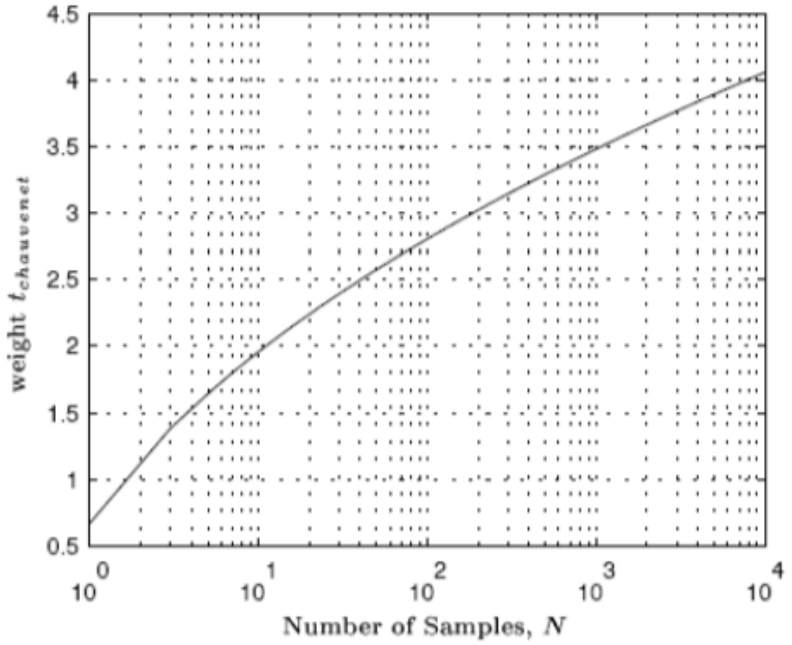

Figure 6.3: The weight t in Chauvenet's criterion for rejection of wild points.

$$t_{chauvenet} \cdot S_x = 0.001228 \tag{6.7}$$

One of two measurements done at J=0.45 deviates significantly from the expected value. See Figure 6.4. This data sample will according to Chau-

venet's criterion, be rejected. For this condition exists it still one data sample. This sample is not rejected by the criterion, and are used as a single value. From now on, Figure 6.5 will be considered as the result. In this figure is the wild point at J=0.45 rejected.

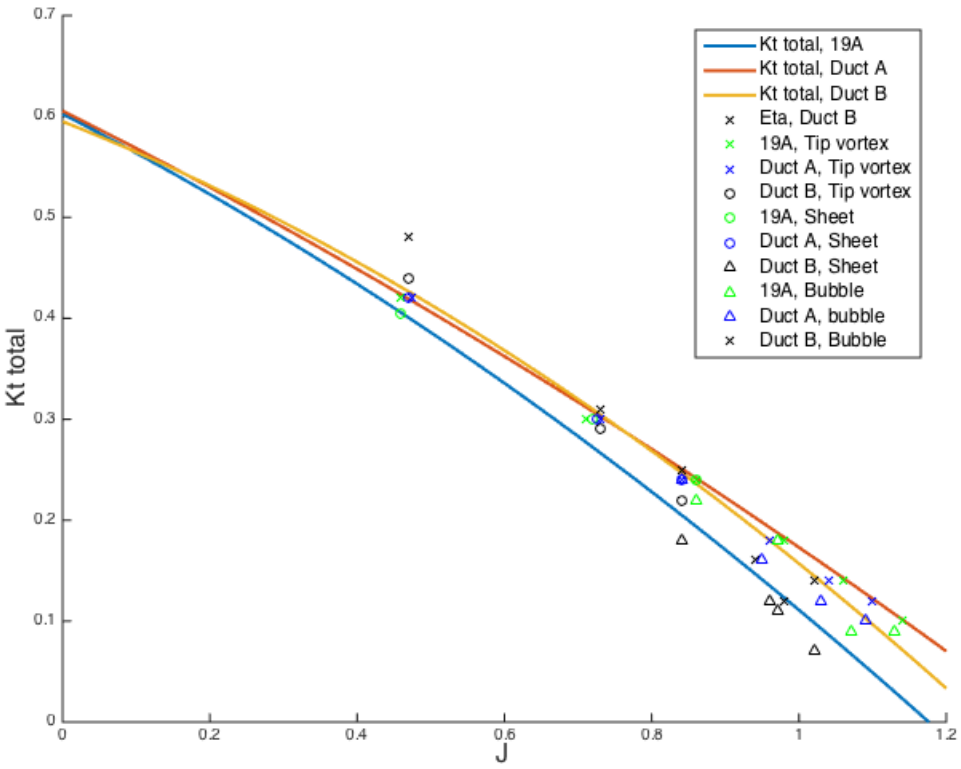

Figure 6.4: Single plot rejected due to Chauvenet's criterion.

6.1.3 Errors - open water diagram

The open water test was done two times for each ducted propeller. The tests was done with a break between the runs. During the break, the engine was shut down and the water was removed from the test section. This was done due to the level of replication, which indicates how large

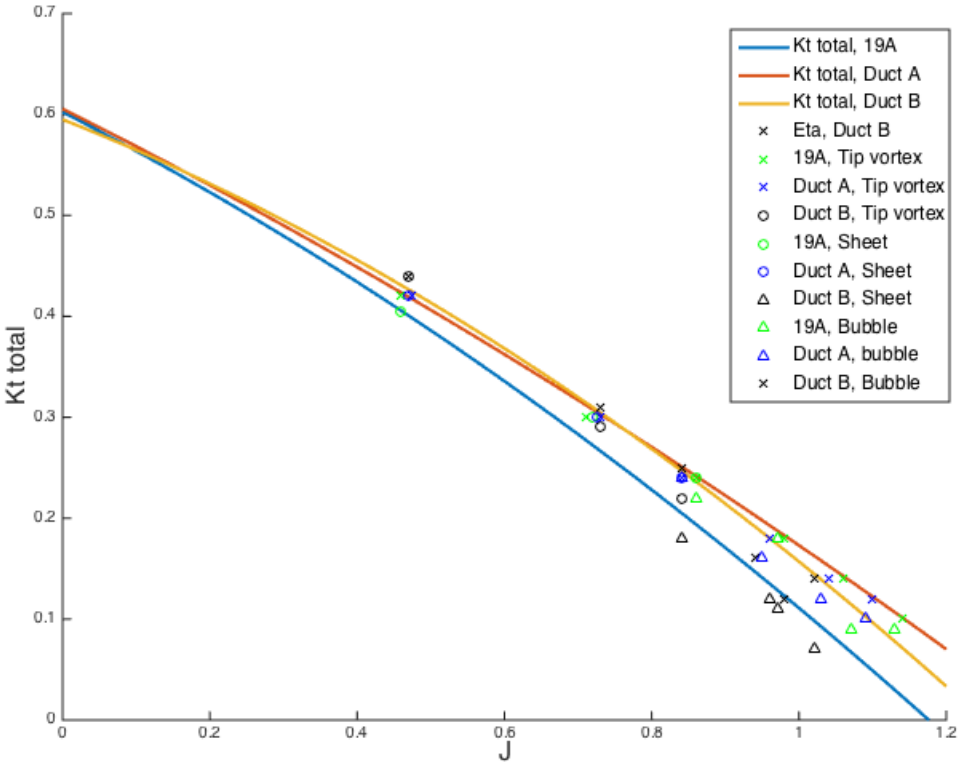

Figure 6.5: Single plot rejected due to Chauvenet's criterion.

part of the set-up that is held the same. Also, for practical reasons is it a compromise between efficiency and accuracy.

The open water tests are plotted as polynomial functions and from single data measurements. Both plots are pictured in Figure 6.6. For presentation and discussion of results will it be used the plots made by polynomials in the thesis. I conclude that the plots made by polynomial fitting is more accurate. When using this method the mean values from continuous measurements are presented, and the uncertainty is reduced.

The open water diagrams are compared, and presented together in Figure 6.7. When presenting results and for calculations is the mean value from the open water tests used.

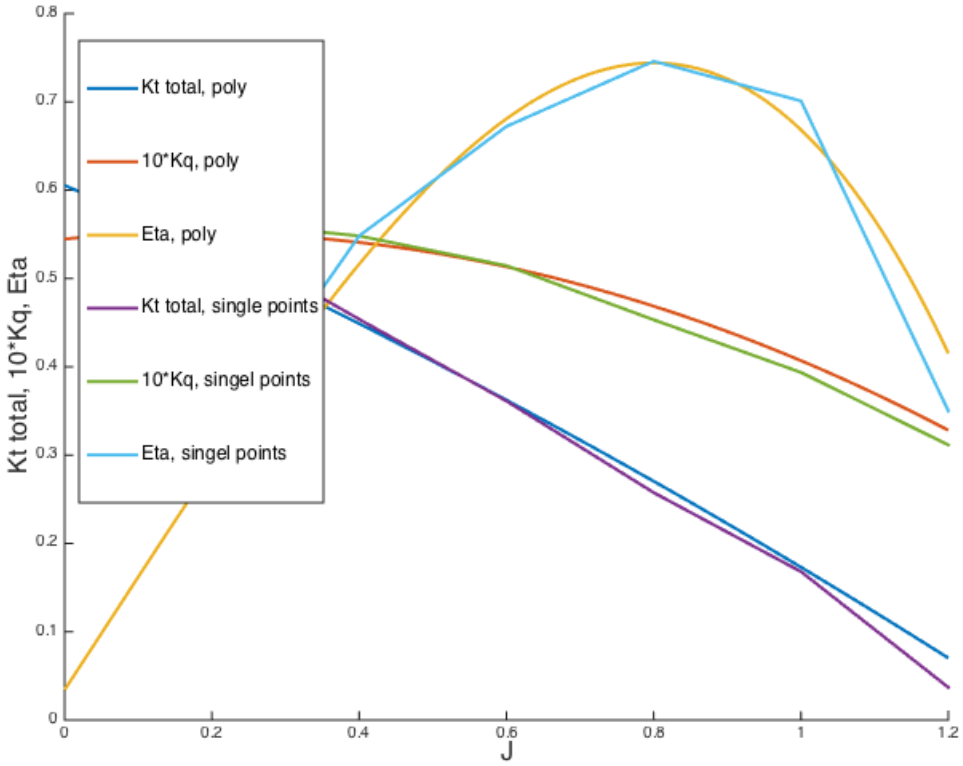

Figure 6.6: Plots of open water test for Duct B. Made by polynomials and single data measurements.

6.2 Bias error

In the following discussion is it tried to quantify the most probable bias error sources, which affects the results during the cavitation test.

Calibration is an important source of bias error. Bias error of the calibration can be hard to determine, thus good calibration routines will minimize the error. For this experiment has Terje Rosten, who is a engineer at the cavitation tunnel, done the calibration. That ensures that the calibration is done in best possible way.

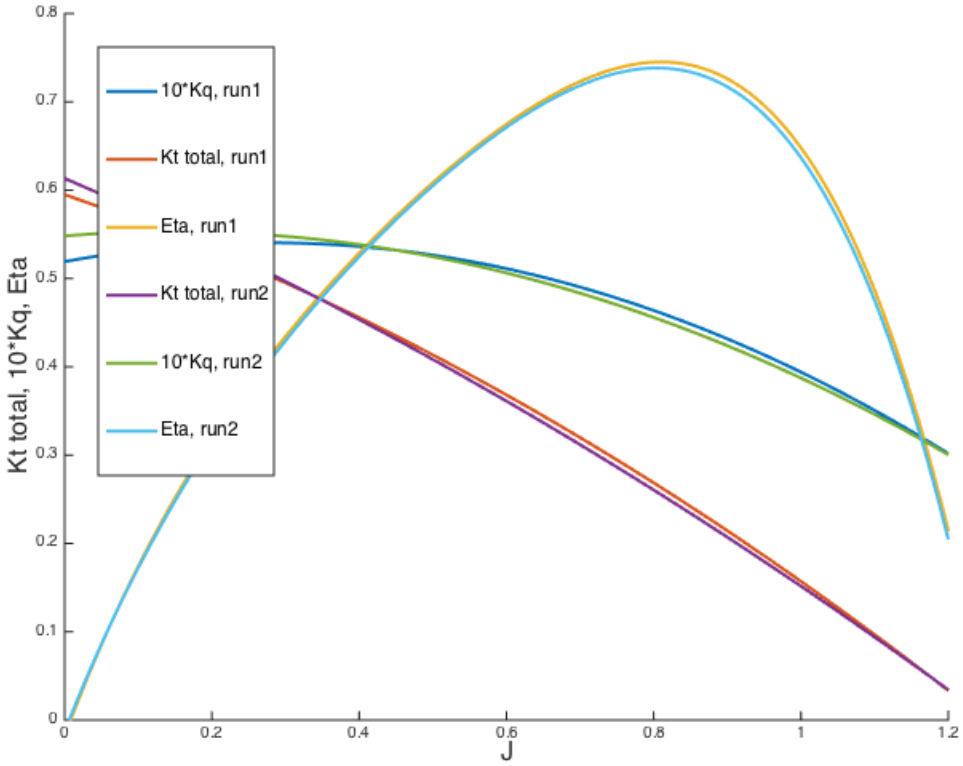

Figure 6.7: Plots of two open water tests, done for Duct B.

Bias errors - cavitation bucket

For designing cavitation buckets, we reduced the pressure in the tunnel. From atmospheric pressure until the the vacuum pump reach its maximum value. The vacuum pump is controlled from the control room. The one observing cavitation inception is studying outside at the working section at the tunnel. When reducing the pressure in the tunnel, the one controlling the pump needs to maintain the pressure by always follow the pressure, because of a leakage.

This means that during a measurement the pressure will rise against atmospheric pressure. As pictured in Figure 6.8 we see how the pressure increases during the measurement. Because of this it can be difficult to

exactly determine when cavitation inception occurs.

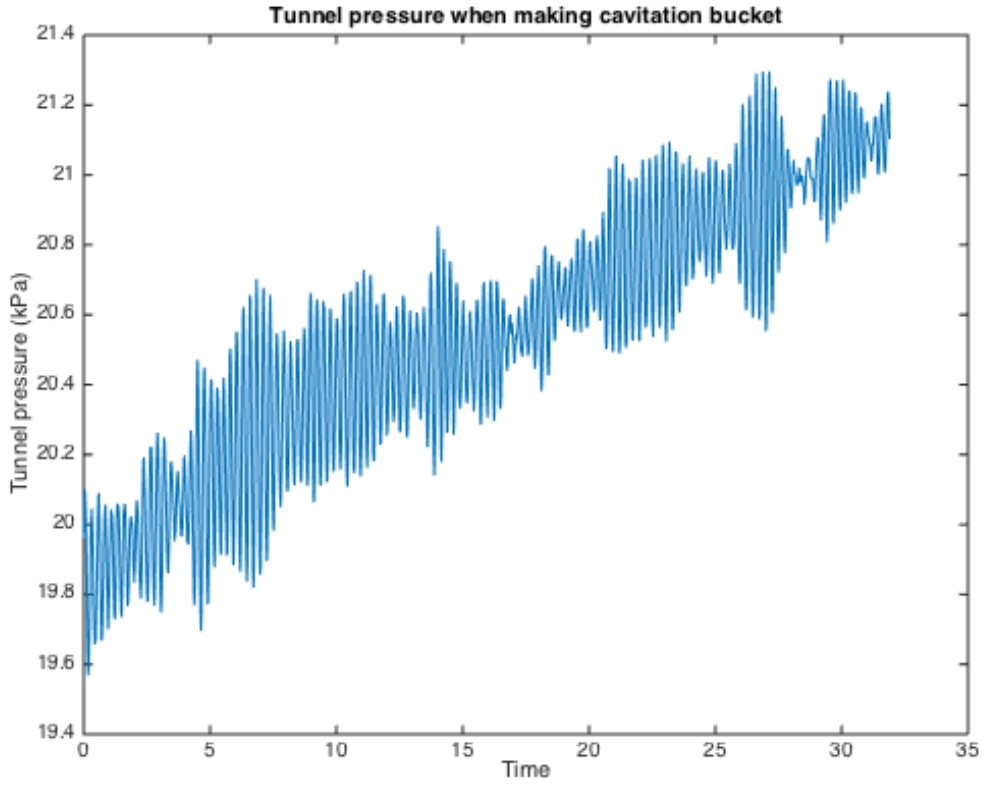

Figure 6.8: Plot showing the variation in the tunnel pressure when measuring a cavitating condition.

The tunnel has some problems with corrosion at the inner walls. Several times during the measurements particles have sticked to the propeller, as shown in Figure 6.9. This particle is not very important, but it could make it more difficult to categorize correct cavitation phenomenon.

Errors regarding electronically smoothing of duct

One of the problems is the smoothing techniques used on the duct. To let the propeller work with constant gap between the propeller tip and duct, is it a horizontal area inside the duct. During smoothing of the duct,

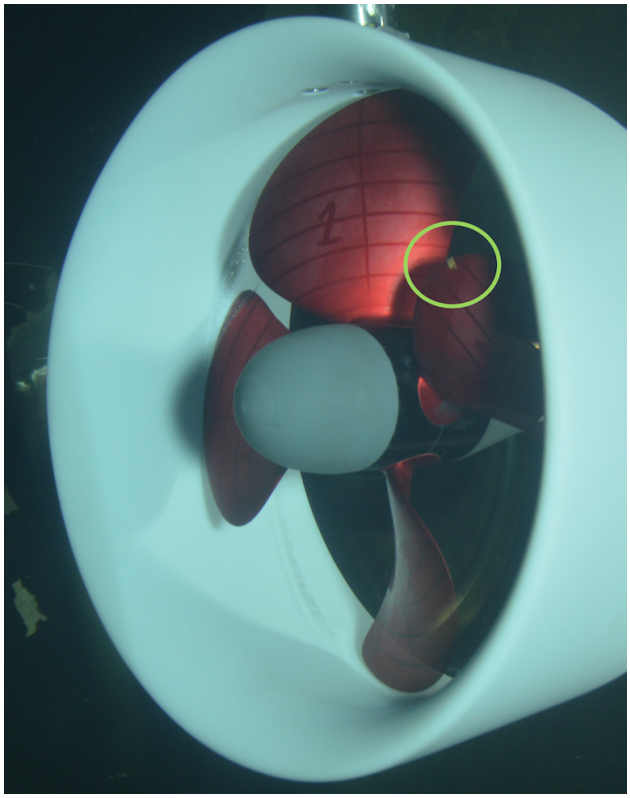

Figure 6.9: Particle from the tunnel placed on the propeller

this horizontal area differ from an exact circle. The result is at 45 degrees from the top position, 1/3 of the gap is lost. This could cause pressure differences which again cause different cavitation pattern, varying with propeller blade position. As seen in Figure 6.10 and 6.11, the cavitation pattern (sheet cavitation) is stronger at the 45 degrees position than at 0 degrees. The reference point, 0 degree, is decided to be when blade 1 is positioned at top (see Figure 6.11).

The pictures in figure 6.10 and 6.11 are taken during the conditions presented in Table 6.2

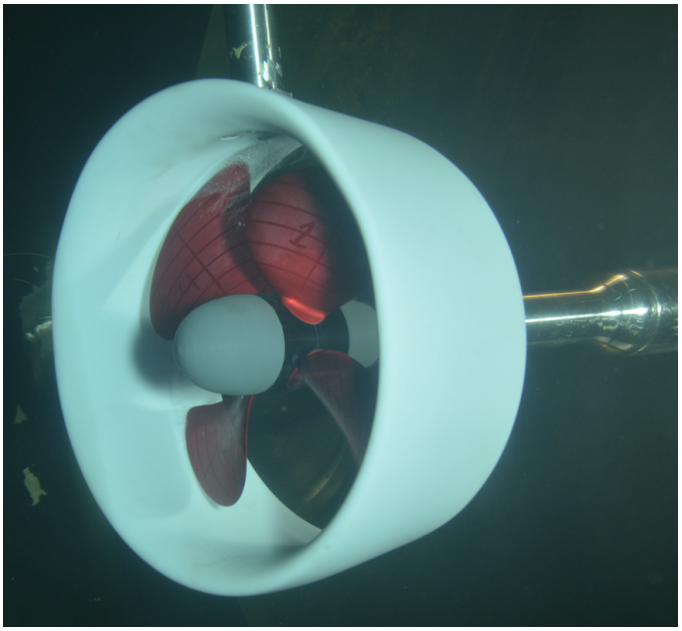

Figure 6.10: Picture showing diverging cavitation pattern on similar ducted propeller at 45 degree.

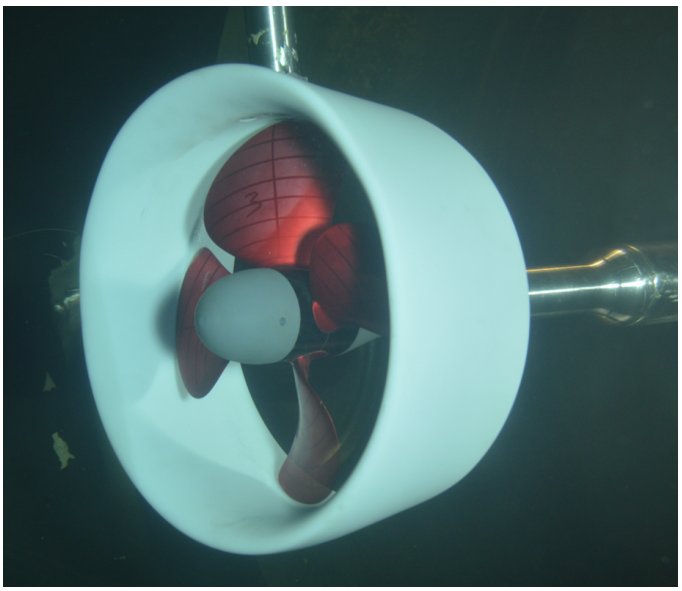

Figure 6.11: Picture showing diverging cavitation pattern on similar ducted propeller at 0 degree.

	n [Hz]	Kt total [-]	Cavitation number [-]
Figure 6.10 on the previous page	18	0.24	2.05
Figure 6.11 on the preceding page	18	0.24	2.05

Table 6.2: Condition where cavitation occur differently with propeller blade position.

Part III

Results and conclusions

Chapter 7

Results

7.1 Open water test

The open water diagrams for the three ducted propellers are presented in Figure 7.1.

From Figure 7.1 is it clear that the efficiency is higher for both non-axisymmetric ducts compared to the 19A duct. The total thrust is lower for the 19A duct. The torque coefficient for Duct A is slightly higher when $J > 0.5$.

7.2 Cavitation buckets

From the figures 7.2, 7.3 and 7.4 one understand that sheet cavitation affects the propulsion properties roughly similar.

Figure 7.5 on page 73 shows that bubble cavitation occur at a higher cavitation number for the 19A than for Duct A and B.

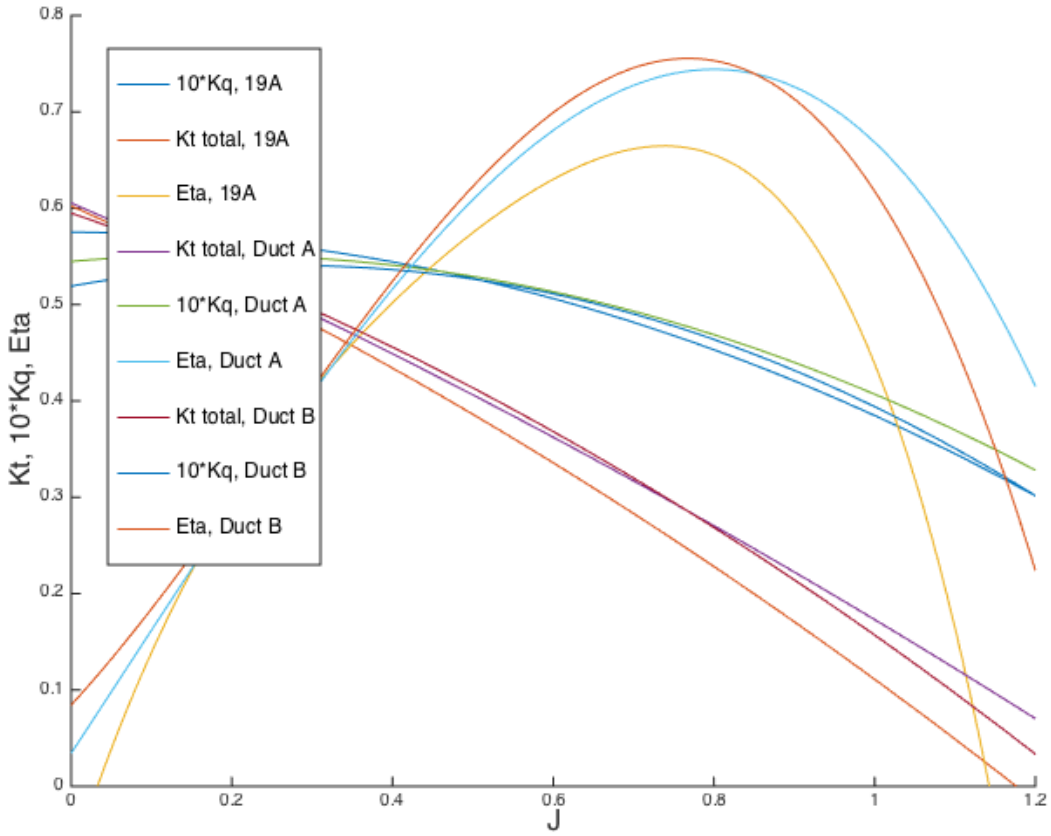

Figure 7.1: Open water diagram for the three ducts.

7.3 Total thrust affected by cavitation

Figure 7.6 shows the total thrust from the open water test together with the cavitation inception plots.

One understand that bubble cavitation reduces the total thrust coefficient, because the triangle (which represents bubble cavitation) always are below the open water line for total thrust.

At advantage number $J = 0.8$ and $J = 1.0$, the reduction in total thrust due to bubble cavitation is given in Table 7.1.

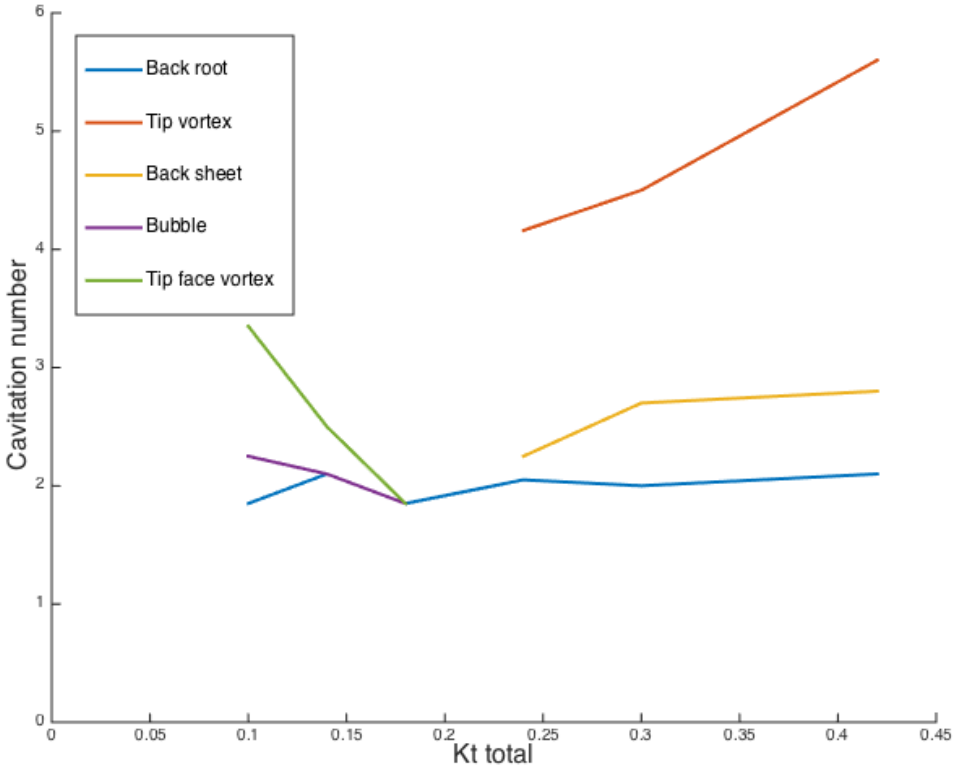

Figure 7.2: Cavitation bucket for the 19A duct.

From Table 7.1 one understand that 19A has a larger reduction in total thrust at a similar advantage number, due to bubble cavitation. It is used linear regression to obtain a comparable J-value for each ducted propeller. The values are compared as single points, thus the uncertainty has to be kept in mind.

Figure 7.6 tells that tip vortex cavitation not affects the total thrust coefficient, as expected due to background theory,

These results (inception of cavitation, plotted for J and $K_{t,total}$) are also available in Table 7.2. In this table the values for $K_{t,total}$ are adjusted so they have similar advance value. This is done to easily be able to compare the results. It is used linear adjustment because the thrust coefficient is

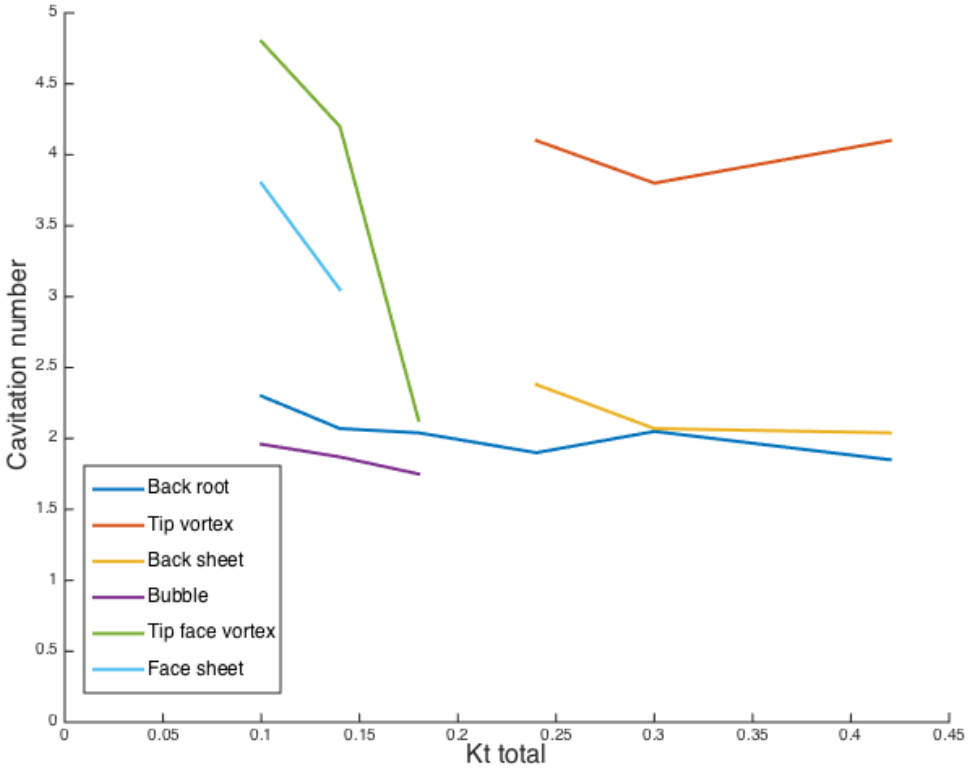

Figure 7.3: Cavitation bucket for duct A.

assumed linear. In Figure 7.6 are the adjustments not done to retain the accuracy.

7.4 Observations from pictures

Pictures of the ducted propellers affected of different cavitation phenomena are presented in Appendix B. From the figures 7.2, 7.3, 7.4 and 7.6 is it possible to identify the inception of different cavitation phenomena.

As explained above, bubble cavitation affects the total thrust. Pictures of the propeller ducts affected by bubble cavitation is presented in Figure 7.7, 7.8 and 7.9. Table 7.1 presents the loss of total thrust.

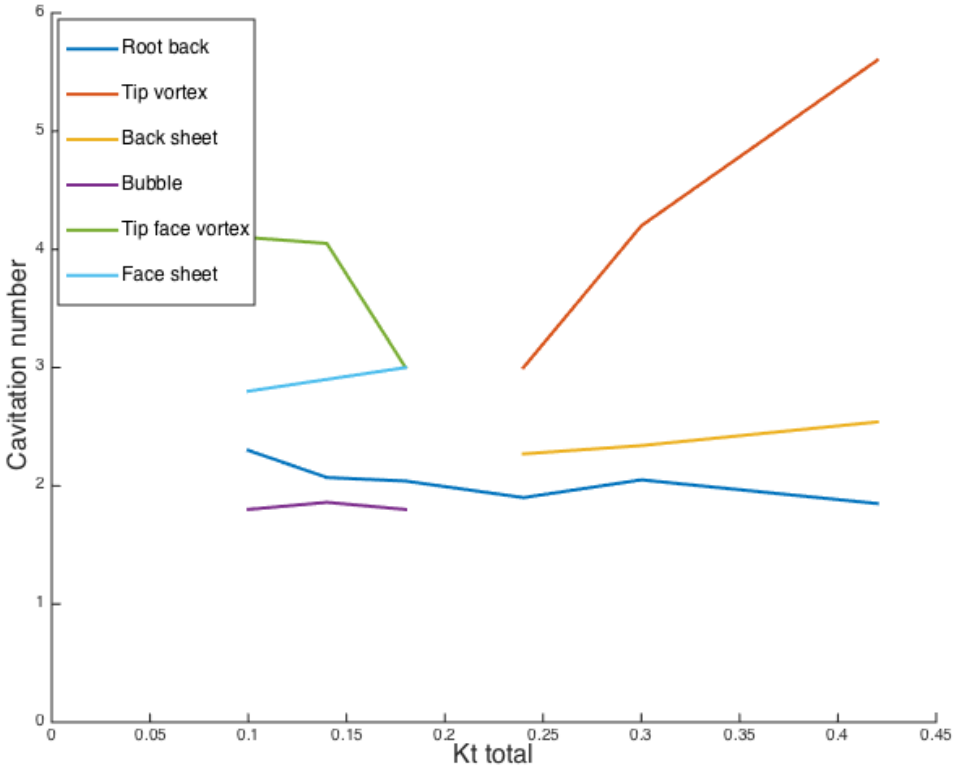

Figure 7.4: Cavitation bucket for duct B.

The picture in Figure 7.10 shows duct cavitation on the 19A duct, especially to the left on the duct. Condition where duct cavitation occurred is presented in Table 7.3.

7.5 Noise measurments

Figure 7.11, 7.12 and 7.13 presents noise measurements as spectra. The measurements are done at similar condition for the three ducts. Sheet cavitation affects the ducted propellers at this condition. The condition is presented in Table 7.4 on page 77. Sheet cavitation is a type of cavitation that generates noise, and is why this condition in presented. The signal is

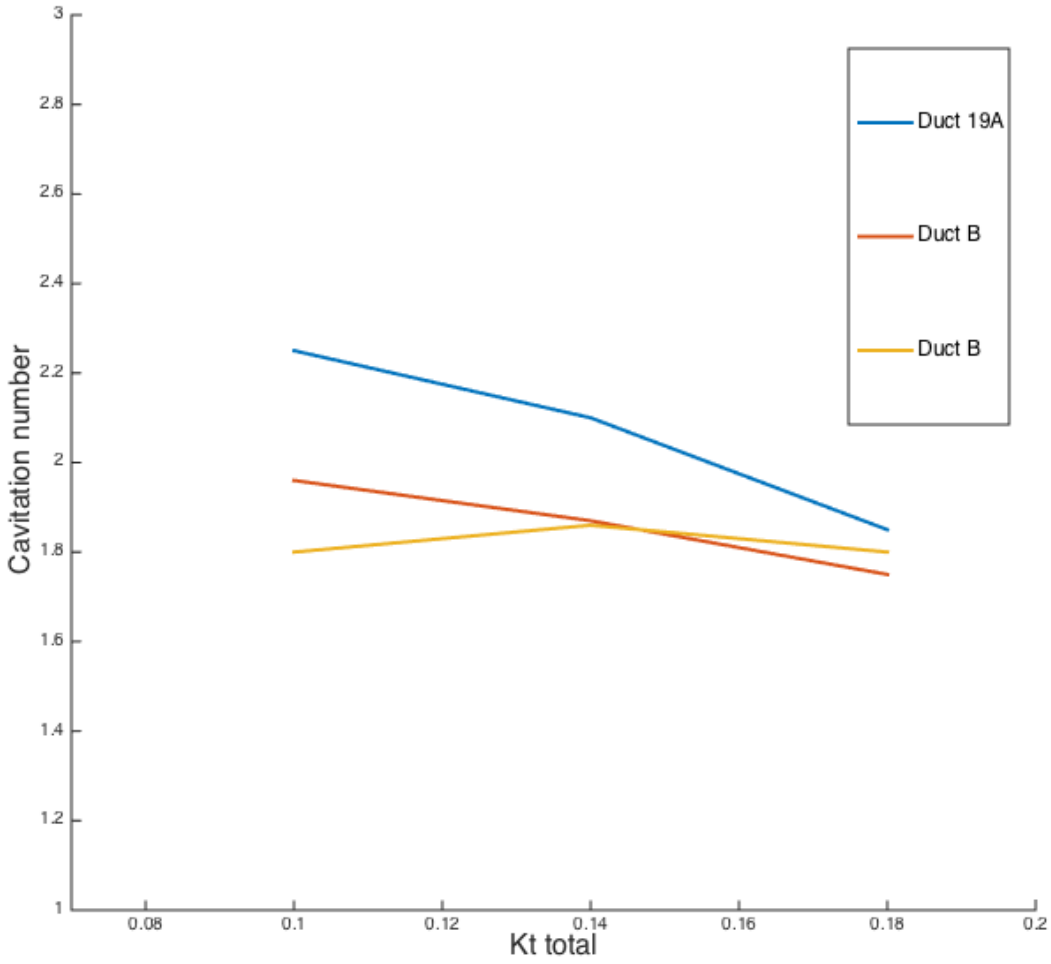

Figure 7.5: Cavitation bucket for bubble cavitation.

presented in Volts.

From the spectra is it difficult to tell if one duct is better than another. One can conclude that all ducts generates noise according to sheet cavitation relative to first blade harmonic. The strength of the signal is roughly of the same size, but the tendency is that Duct B generates slightly less noise than Duct A and the reference duct.

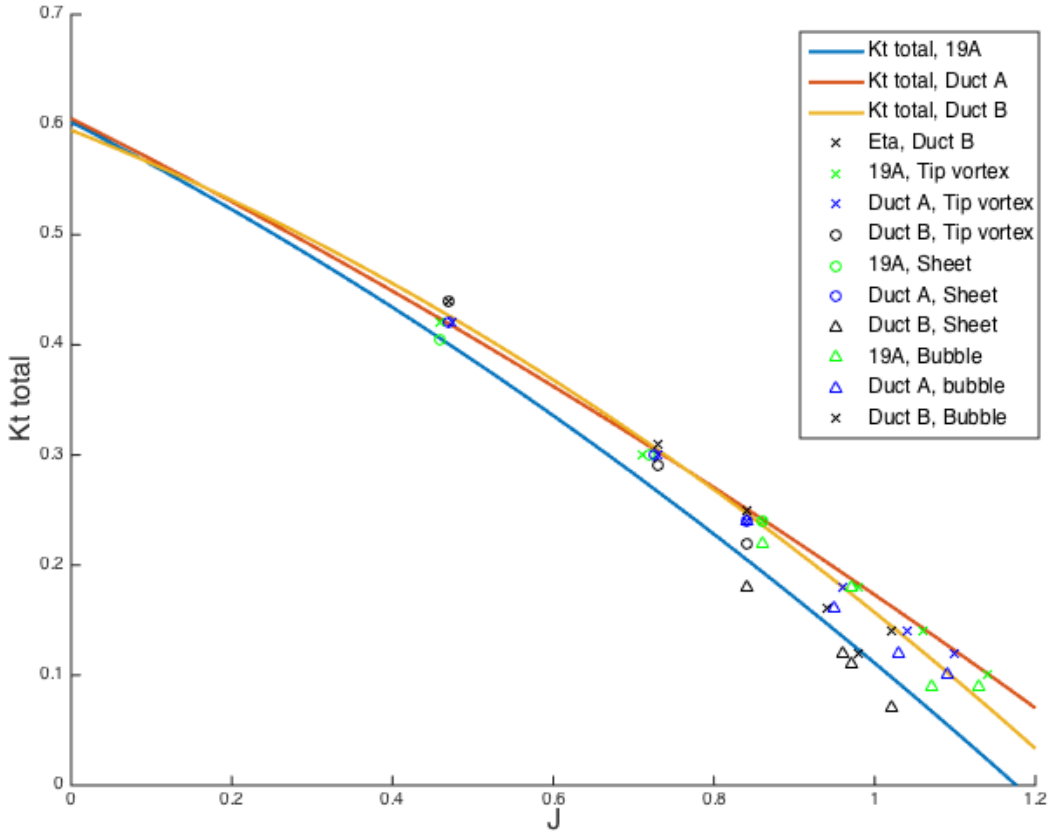

Figure 7.6: Total thrust from open water test together with cavitation inception.

Reduction in total thrust	J=0.8	J=1.0
19A	15 %	16%
Duct A	12%	15%
Duct B	11%	12%

Table 7.1: Presenting the loss in total thrust due to bubble cavitation.

	Tip vortex cavitation		Back sheet cavitation		Bubble cavitation	
	J	**Kt total**	**J**	**Kt total**		
19A	0,47	0,47	0,47	0,44		
Duct A	0,47	0,45	0,47	0,40		
Duct B	0,47	0,48	0,47	0,42		
	J	**Kt total**	**J**	**Kt total**		
19A	0,73	0,32	0,73	0,31		
Duct A	0,73	0,30	0,73	0,29		
Duct B	0,73	0,30	0,73	0,30		
	J	**Kt total**	**J**	**Kt total**	**J**	**Kt total**
19A	0,84	0,26	0,84	0,25	0,84	0,25
Duct A	0,84	0,26	0,84	0,25	0,84	0,24
Duct B	0,84	0,24	0,84	0,24	0,84	0,24
	J	**Kt total**			**J**	**Kt total**
19A	0,94	0,19			0,97	0,15
Duct A	0,94	0,21			0,97	0,18
Duct B	0,94	0,16			0,97	0,14
	J	**Kt total**			**J**	**Kt total**
19A	0,98	0,16			0,98	0,13
Duct A	0,98	0,21			0,98	0,13
Duct B	0,98	0,19			0,98	0,16
	J	**Kt total**			**J**	**Kt total**
19A	1,02	0,14			1,02	0,13
Duct A	1,02	0,2			1,02	0,17
Duct B	1,02	0,19			1,02	0,16

Table 7.2: Table presenting Kt total versus J.

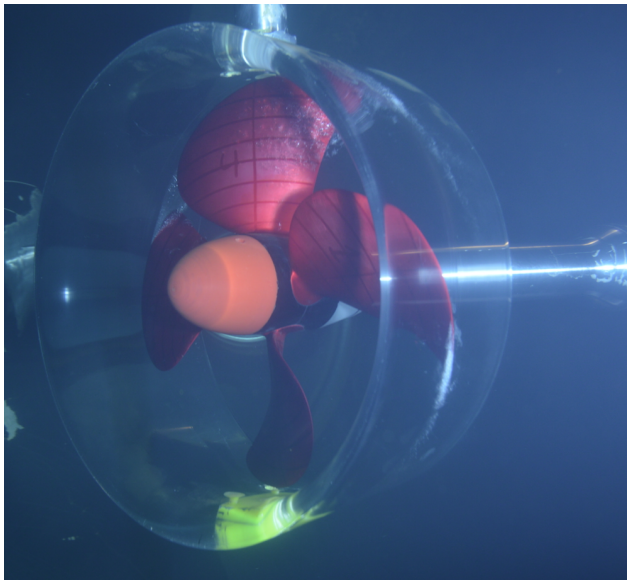

Figure 7.7: Picture of bubble cavitation on the 19A duct.

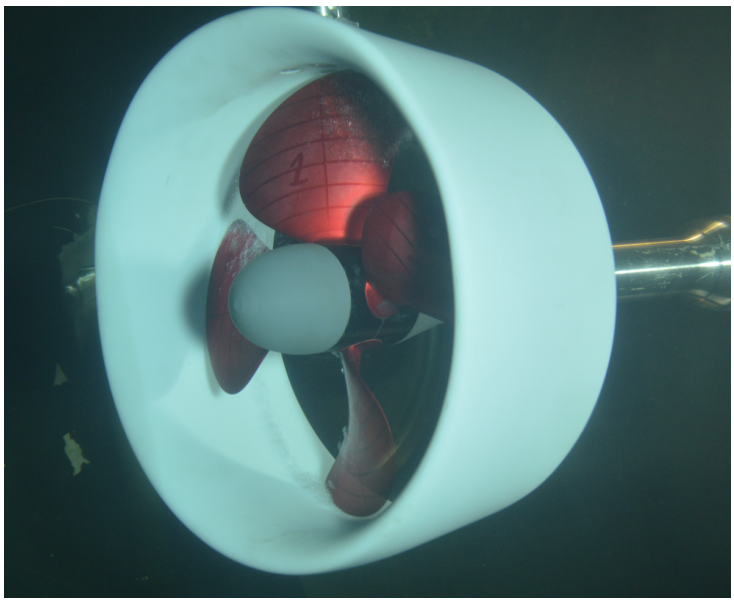

Figure 7.8: Picture of bubble cavitation on Duct A.

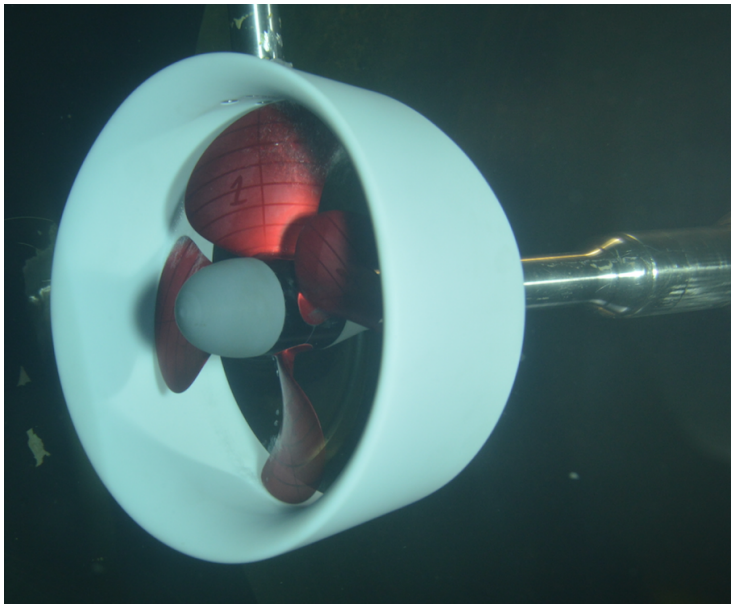

Figure 7.9: Picture of bubble cavitation on Duct B

	Cavitation number [-]	n [Hz]	Kt total [-]	Duct cavitation
Duct 19A	1.2	18	0.24	Yes
Duct A	1.2	18	0.24	No
Duct B	1.2	18	0.24	No

Table 7.3: Presentation of inception of duct cavitation.

Condition:	Rps [Hz]	Kt total [-]	Cavitation number
Transit	15	0.42	2.1

Table 7.4: Condition presented for comparing noise measurements.

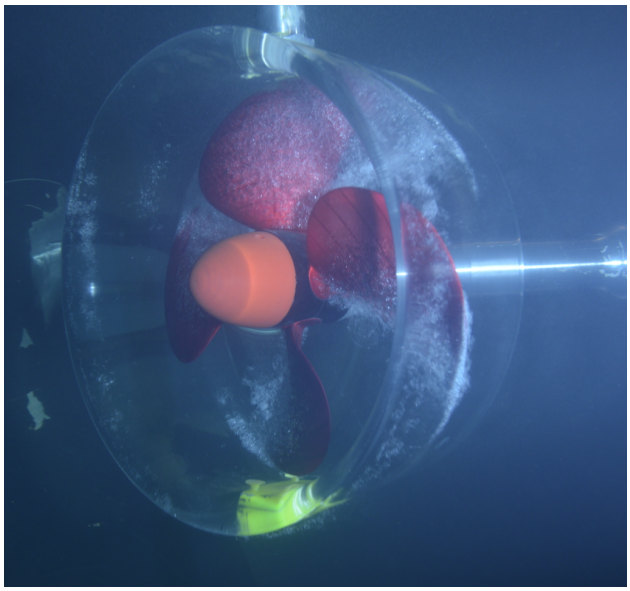

Figure 7.10: Picture of duct cavitation on the 19A duct.

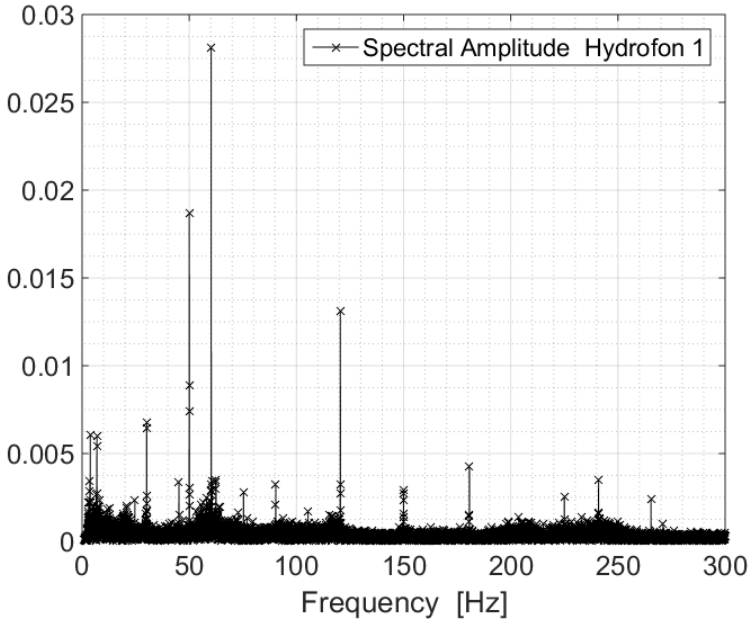

Figure 7.11: Noise measurement for the 19A duct.

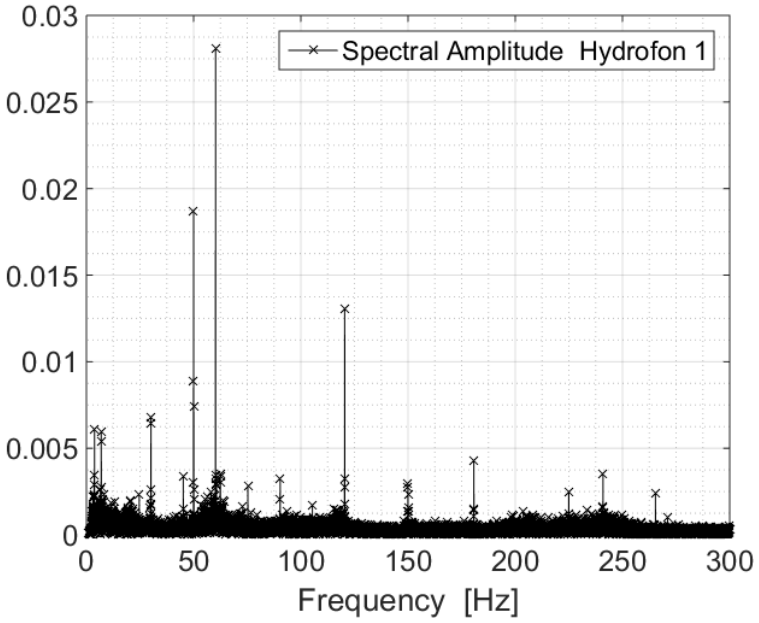

Figure 7.12: Noise measurement for Duct A.

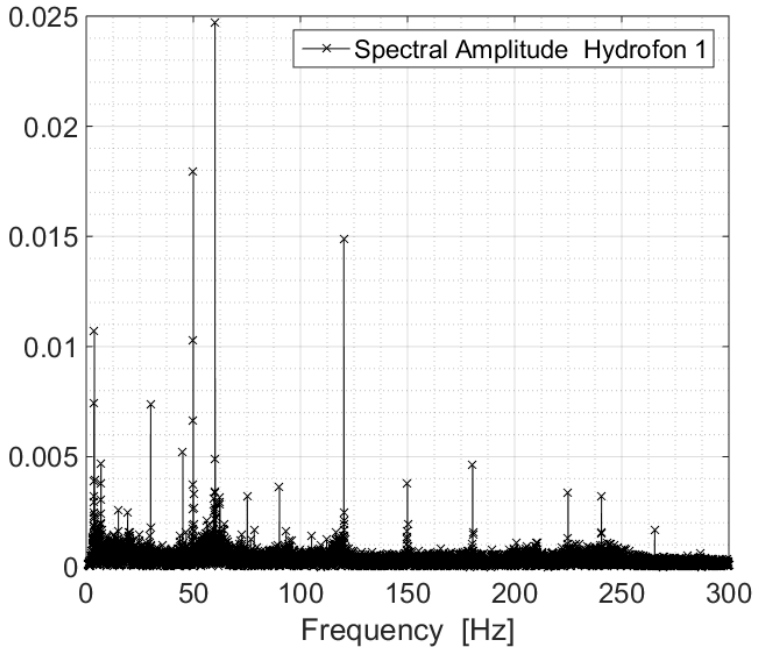

Figure 7.13: Noise measurement for the Duct B.

Chapter 8

Conclusion

In this master thesis, a design procedure for non-axisymmetric ducts is developed. Two ducts (named Duct A and B) have been manufactured and tested in a cavitation tunnel against the axisymmetric reference duct, 19A.

The results from the experiments shows that the non-axisymmetric ducts increase the efficiency and are more resistant to some types of cavitation, compared to the reference duct. How the non-axisymmetric ducts works depends on several aspects, like decision of main goal and design procedure.

The non-axisymmetric ducts designed during this thesis shows increased efficiency compared to the 19A duct. The reason for the increased efficiency is the duct induced velocities, which is maximized at some parts of the duct (depending on the given wake field). The design procedure does not completely aiming for highest possible efficiency, thus further increase in efficiency should be possible. The open water tests show higher thrust coefficient for the non-axisymmetric ducts, and roughly similar torque coefficient.

The cavitation tests, presented as cavitation buckets, shows that bubble cavitation occur at lower cavitation numbers for the non-axisymmetric ducts, especially for Duct B. The effects from sheet cavitation are not sig-

nificant between the asymmetric ducts and the reference duct, regarding thrust loss. The noise measurements show roughly similar results for all three ducts, but the tendency is that Duct A generates slightly more noise.

No differences are found regarding propulsion properties due to tip vortex cavitation. Cavitation number, thrust reduction and noise was studied, but none of them gave clear tendencies.

The cavitation tunnel tests show that duct cavitation is erased on the non-axisymmetric ducts. A probable reason is because of the outside shape of leading edge on the ducts. Sharp edges have consequently been avoided on the outside of leading edge.

Uncertainty analysis has been carried out and shows that scatter in total thrust for cavitation inception probably are the reason for somewhat inaccurate results. The regular open water tests are found to be accurate and reliable.

I mean that the results from the experiments shows high potential regarding efficiency of non-axisymmetric ducts. Also reduction of specific types of cavitation is promising. By further developing and improving the design procedure, one can obtain more uniform flow and more accurate results.

8.1 Recommendation for further work

Optimizing the design

Further developing the design procedure is the most important task for more accurate results. Several simplifications are done to make it possible to design the ducts, during this master thesis.

Accounting for tangential velocities would increase the accuracy of the method. It is possible to divide the ducts into more sections, so the accuracy increases. Transitions between the ducts cross sections are not studied

in detail. It reason to believe that the cross sections interfere and disturb the flow, thus make the flow less homogeneous.

The duct library should expand. At this time the duct profiles induce axial velocity up to $1.34 m/s$. When the library contains more duct cross sections it will also affects the transitions, due to more flexibility. Which again will increase the accuracy in the calculations, because you don't have to configure the duct design for achieving smooth lines.

Horizontal level inside the duct for keeping constant gap between propeller tip and duct

The horizontal level inside the duct is covering $30\% - 70\%$ at the duct length. It affects the efficiency of the duct profile. This effect is accounted for in the AKPA-calculations, but in some cases does it become a sharp edge with the original duct design. The edge can make the water to separate from the duct. Hence, it needs to be removed with help from electronically smoothing, before physically producing the duct. Due to this configuration the duct induced velocities diverge from the pre-calculated induced velocities. Therefore a more sophisticated study on the size and position of this area could increase the accuracy of the method.

Use of CFD

As a part of the scope for this thesis, experimental tests were done in the cavitation tunnel. It is possible that more accurate solutions could be achieved from CFD calculations. When talking about CFD, I mean Computational Fluid Dynamics, i.e. solving viscous fluid flow problems by solving Navier-Stokes equations. By use of CFD one could optimize the duct by visualize the flow into the propeller. With this method one could probably more efficient find how the duct influence the flow into the propeller. It might also be possible to find how the transitions between the duct cross sections affects the flow.

Bibliography

Abbot, J. H. and von Doenhoff, A. E. (1949). *Theory of Wing Sections*. McGraw-Gill N.Y.

Carlton, J. (2007). *Marine Propellers and Propulsion*. Elsevier Ltd., 2nd edition.

Dickmann, H. E. (1940). *Grundlagen zur Theorie ringförmiger Tragflügel (frei umströmte Düsen)*. Ing.-Arch.

Dickmann, H. E. and Weissinger, J. (1955). *Beitrag zur Theorie optimaler Dsenschrauben (Kort-düsen)*. Jahrbuch STG.

Dyne, G. (1967). *A Method for the Design of Ducted Propellers in a Uniform Flow*. The Swedish State Shipbuilding Experimental Tank.

Ersdal, S. (2004). *Lecture Note: Error Analysis of Experiments*. NTNU.

Haavik, A. S. (2014). Design of propeller ducts. Technical report, Norwegian University of Science and Technology.

Horn, F. (1940). *Beitrag zur Theorie ummantelter Schiffsschrauben*. Jahrbuch STG.

Horn, F. and Amtsberg, H. (1950). *Entwurf von Schiffsdüsensystemen (Kort-Düsen)*. Jahrbuch STG.

Hough, G. R. and Ordway, D. E. (1965). *The Generalized Acuator Disk*, volume 2. Developments in Theoretical and Applied Mechanics.

ITTC, editor (2011). *Model - Scale Cavitation Test*.

BIBLIOGRAPHY

Kerwin, J. E. and Hadler, J. B. (2010). *The principles of Naval Architecture Series: Propulsion*. The Society of Naval Architects and Marine Engineers.

Küchemann, D. and Weber, J. (1953). *Aerodynamics of Propulsion*. New York.

Kuiper, G. (1981). *Cavitation Inception on Ship Propeller Models*. NSMB.

Minsaas, K. and Steen, S. (2012). *Foil Theory*. Department of Marine Technology.

Oosterveld, D. I. M. W. C. (1970). *Wake Adapted Propellers*. Netherlands Ship Model Basin Wageningen.

Oosterveld, M. (1965). *Series of Model Tests on Ducted Propellers*. DTMB.

Savio, L. (2011). *Propeller Cavitation*. Department of Marine Technology.

Steen, S. (2013). *Unconventional Propulsion*. Department of Marine Technology.

Steen, S. (2014). *Experimental Methods in Marine Hydrodynamics*. Akademika Forlag.

Steen, S. and Minsaas, K. (2013). *Propeller Theory*. Department of Marine Technology.

Turbal, V. K. (1973). Theoretical solution of the problem on the action of a non-axisymmetric ducted propeller system in a non-uniform flow. In *The Royal Institution of Naval Architects*.

Appendices

Appendix A

The given and measured wake field

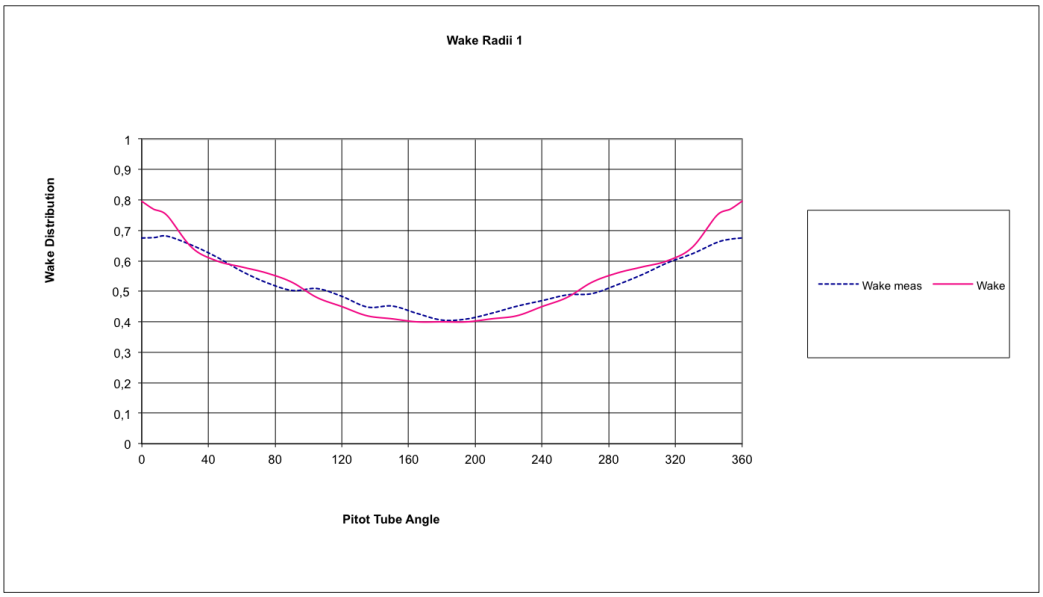

Figure A.1: Difference between the given and the measured wake field, at radii 1.

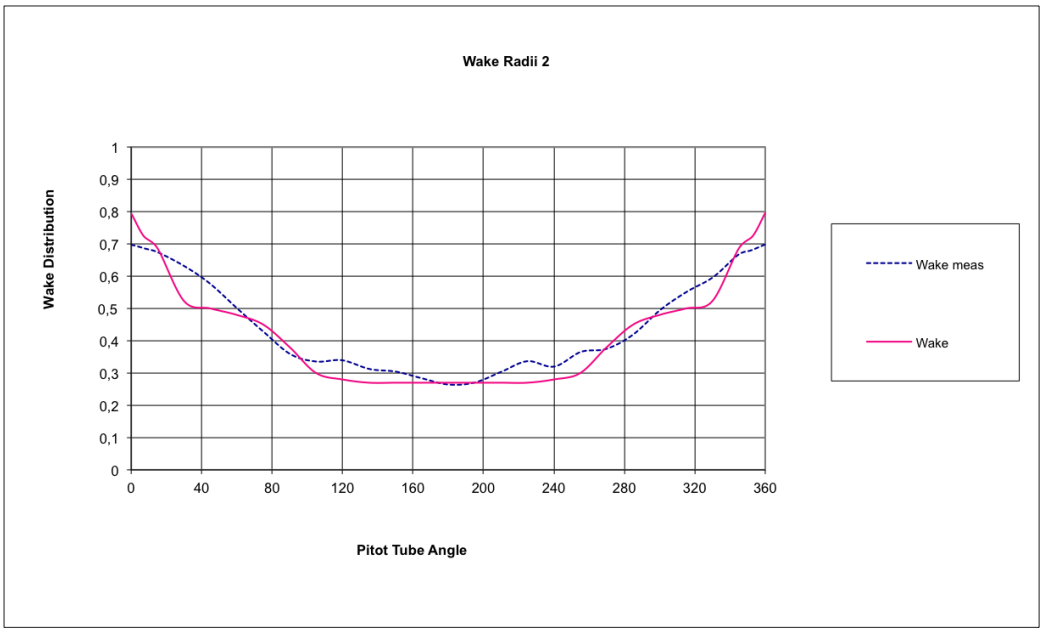

Figure A.2: Difference between the given and the measured wake field, at radii 2.

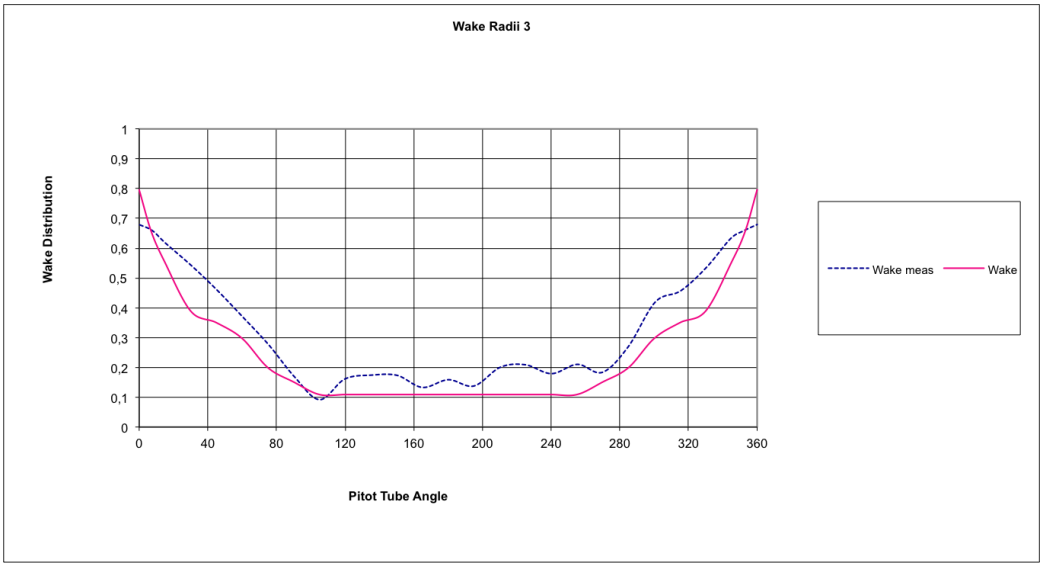

Figure A.3: Difference between the given and the measured wake field, at radii 3.

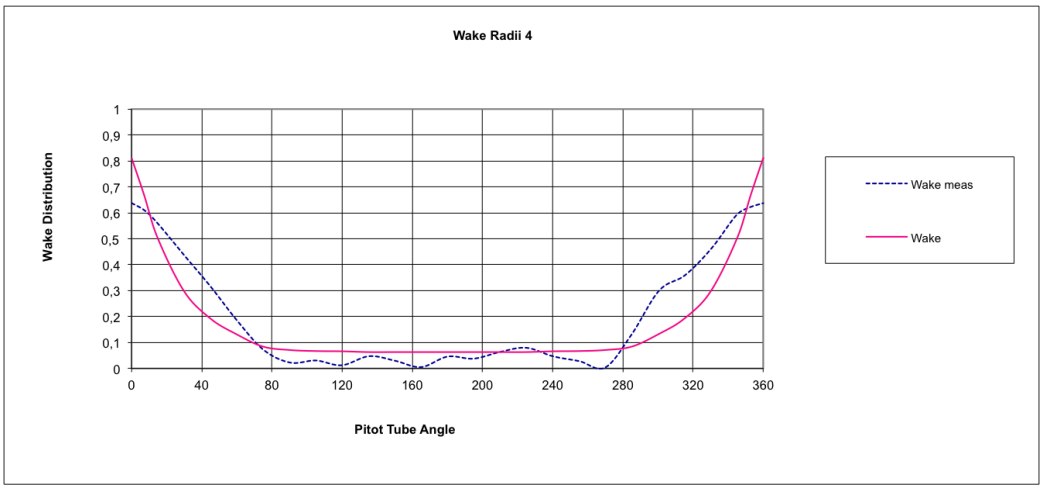

Figure A.4: Difference between the given and the measured wake field, at radii 4.

Appendix B

Pictures of cavitation pattern

Pictures of cavitation patterns on the ducted propellers. The pictures are organized after type of cavitation.

B.1 Bubble cavitaiton

Rps [Hz]	Kt total [-]	Cavitation number [-]
18	0.24	1.75

Table B.1: Condition: bubble cavitaiton.

B.2 Sheet cavitation

Rps [Hz]	Kt total [-]	Cavitation number [-]
18	0.24	2.05

Table B.2: Condition: sheet cavitation.

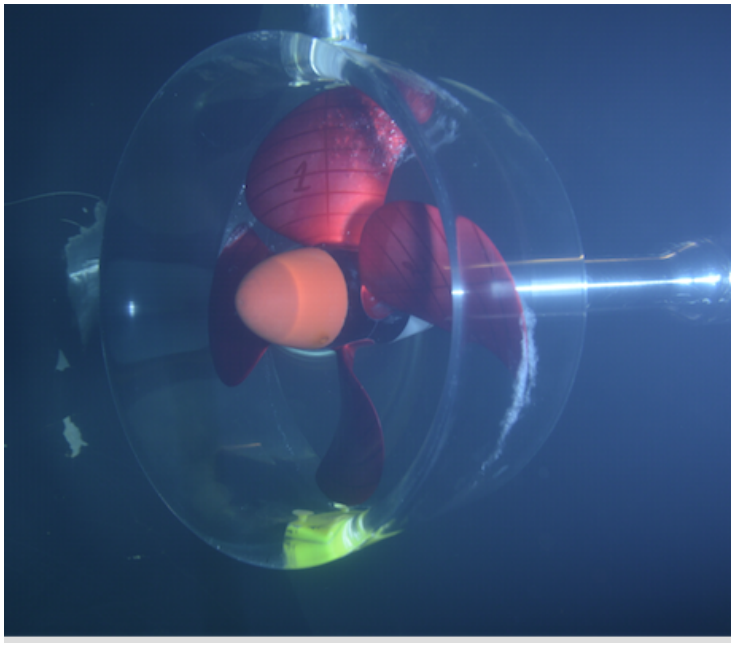

Figure B.1: Bubble cavitation, back side. Duct 19A.

Rps [Hz]	Kt total [-]	Cavitation number [-]
18	0.24	3.0

Table B.3: Condition: tip vortex cavitation.

B.3 Tip vortex cavitation

B.4 Duct cavitation

Rps [Hz]	Kt total [-]	Cavitation number [-]
18	0.24	1.2

Table B.4: Condition: duct cavitation.

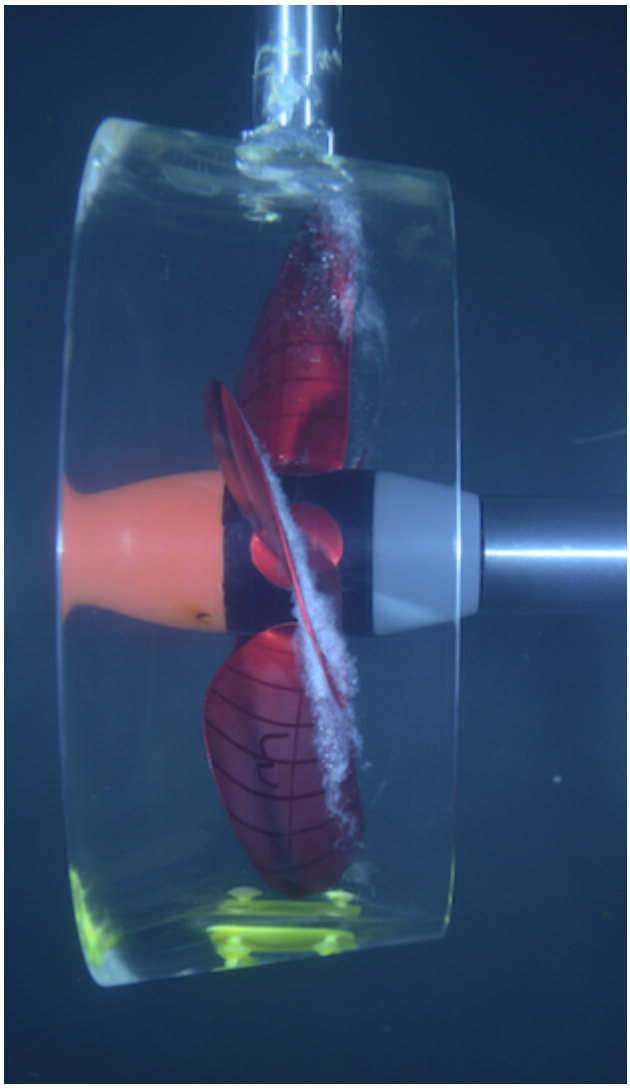

Figure B.2: Bubble cavitation, picture from side. Duct 19A.

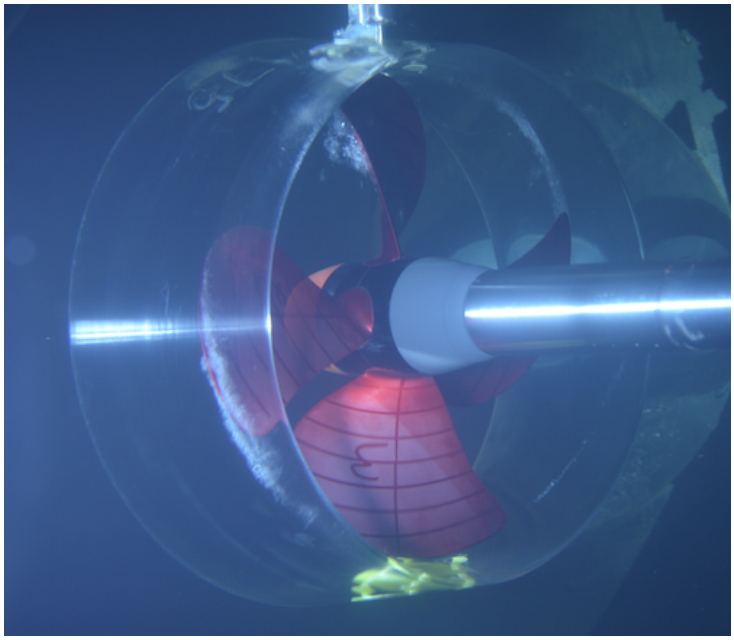

Figure B.3: Bubble cavitation, face side. Duct 19A.

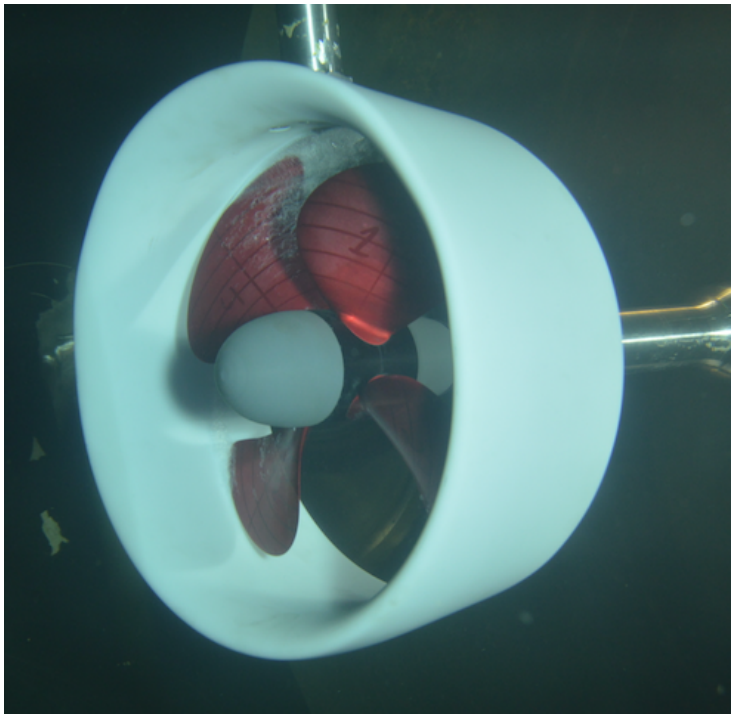

Figure B.4: Bubble cavitation back side. Duct A.

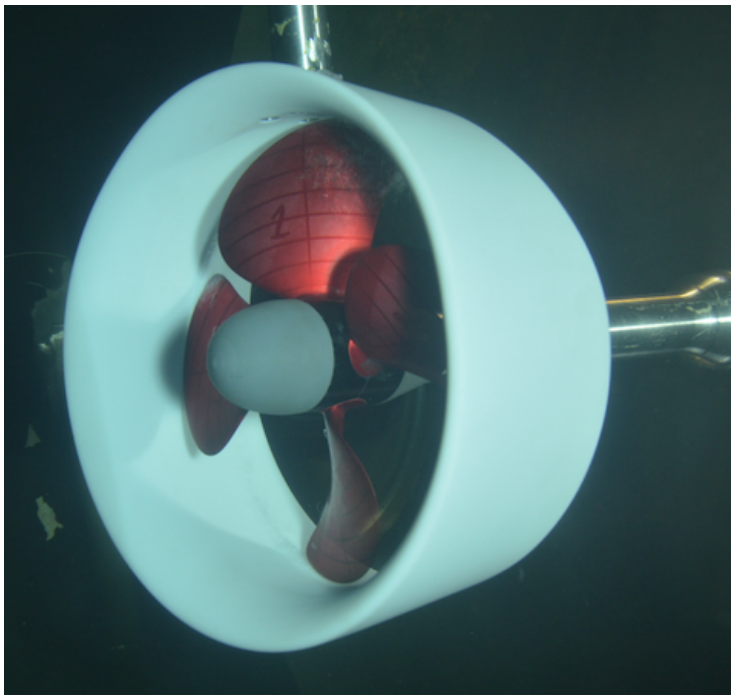

Figure B.5: Bubble cavitation back side. Duct B.

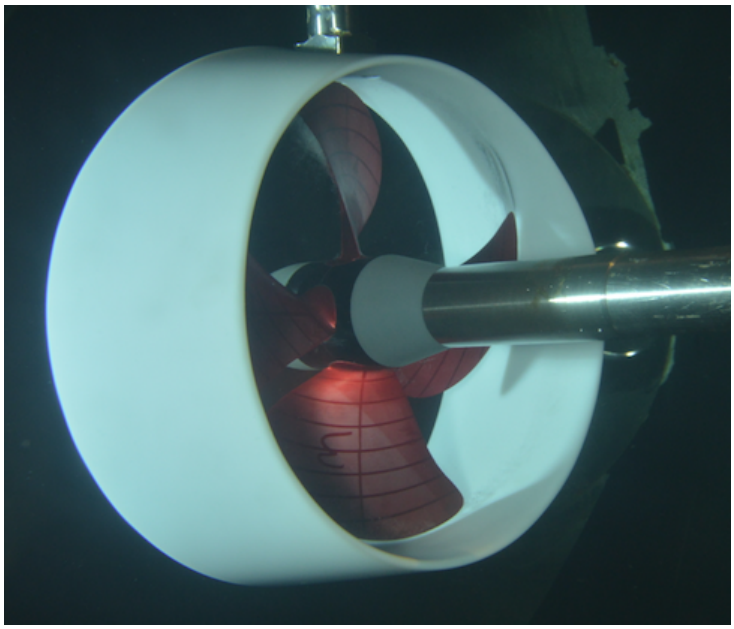

Figure B.6: Bubble cavitation back side. Duct B.

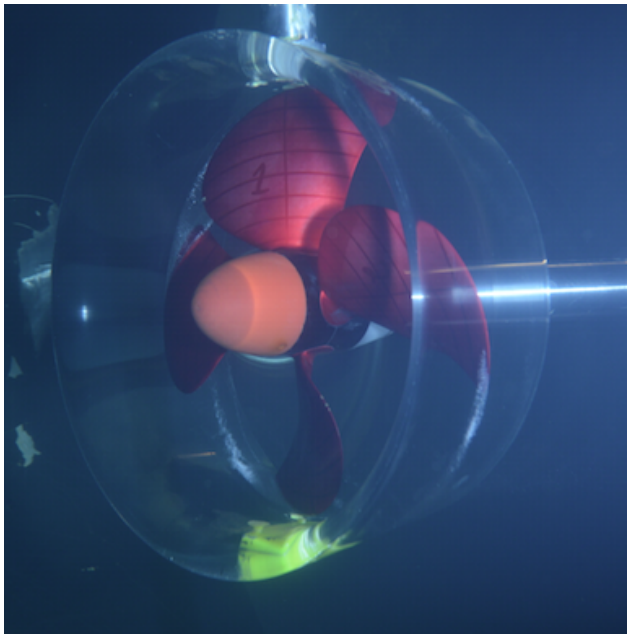

Figure B.7: Sheet cavitation, back side. Duct 19A.

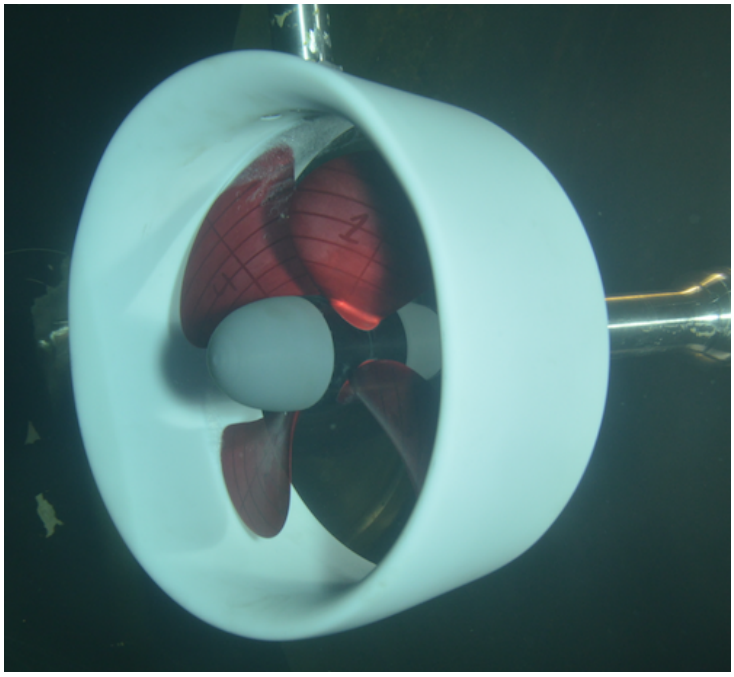

Figure B.8: Sheet cavitation, back side. Duct A.

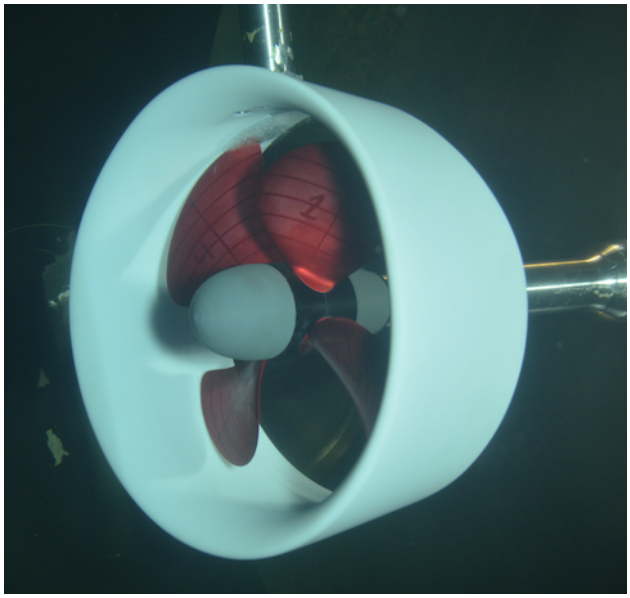

Figure B.9: Sheet cavitation, back side. Duct B.

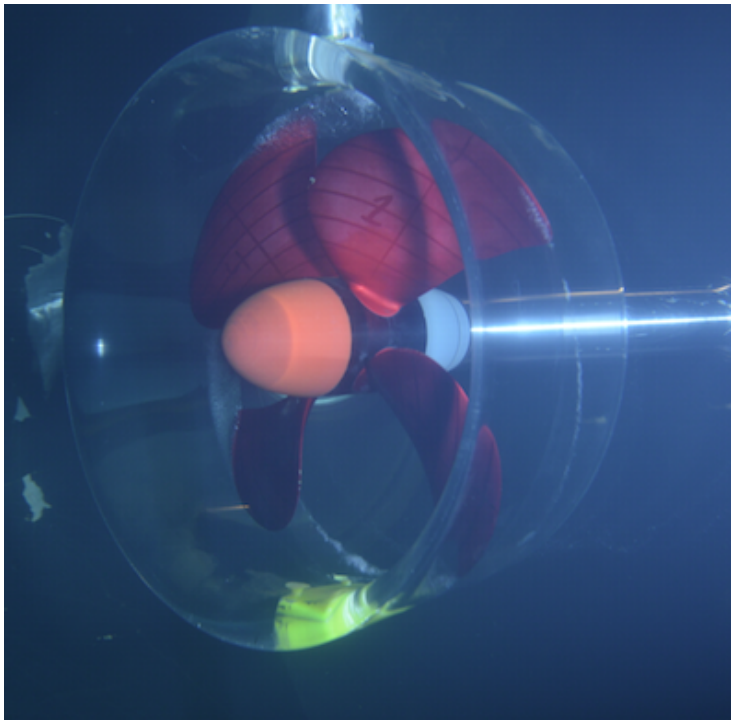

Figure B.10: Tip vortex cavitation, back side. Duct 19A.

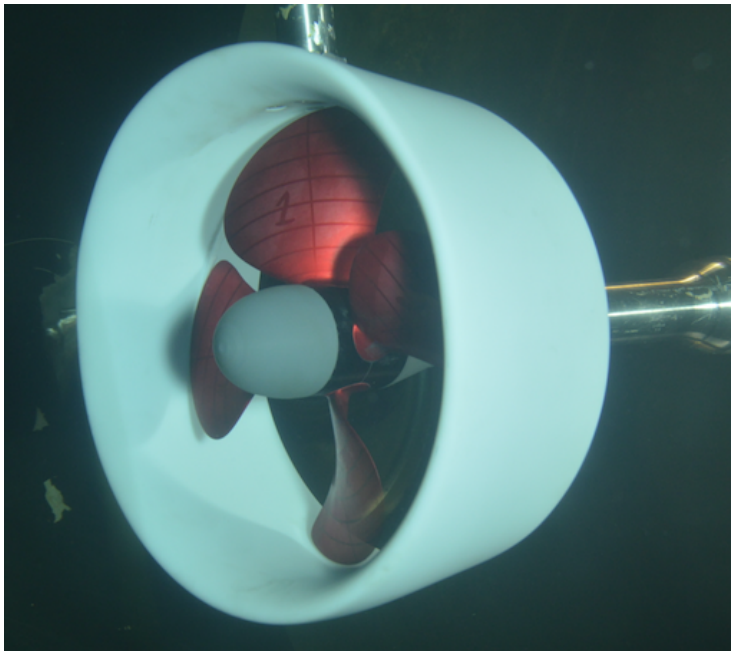

Figure B.11: Tip vortex cavitation, back side. Duct A.

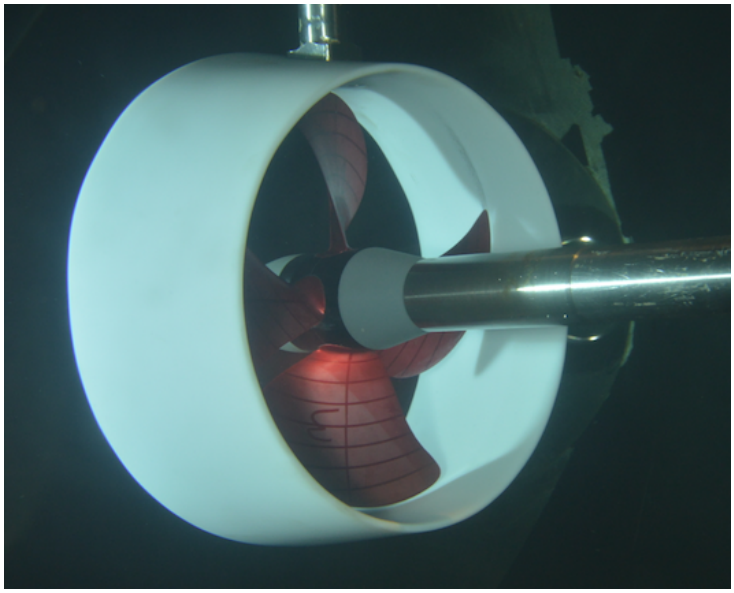

Figure B.12: Tip vortex cavitation, face side. Duct A.

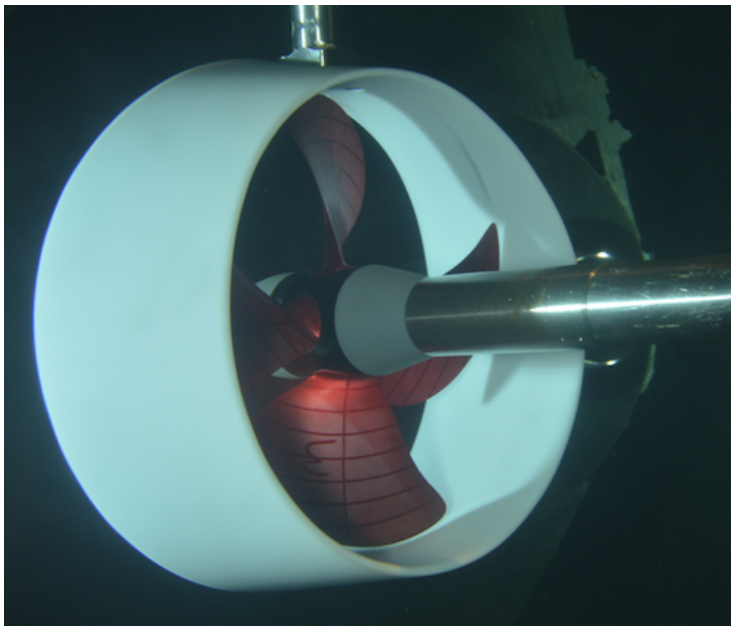

Figure B.13: Tip vortex cavitation, back side. Duct B.

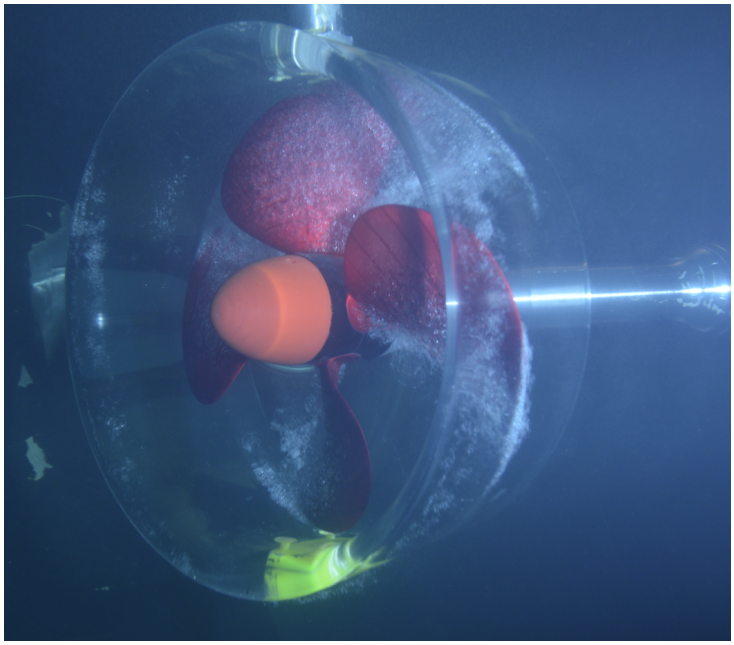

Figure B.14: Duct cavitation. Duct 19A.

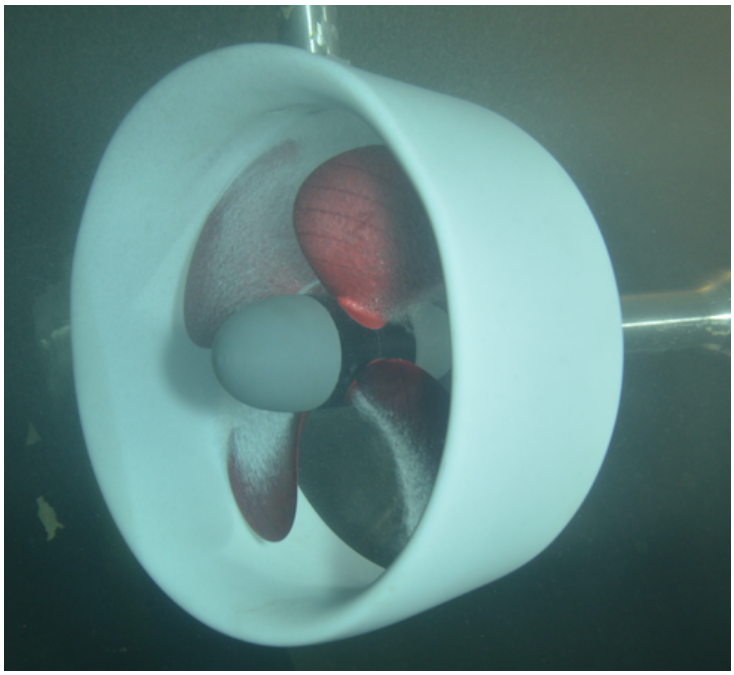

Figure B.15: No duct cavitation, back side. Duct A.

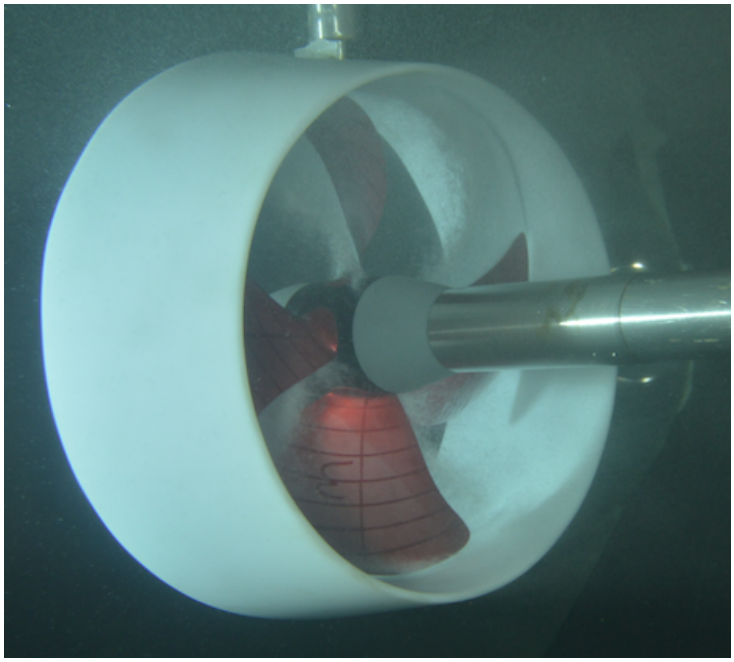

Figure B.16: No duct cavitation, face side. Duct A.

Appendix C

Haaviks Model

```
%%%%%%%%%%%%%%%%%%%%%%%%%%%%%%%%%%%%%%%%%%%%%%%%%%%%%%%%%%%%%%%%%%%%%%%
%
% This program reads a given wake field from a ship. It ... generates
% a matrix that propose a duct which containes different duct
% cross-sections.
%
% The purpose is to achive a homogeneous inflow to the ... propeller.
%
%%%%%%%%%%%%%%%%%%%%%%%%%%%%%%%%%%%%%%%%%%%%%%%%%%%%%%%%%%%%%%%%%%%%%%%

clear all; close all; clc;

wakedistribution = 'test2.xlsx'; %Reads the wake field.
OL = xlsread(wakedistribution);
A=OL(:,1:4); %Seperates the values from the file. Four ... sets of wake values.
B=OL(:,5); % This is the anglular positions.
C=OL(:,6); % Water velocity.


% Seperates the wake into sections of 30 degrees each:

```

```
%for i=1:30:360; %Forsøk på forløkke
 %   grader(i)=i;
  % dimensjon(i)=nonzeros(grader(i));
   % [colu(i),row(i)]=size(dimensjon(i));
   % [R(i),C(i)]=find(grader(i));
    %temp(i)=mean(A(R(i),:));
    %nywake=[temp(i)];
%end


degrees1=B<31;
dimension1=nonzeros(degrees1);
[colu1,row1]=size(dimension1);
[R1,C1]=find(degrees1);

degrees2=(B>31 & B<61);
dimension2=nonzeros(degrees2);
[colu2, row2]=size(dimension2);
[R2, C2]=find(degrees2);

degrees3=(B>61 & B<91);
dimension3=nonzeros(degrees3);
[colu3,row3]=size(dimension3);
[R3,C3]=find(degrees3);

degrees4=(B>91 & B<121);
dimension4=nonzeros(degrees4);
[colu4,row4]=size(dimension4);
[R4,C4]=find(degrees4);

degrees5=(B>121 & B<151);
dimension5=nonzeros(degrees5);
[colu5,row5]=size(dimension5);
[R5,C5]=find(degrees5);

degrees6=(B>151 & B<181);
dimension6=nonzeros(degrees6);
[colu6,row6]=size(dimension6);
[R6,C6]=find(degrees6);

degrees7=(B>181 & B<211);
```

```
63  dimension7=nonzeros(degrees7);
64  [colu7,row7]=size(dimension7);
65  [R7,C7]=find(degrees7);
66
67  degrees8=(B>211 & B<241);
68  dimension8=nonzeros(degrees8);
69  [colu8,row8]=size(dimension8);
70  [R8,C8]=find(degrees8);
71
72  degrees9=(B>241 & B<271);
73  dimension9=nonzeros(degrees9);
74  [colu9,row9]=size(dimension9);
75  [R9,C9]=find(degrees9);
76
77  degrees10=(B>271 & B<301);
78  dimension10=nonzeros(degrees10);
79  [colu10,row10]=size(dimension10);
80  [R10,C10]=find(degrees10);
81
82  degrees11=(B>301 & B<331);
83  dimension11=nonzeros(degrees11);
84  [colu11,row11]=size(dimension11);
85  [R11,C11]=find(degrees11);
86
87  degrees12=(B>331 & B<359);
88  dimension12=nonzeros(degrees12);
89  [colu12,row12]=size(dimension12);
90  [R12,C12]=find(degrees12);
91
92  % Finding the comprimized matrix, which has meanvalues ...
        distributed on each
93  % seaction, per radii:
94
95  temp1=mean(A(R1,:));
96  temp2=mean(A(R2,:));
97  temp3=mean(A(R3,:));
98  temp4=mean(A(R4,:));
99  temp5=mean(A(R5,:));
100 temp6=mean(A(R6,:));
101 temp7=mean(A(R7,:));
102 temp8=mean(A(R8,:));
```

```
103 temp9=mean(A(R9,:));
104 temp10=mean(A(R10,:));
105 temp11=mean(A(R11,:));
106 temp12=mean(A(R12,:));
107
108 tempDegrees=(30:30:360)';
109
110 newwake=[temp1; temp2; temp3; temp4; temp5; temp6; temp7; ...
        temp8; temp9; temp10; temp11; temp12];
111
112 newWakeDistribution=[newwake tempDegrees]; %The wake is ...
        averaged over the section
113
114 %Finding maximum velocity at the propeller. Want to use ...
        this value all over
115 %the propeller.
116
117 AA=newwake(:,1:4);
118 radii=AA(:,2:3); %Finding the value at 0.7*Radii.
119 tempave=mean(radii,2); %Average over the radii at r=0.7.
120 [value, location] = max(tempave(:)); %Finding maximum ...
        value at r=0.7
121
122 bbccc=value-tempave; %The velocity the duct profiles ...
        should accelerate.
123 [bbccc tempDegrees]
124 %bbd=(tempave/value)*100;  %Finding the difference (per cent).
125
126 %Find the position to the duct profiles.
127
128     duct1=bbccc>1.8 & bbccc≤2.0;
129     dimens1=nonzeros(duct1);
130
131     duct2=bbccc>1.6 & bbccc≤1.8;
132     dimens2=nonzeros(duct2);
133
134     duct3=bbccc>1.4 & bbccc≤1.60;
135     dimens3=nonzeros(duct3);
136
137     duct4=bbccc>1.20 & bbccc≤1.40;
138     dimens4=nonzeros(duct4);
```

```
139
140     duct5=bbccc>1.0 & bbccc≤1.20;
141     dimens5=nonzeros(duct5);
142
143     duct6=bbccc>0.8 & bbccc≤1.0;
144     dimens6=nonzeros(duct6);
145
146     duct7=bbccc>0.6 & bbccc≤0.8;
147     dimens7=nonzeros(duct7);
148
149     duct8=bbccc>0.4 & bbccc≤0.6;
150     dimens8=nonzeros(duct8);
151
152     duct9=bbccc>0.2 & bbccc≤0.4;
153     dimens9=nonzeros(duct9);
154
155     duct10=bbccc≥0 & bbccc≤0.2;
156     dimens10=nonzeros(duct10);
157
158     %nywake22=[dyse(i)]
159     newwake2=[duct1 duct2 duct3 duct4 duct5 duct6 duct7 ...
            duct8 duct9 duct10];
160
161     % Generates the matrix that is placing the ducts.
162     placementOfDuctCrossSection=[newwake2 tempDegrees]
163     ductCrossSectionNumber=[1 2 3 4 5 6 7 8 9 10]
```

Appendix D

Raw data from cavitation test

kt=0,10		Sigma			Tunnel pressure (kPa)			Kt_total			
Inception	Tip face vortex	Face sheet	Bubble	Tip face vortex	Face sheet	Bubble	Tip vortex	Face sheet	Bubble	Tip face vortex	
19A	3,35	2,25	2,25	25,95	25,95	18,3728	0,1344	0,1398	0,1398	0,0372	
Duct A	4,8	3,8	2,17	35,6541	28,6078	17,4203	0,0999	0,1007	0,0883	0,0348	
Duct B	3,82	2,78	2,13	28,9047	21,8694	17,1214	0,1127	0,111	0,0956	0,0357	

kt=0,14		Sigma			Tunnel pressure (kPa)			Kt_total			
Inception	Tip vortex	Face sheet	Bubble	Tip vortex	Face sheet	Bubble	Tip vortex	Face sheet	Bubble	Tip vortex	
19A	4,05	2,015	2	27,107	20,042	16,087	0,1578	0,1671	0,1381	0,039	
Duct A	4,2	2,38	2,13	14,045	14,045	12,7062	0,1428	0.1406	0,1351	0,0379	
Duct B	4,05	2,08	2,22	30,214	18,1	15,737	0,1375	0,1346	0,1146	0,0374	

kt=0,18		Sigma			Tunnel pressure (kPa)			Kt_total			
Inception	Tip vortex	Face sheet	Bubble	Tip vortex	Face sheet	Bubble	Tip vortex	Face sheet	Bubble	Tip vortex	
19A	3,3	2,3	1,85	25,59	18,44	15,16	0,1914	0,1828	0,1479	0,0407	
Duct A	2,83	2,38	2,13	21,947	21,98	17,466	0,1841	0,1844	0,1805	0,0407	
Duct B	3,64	2,06	1,8	26,7	16,6882	14,8051	0,1825	0,1765	0,1569	0,0403	

kt=0,24		Sigma			Tunnel pressure (kPa)			Kt_total			
Inception	Tip vortex	Back sheet	Bubble	Tip vortex	Back sheet	Bubble	Tip vortex	Back sheet	Bubble	Tip vortex	
19A	4,6	2,25	2,5	34,473	18	16,6325	0,2547	0,247	0,2462	0,0449	
Duct A	3,6	2,04	1,86	27,7469	16,68	15,2294	0,2395	0,2335	0,222	0,0442	
Duct B	3,6	2,27	1,88	26,998	17,9764	15,4556	0,242	0,241	0,2348	0,0442	

kt=0,30		Sigma			Tunnel pressure (kPa)			Kt_total			
Inception	Tip vortex	Back sheet	Bubble	Tip vortex	Back sheet	Bubble	Tip vortex	Back sheet	Bubble	Tip vortex	
19A	4,5	2,25		34,1503	17,799		0,3205	0,3066		0,049	
Duct A	3,8	2,17		29,5964	16,9876		0,3039	0,2977		0,0266	
Duct B	4,2	2,01		31,6477	18,8065		0,2969	0,2945		0,0475	

kt=0,42		Sigma			Tunnel pressure (kPa)			Kt_total			
Inception	Tip vortex	Back sheet	Bubble	Tip vortex	Back sheet	Bubble	Tip vortex	Back sheet	Bubble	Tip vortex	
19A	4,6	3,3		41,5909	25,4373		0,4407	0,4427		0,0546	
Duct A	4,1	2,38		39,45	19,2951		0,4203	0,4078		0,0537	
Duct B	5,6	2,34		41,6959	20,2662		0,4193	0,4185		0,0532	

Kq			Duct thrust			J			eta	
Face sheet	Bubble	Tip vortex	Face sheet	Bubble	Tip vortex	Face sheet	Bubble	Tip vortex	Face sheet	Bubble
0,0365	0,0365	-36,7197	-30,786	-30,3786	1,0209	1,0159	1,0159	0,768905	0,7422	0,7422
0,0348	0,0332	-64,848	-63,5909	-65,1165	1,1431	1,1393	1,1293	0,5201	0,5231	0,4766
0,0353	0,0338	-59,8967	-60,0875	-65,4801	1,0961	1,0908	1,0879	0,5493	0,5444	0,488

Kq			Duct thrust			J			eta	
Face sheet	Bubble	Tip vortex	Face sheet	Bubble	Tip vortex	Face sheet	Bubble	Tip vortex	Face sheet	Bubble
0,0389	0,0377	-26,5432	-18,424	-38,2	0,979	0,9728	0,9685	0,6308	0,666	0,5647
0,0304	0,0256	-44,88	-48,142	-33,593	1,0626	1,0636	1,067	0,637	0,4944	0,4958
0,0373	0,0351	-47,183	-46,87	-55,266	1,0386	1,036	1,0338	0,6074	0,611	0,5384

Kq			Duct thrust			J			eta	
Face sheet	Bubble	Tip vortex	Face sheet	Bubble	Tip vortex	Face sheet	Bubble	Tip vortex	Face sheet	Bubble
0,0405	0,0386	-9,3457	-16,4535	-36,2396	0,935	0,956	0,9685	0,699	0,6715	0,5669
0,0407	0,0403	-25,109	-25,5185	-26,419	0,9773	0,9773	0,9721	0,7034	0,7039	0,6923
0,0394	0,0375	-26,1087	-27,8615	-34,3489	0,9564	0,9515	0,9493	0,6887	0,6776	0,6316

Kq			Duct thrust			J			eta	
Back sheet	Bubble	Tip vortex	Back sheet	Bubble	Tip vortex	Back sheet	Bubble	Tip vortex	Back sheet	Bubble
0,0446	0,0442	20,611	15,6094	16,2766	0,8398	0,8376	0,8356	0,6891	0,68654	0,6852
0,0438	0,0425	1,3524	-2,2281	-4,568	0,8607	0,8588	0,8562	0,7418	0,7292	0,7117
0,0441	0,0433	3,2638	1,3885	-0,9045	0,8382	0,8377	0,8363	0,7303	0,7278	0,721

Kq			Duct thrust			J			eta	
Back sheet	Bubble	Tip vortex	Back sheet	Bubble	Tip vortex	Back sheet	Bubble	Tip vortex	Back sheet	Bubble
0,0486		55,1958	45,5227		0,7262	0,7271		0,7558	0,732506	
0,0262		35,6623	29,7851		0,7136	0,7179		1,2988	1,2988	
0,0474		31,0082	27,9824		0,725	0,723		0,7211	0,7144	

Kq			Duct thrust			J			eta	
Back sheet	Bubble	Tip vortex	Back sheet	Bubble	Tip vortex	Back sheet	Bubble	Tip vortex	Back sheet	Bubble
0,0547		128,0022	129,9472		0,4701	0,4717		0,6042	0,6079	
0,318		104,5863	96,863		0,4586	0,4561		0,5871	0,5701	
0,0534		102,7367	100,3225		0,4673	0,543		0,5864	0,5654	

Appendix E

Coordinates for Duct A and B

E.1 Coordinates for Duct A

	Length of cross section 0,121 [m]		**Length:** 0,121 [m]		**Length:** 0,121 [m]	
	Degrees on duct: 330-30		**Degrees on duct:** 90-270		**Degrees on duct:** 30-90 and 270-330	
xC/DL						
0	0,20404329	0,20404300	0,12011442	0,12011442	0,16758335	0,16758335
0,0125	0,22830684	0,16770700	0,14820537	0,08760537	0,19324706	0,13264706
0,025	0,23637040	0,14947000	0,15603489	0,07413489	0,19803790	0,11613790
0,05	0,23779753	0,12119800	0,16244806	0,05584806	0,19807787	0,09147787
0,075	0,23312463	0,09892500	0,16627770	0,04207770	0,19650076	0,07230076
0,1	0,22845171	0,08145200	0,16865407	0,03165407	0,19441713	0,05741713
0,15	0,21710583	0,05500600	0,17083332	0,01673332	0,18935288	0,03525288
0,2	0,20575992	0,03626000	0,17068130	0,00718130	0,18347608	0,01997608
0,25	0,19641397	0,01913890	0,16862156	0,00202256	0,17693436	0,01033536
0,3	0,18506800	0,00000000	0,16520000	0,00000000	0,16991798	0,00000000
0,4	0,16237602	0,00000000	0,15605527	0,00000000	0,15508301	0,00000000
0,5	0,14368402	0,00000000	0,13974150	0,00000000	0,13974150	0,00000000
0,6	0,12499202	0,00000000	0,12440000	0,00000000	0,12440000	0,00000000
0,7	0,10630000	0,00000000	0,10875247	0,00000000	0,10875247	0,00000000
0,8	0,08760797	0,00180800	0,09285168	0,00705168	0,09285168	0,00705168
0,9	0,06891594	0,00461600	0,07684536	0,01254536	0,07684536	0,01254536
0,95	0,05956992	0,00697000	0,06874195	0,01614195	0,06874195	0,01614195
1	0,03022389	0,03022400	0,04054356	0,04054356	0,04054356	0,04054356

E.2 Coordinates for Duct B

	Length of cross section	0,101 [m]	**Length:**	0,121 [m]	**Length:**	0,121 [m]	
	Degrees on duct:	315-45	**Degrees on duct:**	90-270	**Degrees on duct:**	45-90 and 270-315	
xC/DL							
0		0,20404329	0,20404300	0,12011442	0,12011442	0,18249943	0,18249943
0,0125		0,22830684	0,16770700	0,14820537	0,08760537	0,20719967	0,14659930
0,025		0,23637040	0,14947000	0,15603489	0,07413489	0,21069980	0,12879931
0,05		0,23779753	0,12119800	0,16244806	0,05584806	0,20800002	0,10139938
0,075		0,23312463	0,09892500	0,16627770	0,04207770	0,20420020	0,07999945
0,1		0,22845171	0,08145200	0,16865407	0,03165407	0,20040034	0,06339952
0,15		0,21710583	0,05500600	0,17083332	0,01673332	0,19280055	0,03869962
0,2		0,20575992	0,03626000	0,17068130	0,00718130	0,18520070	0,02169972
0,25		0,19641397	0,01913890	0,16862156	0,00202256	0,17760080	0,01100080
0,3		0,18506800	0,00000000	0,16520000	0,00000000	0,17000086	0,00000000
0,4		0,16237602	0,00000000	0,15605527	0,00000000	0,15480093	0,00000000
0,5		0,14368402	0,00000000	0,13974150	0,00000000	0,13960096	0,00000000
0,6		0,12499202	0,00000000	0,12440000	0,00000000	0,12440099	0,00000000
0,7		0,10630000	0,00000000	0,10875247	0,00000000	0,10920099	0,00000000
0,8		0,08760797	0,00180800	0,09285168	0,00705168	0,09285168	0,00705168
0,9		0,06891594	0,00461600	0,07684536	0,01254536	0,07684536	0,01254536
0,95		0,05956992	0,00697000	0,06874195	0,01614195	0,06874195	0,01614195
1		0,03022389	0,03022400	0,04054356	0,04054356	0,04054356	0,04054356